Subsea Tracked Trencher Mobility

The development of a model to gain insight of the mobility of a subsea tracked trencher in granular and cohesive soils

F.C. Holzhaus

Technische Universiteit Delft

TU Delft

Subsea Tracked Trencher Mobility

The development of a model to gain insight of the mobility of a subsea tracked trencher in granular and cohesive soils

by

F.C. Holzhaus

to obtain the degree of Master of Science
at the Delft University of Technology,
to be defended publicly on Monday September 15, 2021 at 13:00 AM.

Student number:	4401085	
Project duration:	December 1, 2020 – September 15, 2021	
Thesis committee:	Prof. dr. ir. C. Van Rhee,	TU Delft, Chairman
	Dr. ir. S. A. Miedema,	TU Delft
	Dr. ir. R. L. J. Helmons	TU Delft
	Dr. Ir. A. J. Nobel,	Boskalis

TU Delft

Preface

Before you lie, the thesis ”Subsea tracked trencher’s mobility”, in which, with the help of a mathematical model, the influence of various factors on the deployability, regarding mobility, of different trenchers is examined. Ultimately, the aim is that the resulting model can also be used in earlier phases of the construction process to capture the risks of the route. This thesis was written as part of my graduation project in Hydraulic Engineering at the Delft University of Technology and commissioned by Boskalis. From December 2020 to September 2021, I have been busy with the research and writing of the thesis.

To begin with, I would like to thank my supervisor from Boskalis, Arno Nobel. First of all, for the opportunity, he gave me to graduate within the Research and Development team. Secondly, for the daily guidance in the form of many video calls. Arno has been able to help me further with his critical view and thinking along, and I have been able to learn a lot from him. I would also like to thank my sounding board group within Boskalis. This group was set up especially for me and ensured that the problem and intended objective were quickly apparent.

I would also like to thank my supervisors from TU Delft, Sape Miedema, Cees van Rhee and Rudy Helmons. I would like to thank Cees van Rhee for his contribution during the progress meetings and finding a thesis topic. In particular, I would like to thank Sape Miedema. The fortnightly meetings were an excellent way for me to keep in touch in corona. Both the discussions about the content and the peripheral issues helped me a lot.

Finally, I would like to thank my family and girlfriend who supported me through the process and ensured that all the peripheral matters were always in order. I hope you enjoy reading my thesis.

F.C. Holzhaus
Amsterdam, September 2021

Abstract

The deployability, regarding mobility, of Boskalis trenchers, is currently determined by practical knowledge. The lack of theoretical knowledge means that risk assessments in the tender phase are less accurate. This reduced accuracy has two negative consequences. First, the trencher may fail. Secondly, the safety margins can be too large. Both consequences result in additional duration and costs. This research considers two ways of failure. The first one is slipping; as a result of this, the track does not have enough traction, which causes the tracks to turn while the trencher does not move forward. The slipping can happen in two ways. The first way is due to soil failure with the grousers fully penetrated. This results in the trencher digging itself in. The other way is that the grousers are not penetrated and the trenchers slips due to the track-soil interaction. In order to prevent the trencher from slipping, horizontal stability between the soil and tracks should be obtained. The second way of failure is that the trencher sinks into the soil. Vertical stability between the applied pressure and the bearing capacity should be achieved to prevent this kind of failure. In this research a model has been developed that can approximate the operating range of different trenchers. With the help of these operating ranges, the model can make risk assessments in an early phase of the project. There will be little knowledge about the soil-specific parameters and the exact external conditions in this phase. Should there be a risk in the area of mobility along with the project, the model is also able to provide a more in-depth analysis. In addition, the model aims to apply to different types and sizes of trenchers. The research answers the following question:

”Which different operational environments and soil conditions have a critical influence on the deployability of a subsea tracked trencher regarding the vertical stability and horizontal stability of the soil¬track interaction system?

The model considers the trencher’s mobility in terms of vertical and horizontal stability, where the axes rotate with the slope. Meyerhof’s effective area method approximates the vertical stability. This method is used to take into account the eccentric loads. A traction calculation model approaches horizontal stability. Based on the penetration depth of the individual elements of a track, a shear mode is determined. The available traction force per element can be calculated using these shear modes using the Mohr-coulomb shearing theory. With a case study for the CBT2400, the research question is answered. In this case study, we first look at the different external processes that influence mobility. In addition, the various soil parameters and trencher dimensions are examined. Finally, the results of this study will be compared with two real-life projects.

The results show that the mobility of the trencher is better in granular soils than in cohesive soils. In cohesive soils, the trencher’s mobility depends on the external factors that change in the driving direction, like pitch slopes and currents that have a frontal impact. In cohesive soils, the sensitivity is a vital soil parameter besides the undrained shear strength. Since the sensitivity is not included in the soil research, it is recommended to do it in future projects. In granular soils, external factors from all angles must be taken into account, like pitch and roll angles and currents from all directions. With granular soils, especially the relative density and internal friction angle are essential; in addition, the grain size must be taken into account. The grain size influences the permeability of the soil. The permeability, together with the relative density, determine if contractancy and dilatancy will take place in the soil. It could be interesting to change the grouser and track dimensions to improve the trencher’s mobility. However, this depends on the circumstances in which the trencher would have to operate. The model was validated using two cases involving the Borssele and Moray East projects. An important conclusion is that the model can be used to estimate the potential risk areas reasonably. However, it is recommended to test the model in predefined circumstances and soil parameters.

Nomenclature

α	Adhesion factor
γ	Soil unit weight [kPa]
γ'	Effective unit weight [kN/m^3]
$\delta\eta$	Porosity difference [-]
δh_{avg}	Head pressure difference [m]
δP_{avg}	Pressure difference [kPa]
ϵ	Dilatancy [-]
η_{cs}	Critical state porosity [-]
η_i	Initial porosity [-]
$\theta_{current}$	Impact angle current [°]
μ_{emb}	Embedment factor [-] (=1 assumed)
μ_s	Shape factor (=B_{track}/L_{track}) [-]
μ_{wall}	Side wall factor [-] (=1 assumed)
v_u	Poisson's ratio undrained condition (0.3-0.45)[-] (v' in case of granular soils(0.2-0.455))
ρ'	Effective density [kg/m^3]
ρ_s	Specific density [kg/m^3]
ρ_t	In-situ density [kg/m^3]
ρ_w	Water density [kg/m^3]
σ_1	Principal stress 1 [kPa]
σ_3	Principal stress 3 [kPa]
σ'	Effective stress [kPa]
$\sigma'_{n,f}$	Effective pressure at critical state [kpa]
σ_{pore}	Total pore pressure [kpa]
σ_{total}	Total pressure [kpa]
σ_{xy}	Applied shear stress[kPa]
σ_{yy}	Applied normal stress in y direction[kPa]
σ_{yx}	Applied shear stress[kPa]
τ_{cs}	Critical state shear strength [kpa]
τ_f	Shear strength [kPa]
$\tau_{t-s,max}$	Shear strength track-soil [kPa]
ϕ'_{cs}	Critical state internal friction angle [degree]
a	Adhesion [kPa]
A_{trench}	Area of cutting sword [m^3]
A_{shear}	Shear area [m^2]
B'	Effective width of track [m]
$B_{trencher}$	Width trencher [m]
c	Cohesion[kPa]
cd	Drag coefficient[-]
d_{10}	Effective particle size[mm]
d_{50}	Median soil particle size [kPa]
$d_{c,q,\gamma}$	Depth factors[-]
e	Void ratio [-]
e	Eccentricity parameter[m]
e_{max}	Maximum void ratio [-]
e_{min}	Minimum void ratio [-]
E_u	Undrained elastic modulus [kPa] (E' in case of granular soils)
$F_{current,y,x}$	Current force[kN]
$F_{cut,hor}$	Horizontal cutting force[kN]
$F_{cut,ver}$	Vertical cutting force[kN]
f_{vert}	Vertical cutting factor [-] (-0.5-0.5)
$h_{grouser}$	Grouser height [m]
$H_{trencher}$	Height trencher [m]
i	Slip ratio [-]
I	Moment of inertia [mm^4]
$i_{c,q,\gamma}$	Inclination factors[-]
j	Shear displacement [m]
$j_{residual}$	slip displacement before residual shear strength [m]
kc	undrained elasticity modulus correlation factor [-]
K_p	Passive earth coefficient [kN]
k_w	Soil permeability [-]
l'	Effective Length of track [m]
$L_{element}$	Element length [m]
$L_{grouser}$	Grouser length [m]
l_{flow}	Average flow length [m]
L_{track}	Track length [m]
M	Momental force [kNm]
N_c	Cutting factor [-] (5-10)
$N_{c,q,\gamma}$	Bearing capacity factors[-]
$N_{element,res}$	Number element residual shear strength [-]
q_0	Overburden pressure[kPa]
$Q_{avg,shear}$	Average flow rate [m^3/s]
Q_b	Bearing capacity[kPa]
R_b	Bulldozing resistance [kN]
R_c	Compaction resistance force [kN]
$S_{c,q,\gamma}$	Shape factors[-]
S_u	Undrained shear strength [kpa]
S_t	Sensitivity [-]
$S_{u,res}$	Residual undrained shear strength [kpa]
Th_{shear}	Shear plane thickness [m]
$u_{current}$	Current velocity [m/s]
v_1	Kinematic viscosity [m^2/s]
V	Actual progression speed vehicle[m/s]
V	Vertical resultant force [kN]
V'	Progression speed track [m/s]
$v_{progress}$	Progress speed track [m/s]
V_s	Solids Volume [m^3]
V_{shear}	Shear volume [m^3]
V_t	Mixture Volume [m^3]
V_v	Voids Volume [m^3]
X	Distance from start of track [m]
z_0	Elastic settlement [m]
z_i	Dynamic settlement [m]

List of Figures

List of Tables

Contents

1 Introduction

1.1. Background information

In the construction of offshore wind farms, large wind tubines are installed to generate electricity. This electricity must be transported via cables. These cables run along the seabed from wind turbine to wind turbine as well as to onshore facilities to transport the electricity further on land. In order to protect these cables from external hazards, they can be covered with rocks. Another option is to bury the cables. To bury the cables a trench is made. This trenching can be done in two ways: with a tool on sledges behind a vessel or with the help of subsea tracked trenchers. These subsea tracked trenchers are vehicles that use tracks to drive on the seabed, where they dig a trench to guide the cable. This can be done using a mechanical cutter and/or a jet sword. Boskalis owns three trenchers, all of which have their own specifications. Therefore each trencher will respond differently in different conditions. The mobility of a trencher can be explained as the ability of a vehicle to move over a certain soil in certain external conditions.

1.2. Problem definition

The knowledge on the deployability in terms of mobility of Boskalis' subsea trenchers is currently limited, due to a gap in the available knowledge about the mobility of different tracks/trenchers in different conditions. The mobility - and thus deployability - is determined using data from previous projects. The lack of theoretical knowledge about the mobility of the subsea trenchers leads to two issues: Firstly, the trencher could fail, causing damage and/or delays and thus introducing additional costs. Secondly, the safety margins imposed may be too strict, which also results in additional costs. The trencher's mobility is expected to be insufficient in the following conditions:

- Soft cohesive soil (<15 kPa) and loose granular soils (RD < 30 %), where the trencher might sink (= vertical stability) or traction may not be good enough and the tracks may slide (= horizontal stability).
- Steep slopes (>15°), especially of sand dunes. Steeper slopes are generally dredged first.
- Cohesive soils (>50 kpa, trenching depth = 3.3 m), where the jet swords work more like a plough; this introduces additional resistance and cutting forces. This research only regards a trencher operating a jet sword without mechanical cutter.

1.3. Research goal

The goal of this thesis is to determine the deployability in terms of mobility of a general subsea tracked trencher. In order to achieve this goal, the processes that influence the mobility - and thus the deployability - of the trencher need to be known theoretically. As the mobility issue depends on many factors and processes, the aim is to produce a python model for subsea trencher mobility. With this computational model the operational borders discussed in the problem definition should be assessed. The model uses a simplified trencher, whereby the most important parameters can be changed. It

calculates whether a seafloor has enough horizontal traction capacity and vertical bearing capacity to support the operations of a subsea trencher. Different situations can be considered, such as the type of tracks (track dimensions, grouser sizes, materials), the soil type (cohesive and granular soils), the current conditions and different driving states (resting, driving, pitch and roll angles). The model ideally provides the circumstances and soil conditions under which the trencher should be able to operate. It should be applicable to a wide variety of trenchers, so as to determine the deployability of the various trenchers currently owned by Boskalis, any future trenchers Boskalis might acquire and trenchers owned by external parties.

1.4. Research questions

In order to achieve the above goal, insights must be gathered in the mobility of subsea tracked trenchers. The following main research question was formulated to incorporate this goal:

”Which different operational environments and soil conditions have a critical influence on the deployabilty of a subsea tracked trencher regarding the vertical stability and horizontal mobility of the soil-track interaction system?”

In order to answer this question properly, it will be divided into several parts and their associated subquestions. The different parts are: the trencher-specific questions, the soil-specific questions, the external influence-specific questions and the modelling-specific questions.

- Trencher-specific questions:
  - Which different tracks are being used?
  - How do different tracks influence horizontal traction?
  - How do different tracks influence vertical stability?
  - Which trencher components and dimensions influence the mobility process?
  - How do these different components and dimensions influence the mobility process?
- Soil-specific questions:
  - Which different soil types can be expected when operating?
  - Which kind of soil failure would influence the mobility of the trencher?
  - How do the soil characteristics influence the trafficability of the soil?
  - How do the soil characteristics change during the driving process of tracks?
  - How can the different mobility/trafficability processes be calculated?
- External-influence questions:
  - What external factors exert a force on the trencher?
  - What resistances will the trencher encounter during operations?
  - Under which pitch and roll should the trencher operate, and how do these angles change the soil’s bearing capacity?
  - How fast does the trencher operate?
- Modelling questions:
  - How could the entire process be combined into a model?
  - Which parameters should input and which should output?
  - Is the model representative of reality?

1.5. Research outline

The study can be divided into three parts: a literature study, modelling and a case study. In the literature review, several issues need to be clarified: firstly, how granular soils and cohesive soils absorb shear forces and how these soils can fail. In order to present a proper picture, it is important that the failure mechanisms can be approached with existing theories. A review of these mechanisms and theories will be presented in chapter 2. Also, a method will need to be devised to simplify the different trenchers to a general vehicle without losing key dimensions. This process is outlined in chapter 3. In addition, it is important to find out which external factors can affect trencher mobility, e.g. flow conditions, driving resistances and slopes. These will be discussed in chapter 4, section 1.

In the modelling section of this study, all findings from the literature research must be applied to the mobility problem of the subsea tracked trencher. This is done in chapter 4, section 2 and in chapter 5. After this step, it is important to understand the influences of and relationships between the different processes. Subsequently, these processes must be programmed into an iterative model, which must ultimately work towards a mobility envelope that shows where the trencher can and cannot operate under certain conditions. This model will be presented in chapter 6. As mentioned earlier, it is important that the model is easily adaptable, for use with different trenchers. Cutting forces and other forces exerted on the trenching tool are not considered in this research. However, it should be possible to add these as inputs. The outline of the model will be as follows: The model checks the load applied to the soil by the trencher via the tracks. First, the vertical capacity of the soil will be checked. The resultant force that works perpendicular to the soil should be checked against the vertical bearing capacity. The second part of the model should check the horizontal traction capacity of the soil-track interaction. Again, a balance of forces should be created. The capacity of the soil should be sufficient to support the applied force. If one of the capacities is not sufficient, slip will occur and mobility will be insufficient. The soil's horizontal traction will first be modelled for one track element and then expanded to multiple tracks.

The case-study section has been included for two reasons. The first is to be able to estimate the important parameters and processes. The second reason is to validate the model. This is done using two cases: the construction of the Borssele wind farm and the construction of the wind farm at Moray East, both of which will be discussed in Chapter 7. The conclusion, discussion and recommendations for further research are presented in Chapter 8.

2

Basic soil mechanics

This chapter explains the fundamental soil mechanics used in this research. Alongside the soil mechanics, it will also provide the basic explanations and definitions of different parameters. This is important because the model formed in this research rests on these basic ideas. If these processes are known, the next steps can be more targeted to the specific problem.

2.1. Soil classification

Each soil consists of different particles, the ratio of which defines the soil type. The particles that make up the soil can be distinguished by size. Particle size is represented by the equivalent diameter of the particle. The equivalent diameter is the diameter of a sphere which behaves like the respective soil particle and can be measured through various tests, such as mechanical sieving. Four particle groups can be classified following the USDA standard, moving from larger to smaller particle size: gravel, sand, silt and clay. Gravel consists of particles with a particle size larger than 2.0 mm. Sand particles have a size of between 2.0 mm and 0.05 mm. Particles sized between 0.05 mm and 0.005 mm are categorized as silt, while clay consists of all particles smaller than 0.005 mm. Once the ratio of the different particles is known, Figure 2.1 can be used to determine the soil type.

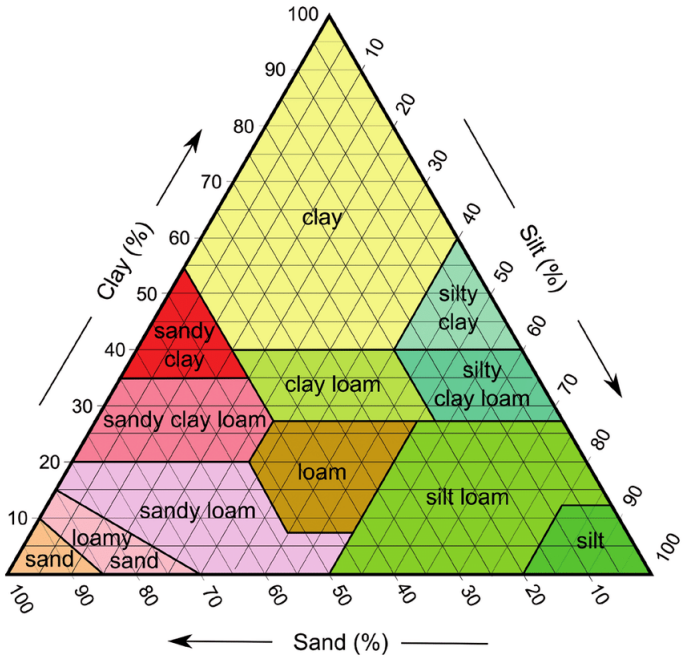

Figure 2.1: Soil types by the USDA

In this research the soil is divided into two groups: cohesive soils and granular soils, also known as non-cohesive soils. The difference between both groups is the tendency of soil particles to stick together. Cohesive soil consists of a large percentage of clay. It tends to be brittle when dry and plastic when wet. Another important feature of cohesive soil is its low permeability. This ensures that cohesive soils usually react undrained. The soil types in Figure 2.1 that belong to the cohesive soils are clay, sandy clay and silty clay. Contrary to cohesive soils, granular soils consist of larger-grained particles and tend to lack cohesive strength. Nevertheless, certain granular soils can exhibit a force that looks like cohesive strength. This force is caused by water under pressure and is therefore different from cohesion. Whether it occurs depends on the permeability of the granular soil: Soils with higher permeability will show drained behaviour. If permeability is lower, the granular soil will behave partially drained and can therefore temporarily absorb pore water pressures. Granular soils cannot be molded because they are drained, and they crumble when dry. Soil types that belong to the granular soils are gravel, sand, silt, loam and all relevant hybrids.

2.2. Soil mechanical parameters

2.2.1. Shear strength

One of the main characteristics of a soil mixture is its shear strength. When a soil is loaded on shear and the load increases, the shear deformation will increase during that process. When the deformation is large enough, eventually, the soil will fail. Shear strength can be explained by different terms and theories. The theory used in this research is that of Coulomb. Coulomb described the maximum shear force using the analogy of a sliding rigid block on a soil slope, arguing that failure would occur if the ratio of the shear force to the normal force became too large. From the force equilibrium, the shear force in the plane is $T = W * sin(alpha)$, and the normal force is $N = W * cos(alpha)$. The ratio of shear is $T/N = tan(alpha)$. As long as this ratio remains under the critical value, there will be no shearing. If alpha becomes larger than the critical value, there will be no equilibrium and the block will slide down the slope (Verruijt, 2010).

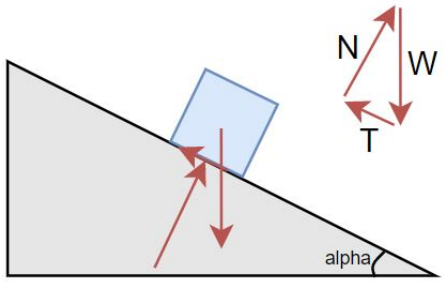

Figure 2.2: Sliding block, Coulomb

From this analogy, Coulomb proposed an equation for the critical shear stress, shown in equation 2.1. If the shear stress is smaller than this value, the deformations in this plane will be limited. If the shear stress reaches this value, the deformations are unlimited. This research exclusively pertains to submerged environments, i.e. only fully saturated soils. Thus, the effective parameters should be used in the shear calculations. It is assumed that only cohesive soils show cohesive strength. Cohesion will be denoted as c. σ' is the effective normal pressure on the shear plane, and ϕ is the internal friction angle. The effective pressure is the total pressure minus the water pressure in the soil (Verruijt, 2010). Further interpretation of these parameters will be provided in the following sections.

$$\tau_f = c + \sigma' tan(\phi) \tag{2.1}$$

Where:

τ_f	Shear strength [kPa]
c	Cohesion [kPa]
σ'	Effective stress[kPa]
ϕ	Internal friction angle [°]

The internal friction angle
When a soil is loaded on shear, the limit is determined by the ratio of the shear force to the normal force. The internal friction angle is the limit ratio of internal soil failure, also called soil-soil shearing interaction. This internal friction angle usually varies from $\phi = 30°$ to $\phi = 45°$ for granular soils, depending on the type of sand and its packing. Round particles have smaller friction angles than granular soils with many sharp angles. Also, compact soils have larger friction angles than loose soils. The internal friction angles can be determined with the help of the table below (Miedema, 2019). Figure 2.3 also could be used for this relation (Schmertmann, 1978).

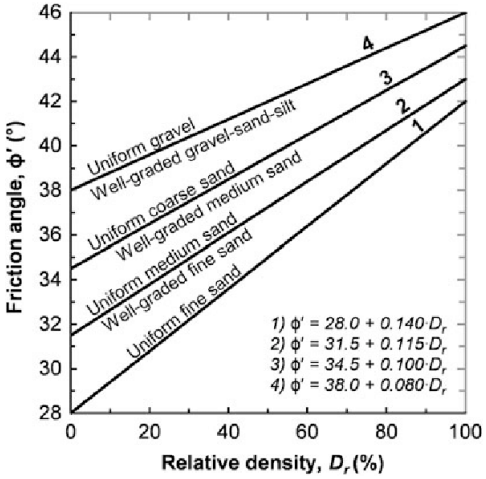

Figure 2.3: Internal friciton angle as a function of relative density (Schmertmann, 1978)

Density of sand	Relative density	ϕ[degree]
Very loose	0-20	<30
Loose	20-40	30-35
Medium	40-70	35-40
Dense	70-85	40-45
Very dense	85-100	>45

Table 2.1: Relationship between ϕ and relative density (From Meyerhof 1956, Foundation Engineering Handbook and Lambe and Whitman, 1969 combined).

The external friction angle
The external friction angle is a way to describe the friction between a soil mixture and another material, such as a track of a trencher. The external friction angle is mostly given as a percentage of the internal friction angle. For smooth surfaces, the external friction angle can be estimated as $\frac{1}{3}\phi$. For rough surfaces, the external friction angle can be estimated as $\frac{2}{3}\phi$. When there is a lack of information, the assumption of $\frac{2}{3}\phi$ is generally made (Miedema, 2019). For the tracks of the trencher the same assumption is made.

Cohesion
Cohesion could be described by two definitions. One definition is: ”the cohesive force that takes place between adjacent particles.” The other definition is: ”the shear strength when the compressing stresses

are equal to zero." In other words, cohesion is the force that keeps the mixture particles together. In this research, granular soils are assumed to show no cohesion. For cohesive soils, on the other hand, it will be a governing parameter. The cohesion of a soil can be examined in the laboratory using a Direct shear test (Verruijt, 2010).

Adhesion

Adhesion is the tendency of soil particles to stick to any other material, such as steel or concrete. Adhesion can be expressed as an adhesion factor times the cohesion of the soil, as shown in equation 2.2 (Miedema, 2019).

$$a = \alpha * c \tag{2.2}$$

Where:

α	Adhesion factor
a	Adhesion [kPa]

Little is known about the exact values of the adhesion factor (Miedema, 2019). Therefore, the relationship depicted in Figure 2.4 is used in this study (Chen et al., 2019).

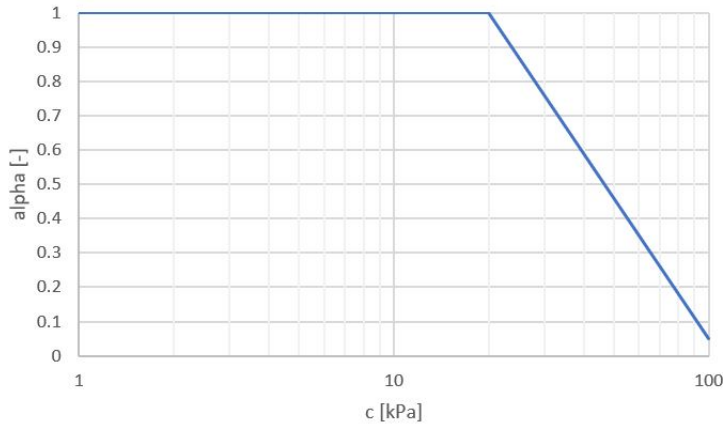

Figure 2.4: Cohesion versus adhesion (after Chen et al., 2019)

However, adhesive factors also have been determined for pile foundations. These results are shown in the figure below (Cherubini and Vessia, 2008). Here it can clearly be seen that the factor drops less, not lower than 0.2, than in the case of Chen. This will result in higher adhesive forces than with Chen's relation. Since the pile foundation is something different from the traction of a trencher, the relation of Chen is used in this research.

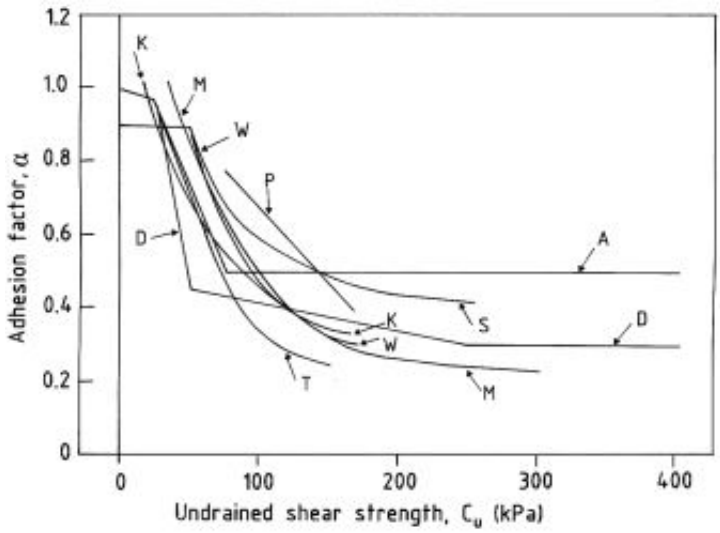

Figure 2.5: Trends of the adhesion factor recommended by various authors: K = Kerisel 1965, T = Tomlinson 1957, W = Woodward and Boitano 1961, P = Peck 1958, D = Dennis and Olson 1983, A = API 1974, S = Sowers and Sowers 1970, M = McCarthy 1977 (adapted from Sladen 1992) (Cherubini and Vessia, 2008)

Undrained Shear strength

The undrained shear strength is the peak shearing resistance at a constant volume, i.e. without any changes to the water volume (undrained situation). The undrained shear strength is defined by the Tresca theory, based on Mohr's circle and shown in equation 2.4. Mohr's circle will be discussed in a later section. In undrained situations, an increase of the cell pressure can be expected to result in an increment of the pore pressures by the same amount as the increment of the cell pressure. So, the increase in stress will cause no change in the effective stress, as shown in equation 2.3. When the same soil is loaded with two different total stresses, the effective stresses will be the same, where, for both cases, the shear strength will also be identical. This is shown in Figure 2.6. The critical circles for the total stresses are shown as dotted circles, while the critical circle for effective stress is shown as a solid circle. It can be noted that the solid circle overlaps for both situations. Therefore, when the soil is undrained, the shear strength will be the same for every total pressure. This strength is the undrained shear strength, leading to the conclusion that, in undrained situations, the critical shear strength is independent of the internal friction angle (Verruijt, 2010).

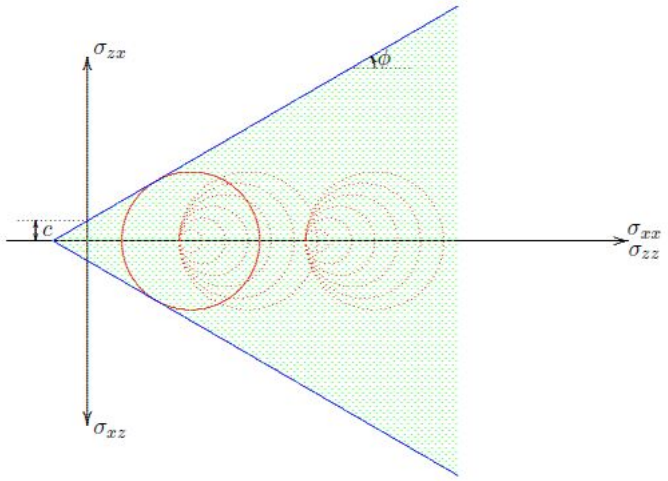

Figure 2.6: Mohr circles for undrained tests (Verruijt, 2010)

$$\sigma' = \sigma_{total} - \sigma_{pore} \tag{2.3}$$

Where:

σ'	Effective pressure [kPa]
σ_{total}	Total pressure [kpa]
σ_{pore}	Total pressure [kpa]

$$\sigma_1' - \sigma_3' = 2 \cdot S_u \tag{2.4}$$

Where:

σ_1'	Principal stress 1 [kPa]
σ_3'	Principal stress 3 [kPa]
S_u	Undrained shear strength [kpa]

$$(\sigma_1' - \sigma_3')/2 = \tau_{f,max}(\text{if:}\phi = 0) = S_u \tag{2.5}$$

The consistency of cohesive material in terms of undrained shear strength is shown in the table below (based on Terzaghi et al., 1996).

Very soft	<12.5 kPa
Soft	12.5-25 kPa
Medium	25-50 kPa
Stiff	50-100 kPa
Very stiff	100-200 kPa
Hard	>200 kPa

Table 2.2: Consistency of cohesive material in terms of undrained shear strength

Residual shear strength

The residual strength of a cohesive soil mixture is the amount of shear strength of the soil after having been fully remolded by the shear displacement (Mitchell and Soga, 2005). The residual shear strength is assumed to be lower than the peak shear strength. The residual shear strength for granular soils is the shear strength when the pore volumes are at the critical state.

Sensitivity

The sensitivity is the ratio of the decrease in shear strength due to the remolding of the soil mixture. It can be calculated using equation 2.6 (Mitchell and Soga, 2005). In the table below the a classification of the sensitivity parameters are given. Sensitivity of two to four is common under normally consolidated cohesive soils (Abuhajar et al., 2010). If the sensitivity is not known a value of four will be used in this research.

$$S_t = \frac{S_u}{S_{u,res}} \tag{2.6}$$

Where:

S_t	Sensitivity [-]
$S_{u,res}$	Residual undrained shear strength [kpa]

Insensitive	1
Slightly sensitive	1-2
Medium sensitive	2-4
Very sensitive	4-8
Slightly quick	8-16
Medium quick	16-32
Very quick	32-64
Extra quick	>64

Table 2.3: Classification of Clay Sensitivity Values (Rosenqvist, 1952)

Stress-strain relation

The stress-strain relation shows the shear strength as a function of the shear strain of the soil. The stress-strain relation is different for every type of soil but can be compared to one of the three basic graphs shown in Figure 2.7. All three different graphs can be brought back to a peak shear strength and a residual shear strength. The $\tau_{f,max}$ can be calculated using Coulomb's formula. In cohesive soils, the peak shear strength and the residual shear strength can be distinguished.

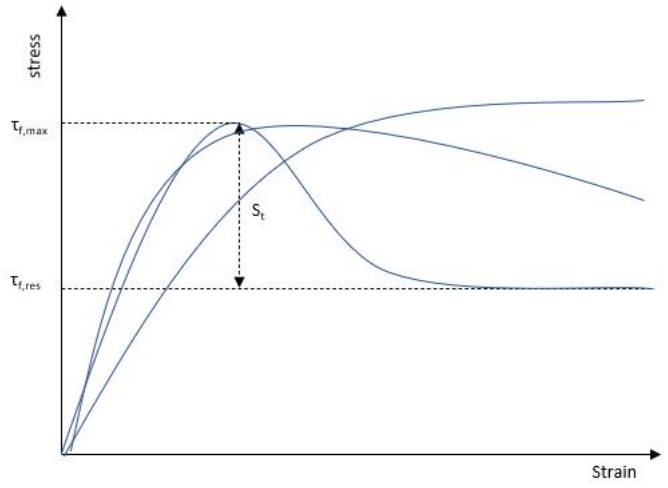

Figure 2.7: Example of a stress-strain curve

In granular soils this works differently: here, the residual state is called the critical state, which, for a particular granular soil, will shear in the same packing. The porosity of that packing is called the critical state porosity. If the packing of a granular soil is denser than the critical state, the shear-strain graph will contain a peak shear strength and afterwards a residual strength shear strength in the critical state. The peak shear strength is caused by water under pressure created by dilatancy. If the granular soil is less dense, the soil will become denser to shear, and therefore there will be overpressure due to contractancy, which causes the shear strength to decrease before the critical state is met (Verruijt, 2010). These processes are shown in figure 2.8. Dilatancy and contractancy will be further elaborated upon in a later section. The critical shear parameter can be determined through the stress-strain graph using equation 2.7 (Mitchell and Soga, 2005).

$$\phi'_{cs} = \arctan(\tau_{cs}/(\sigma'_n)_f) \tag{2.7}$$

Where:

ϕ'_{cs}	Critical state internal friction angle [degree]
τ_{cs}	Critical state shear strength [kpa]
$\sigma'_n)_f$	Effective pressure at critical state [kpa]

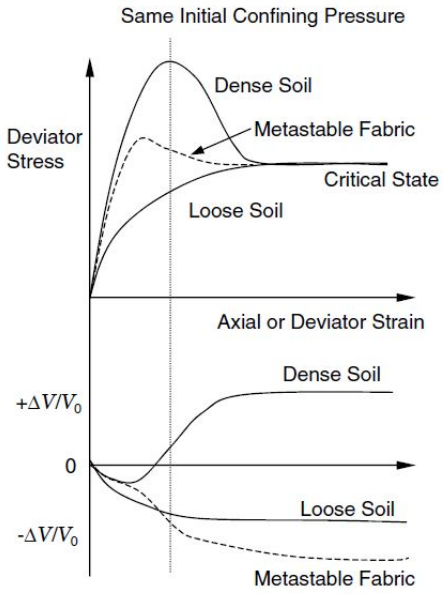

Figure 2.8: Volume and pore pressure changes during shear, drained conditions (Mitchell and Soga, 2005)

Slip ratio

The slip ratio is the ratio of displacement of the track by shear to the place under the tracked vehicle. It can be assumed that shear displacement gradually increases with the length of the tracks, as shown in Figure 2.9. Therefore the slip ratio is constant over the entire track (Wang et al., 2016).

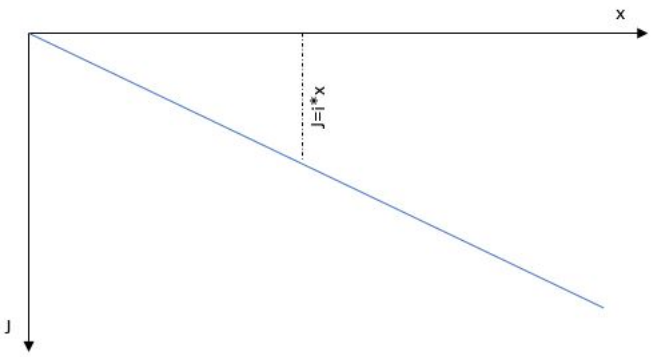

Figure 2.9: Shear displacement development under tracks

Slip ratio is a parameter that is closely related to the soil parameters. The slip ratio can be calculated in two different ways. One way is by using the shear displacement at a certain position under the track. With the help of equation 2.8, the slip ratio can be calculated. The other method is by measuring the speed of the tracks and comparing it to the actual vehicle speed, using equation 2.9. This research uses equation 2.8 since it links soil parameters to track displacement. Equation 2.9 is a good tool to measure the slip during operations (Wong, 2010). The usual range of the slip ratio is between zero and 0.8 (Wang et al., 2016). It is preferable to maintain the slip ratio below 0.2 for off-road tracked vehicles (Wong, 2001). Therefore a slip ratio of 0.2 is used as a common basis to compare the performance (Baek et al., 2020).

$$i = \frac{X}{j} \tag{2.8}$$

Where:

i	Slip ratio [-]
X	Distance from start of track [m]
j	Shear displacement [m]

$$i = 1 - \frac{V}{V'} \tag{2.9}$$

Where:

V	Actual progression speed vehicle[m/s]
V'	Progression speed track [m/s]

Three parameters directly influence each other, so the relationship between them must be known. These parameters are sensitivity, slip displacement for the residual shear strength and slip ratio. Sensitivity indicates the loss of strength of the soil. Slip displacement for the residual shear strength indicates how much the soil must move before it reaches the residual shear strength. Slip ratio, in combination with the length of a single element, indicates how fast the displacement is caused in relation to the track. Through equation 2.10, it can be determined at which track element the residual shear strength comes into play. In order to properly assess the influence of individual phenomena, it is important to include this relationship.

$$N_{element,res} = \frac{j_{residual}}{L_{element} * i} \tag{2.10}$$

Where:

$N_{element,res}$	Number element residual shear strength [-]
$j_{residual}$	slip displacement before residual shear strength [m]

2.2.2. Mass Volume relations

Density

The density of the soil is determined by the ratio of the mass and volume of the soil mixture. This density is also called the in-situ density. The in-situ density is calculated based on the total mass volume of the mixture, including solids, liquids and gas. In submerged environments, the mass of the gas can be assumed to be zero. A subsea tracked trencher only operates in submerged environments, and therefore the in-situ density can be calculated using equation 2.11.

$$\rho_t = \rho_w * \eta_i + (1 - \eta_i)\rho_s \tag{2.11}$$

Where:

ρ_t	In-situ density [kg/m^3]
ρ_w	Water density [kg/m^3]
η_i	Initial porosity [-]
ρ_s	Specific density [kg/m^3]

The submerged - or effective - density is the density of the mixture minus the density of any liquid it contains. In hydraulic engineering, that liquid is usually water. Equation 2.12 is used to calculate the effective density.

$$\rho' = \rho_t - \rho_w \tag{2.12}$$

Where:

ρ'	Effective density [kg/m^3]

Closely related to density is the unit of weight. The unit of weight is the weight of the mixture divided by the volume, as shown in equation 2.13 (Miedema, 2019). For granular soils a submerged unit weight of 8.0 kN/m^3 is assumed and for cohesive soils it is 6.5 kN/m^3 (Mitchell and Soga, 2005).

$$\gamma' = \rho' * g \tag{2.13}$$

Where:

γ'	Effective unit weight [kN/m^3]

Porosity
Porosity is the ratio of the pore volume of the mixture to the total volume of the soil mixture. Porosity can be calculated using equation 2.14.

$$\eta = \frac{V_v}{V_t} \tag{2.14}$$

Where:

V_v	Voids Volume [m^3]
V_t	Mixture Volume [m^3]

Void ratio
Void ratio is the ratio of pore volume to the volume of solids in the soil mixture. It can be calculated through equation 2.15.

$$e = \frac{V_v}{V_s} \tag{2.15}$$

Where:

e	Void ratio [-]
V_s	Solids Volume [m^3]

Porosity and void ratio are directly linked with the following equations. Porosity cannot be smaller than zero or larger than one; the void ratio can be greater than one.

$$e = \frac{\eta}{1-\eta}; \eta = \frac{e}{1+e} \tag{2.16}$$

Relative density
Relative density is also closely connected to the void ratio and porosity. Formula 2.17 shows the correlation between the parameters. Relative density is an index that shows the state of compactness of granular soils and can be used to estimate the internal friction angle.

$$RD = \frac{e_{max} - \epsilon}{e_{max} - e_{min}} \tag{2.17}$$

Where:

e_{max}	Maximum void ratio [-]
e_{min}	Minimum void ratio [-]

It is assumed, in this research, that the minimum void ratio is 0.35 and the maximum is 0.9. These are the theoretical maximum and minimum void ratios for soils with uniform and perfectly round particles (M. Takechi, C. Uno, 1994).

Dilatancy
When a granular soil is shearing, there could be an increase in volume. This happens when a soil is densely packed, i.e. when the soil mixture is denser than the critical state of the soil. If a densely packed granular soil is loaded on shearing, the only way the particles can move is by rolling over each other. During that process, pore volume will increase. This increase in pore volume will cause an underpressure in the mixture, which could introduce an additional force that keeps the particles

together and increases the soil's shear strength. This process is more likely to occur in less permeable soils. Figure 2.11 shows the densely packed soil particles. Figure 2.10 shows the composition of a loosely packed soil (Verruijt, 2010).

Figure 2.10: Densely packed

Figure 2.11: Loosely packed

As mentioned earlier, the additional pore volume must be filled with water in saturated soils. However, if the water supply is not instant, this will lead to water underpressure. This underpressure causes an increase in effective stress, making the soil stronger until the shear layer is fully filled with water (Verruijt, 2010). This increase is sometimes called apparent cohesion, but to call it cohesion would be a misconception. The increase in volume can be calculated using equation 2.18 (Miedema, 2019). The critical state void ratio depends on the effective vertical stress and the content of the soil specimen. Therefore in reality each soil will fail in another critical state. For this research a constant critical void ratio is chosen, with the help of this constant value the influence of dilatancy and contractancy can be determined. However, the real impact of these processes, dilatancy and contractancy, will require a soil specimen investigation and is different for each project. Figure 2.12, shows multiple critical state lines in terms of void ratio and effective normal stresses, for quartz silty sand particles with different uniformity coefficients (Papadopoulou and Tika, 2008). The critical void ratio varies between 0.8 and 0.4, which is a large spectrum. In order to give a clear view of the dilatancy or contractancy influence the assumed critical void ratio in this research is chosen at a relative density of 50%. This will correspond to a critical void ratio of 0.63 and a critical state porosity of 0.39.

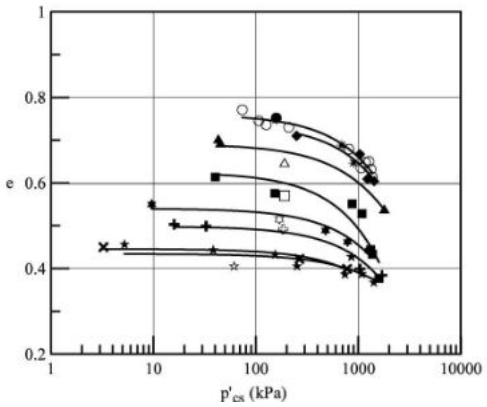

Figure 2.12: Critical state lines of sand-silt mixtures in terms of void ratio,e (Papadopoulou and Tika, 2008)

$$\epsilon = \frac{dV}{V} = \frac{\eta_{cv} - \eta_i}{1 - \eta_{cv}} = \frac{\delta\eta}{1 - \eta_{cv}} \tag{2.18}$$

Where:

ϵ	Dilatancy [-]
η_{cs}	Critical porosity [-]
η_i	Initial porosity [-]

Contractancy

The opposite of dilatancy is contractancy. It means that the initial pore volume is larger than the critical-state pore volume. Thus, when the soil is loaded on shear, it should be contracted in order to create the shear layer, leading to a smaller pore volume. In submerged soils, this means that the water needs

to flow out of the soil mixture. If the water outflow is not quick enough, water overpressure will develop. This overpressure causes a decrease in the shear strength of the soil (Al-Karni, 2011). The decrease in pore volume can be calculated using the same equation that reflects pore increase, i.e. equation 2.18.

Permeability
The permeability of the soil is the ease with which a fluid can flow through a soil medium. Soil permeability is influenced by the packing, shape and sorting of the granular materials. Only granular soils will exhibit permeability, as cohesive soils are assumed to be impermeable. In this research, the Kozeny-Carman equation is used to determine permeability, as expressed in the Kozeny-Carman equation 2.19 from 1956. For this relationship to exist, there must be laminar flow and the soil particles can be no larger than 3 mm (Carman, 1956).

$$\mathrm{k} = 8.3 \cdot 10^{-3} \cdot \frac{\mathrm{g}}{\mathrm{v}_1} \cdot \frac{\eta^3}{(1-\eta)^2} \cdot \mathrm{d}_{10}^2 \tag{2.19}$$

Where:

v_1	Kinematic viscosity $[m^2/s]$
d_{10}	Effective particle size[mm]

2.3. Failure basics

In this section, three failure mechanisms will be discussed: the Mohr-Coulomb failure criterion; the passive soil failure of Rankine; and, finally, the shallow foundation bearing capacity. All three theories represent fundamental failure modes and will be assessed in relation to the mobility problem of the tracked vehicles under study.

2.3.1. Mohr-Coulomb failure criterion

Mohr's circle is a graphical way of solving the shear stresses in different planes present in the soil. In the derivation of Mohr's circle, there are two perpendicular principal stresses: σ_1 and σ_3. These two stresses work in a plane, with any orientation, where no shear stresses work. In order to set up Mohr's circle, it is key to express the applied pressures into the principal stresses. This can be done with the help of equilibrium of forces and is shown in the figures below.

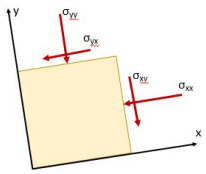

Figure 2.13: Applied stresses

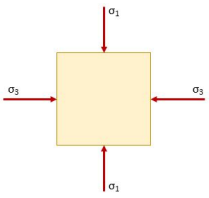

Figure 2.14: Principal stresses

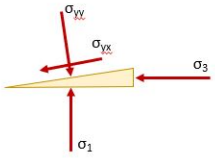

Figure 2.15: Slice one

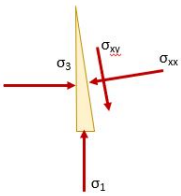

Figure 2.16: Slice two

Equation 2.20 is the force equilibrium in the x direction, for Figure 2.16. Equation 2.21 represents the equilibrium in the y direction.

$$\sigma'_{xx} = \sigma'_1 \sin^2 \alpha + \sigma'_3 \cos^2 \alpha \tag{2.20}$$

Where:

σ'_{xx}	Applied normal effective stress in the x direction[kPa]
σ'_1	Effective principal stress 1 [kPa]
σ'_3	Effective principal stress 3 [kPa]
α	Angle of considered plane [°]

$$\sigma'_{xy} = \sigma'_1 \sin \alpha \cos \alpha - \sigma'_3 \sin \alpha \cos \alpha \tag{2.21}$$

Where:

σ'_{xy} | Applied shear stress[kPa]

The other two stresses can be calculated using the force equilibrium in figure 2.15. Equation 2.22 and equation 2.23 are the equilibrium equations for this soil cut. From equations 2.21 and 2.23 it can be concluded that $\sigma'_{xy} = \sigma'_{yx}$.

$$\sigma'_{yy} = \sigma'_1 \cos^2 \alpha + \sigma'_3 \sin^2 \alpha \tag{2.22}$$

Where:

σ'_{yy} | Applied normal effective stress in y direction[kPa]

$$\sigma'_{yx} = \sigma'_1 \sin \alpha \cos \alpha - \sigma'_3 \sin \alpha \cos \alpha \tag{2.23}$$

Where:

σ'_{yx} | Applied effective shear stress[kPa]

The basic trigonometric formulas 2.24 and 2.25 will be used in equations 2.20 and 2.22 and 2.21.

$$\cos 2\alpha = 1 - 2 \sin^2 \alpha \tag{2.24}$$

$$\sin 2\alpha = 2 \sin \alpha \cos \alpha \tag{2.25}$$

Equation 2.26 till equation 2.28 are the formulas for the stresses, including the trigonometric formulas.

$$\sigma'_{xx} = \frac{1}{2}\left(\sigma'_1 + \sigma'_3\right) - \frac{1}{2}\left(\sigma'_1 - \sigma'_3\right) \cos 2\alpha \tag{2.26}$$

$$\sigma'_{yy} = \frac{1}{2}\left(\sigma'_1 + \sigma'_3\right) + \frac{1}{2}\left(\sigma'_1 - \sigma'_3\right) \cos 2\alpha \tag{2.27}$$

$$\sigma'_{xy} = \sigma'_{yx} = \frac{1}{2}\left(\sigma'_1 - \sigma'_3\right) \sin 2\alpha \tag{2.28}$$

When equations 2.26 and 2.28 are squared and added up, this will give equation 2.29.

$$\left(\sigma'_{xx} - (\frac{\sigma'_1 + \sigma'_3}{2})\right)^2 + \sigma'^2_{xy} = \left(\frac{\sigma'_1 - \sigma'_3}{2}\right)^2 \cdot (\sin^2(2 \cdot \alpha) + \cos^2(2 \cdot \alpha)) \tag{2.29}$$

Equation 2.29 can be simplified to a circle equation 2.30. With the help of this equation, the stresses in every angle in the soil can be calculated.

$$\left(\sigma'_{xx} - \left(\frac{\sigma'_1 + \sigma'_3}{2}\right)\right)^2 + \sigma'^2_{xy} = \left(\frac{\sigma'_1 - \sigma'_3}{2}\right)^2 \tag{2.30}$$

Since the equation is in the form of a circle, it can also be represented graphically. In equation 2.31, (k,h) is the center of the circle and r is the radius.

$$(x - h)^2 + (y - k)^2 = r^2 \tag{2.31}$$

So for equation 2.30, the center will be located at $(0, \frac{\sigma'_1 + \sigma'_3}{2})$ and the radius will be $\frac{\sigma'_1 - \sigma'_3}{2}$. The x parameter will be σ'_{xx} or σ'_{yy}, and the y value will be σ'_{xy}. The angles in real life will be displayed in the circle with two times the angle.
Figure 2.17 shows an example of a graphical representation of the equation.

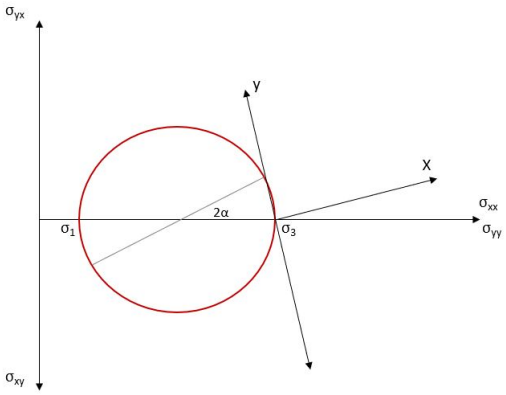

Figure 2.17: Mohr's circle

Every point on Mohr's circle represents a different plane in the soil with its corresponding normal and shear stresses. The angle of the plane under consideration appears as the doubled angle in Mohr's circle. Coulomb's critical shear stress can be integrated into the figure as a failure envelope. With the stresses in every plane and the failure envelope known, it can be checked whether the soil fails and in which angle it will fail. This can be done by determining the different intersections. In this research, it is assumed that the cohesive soils' shear strength does not have an internal friction angle component so the failure envelope will be horizontal. Besides, granular soils do not exhibit cohesive strength, and therefore their failure envelope will intersect the origin. Figure 2.18 shows that cohesive soils will always fail in planes that are $45°$ to the fundamental stresses while granular soils will fail in planes with angles of $45 - \phi/2°$ to the fundamental stresses.

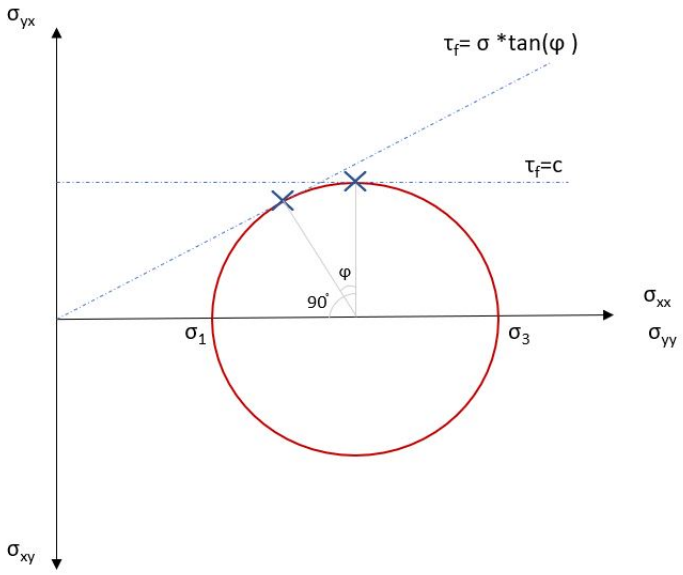

Figure 2.18: Mohr-Coulomb failure criterion

2.3.2. Rankine's passive lateral earth theory

There is a difference between active and passive lateral soil failure. In this study, it is a trencher that applies forces to the soil. This is called passive earth failure. In other words, passive failure takes place when the outside world exerts pressure on the soil. An example of passive soil failure is the pushing of soil by a bulldozer. In order to derive Rankine's passive earth theory, the problem can be simplified to Figure 2.19. The failure stresses and soil strengths can be calculated using a Mohr-Coulomb problem, shown in Figure 2.20, assuming that σ'_{zz} and σ'_{xx} are principal stresses.

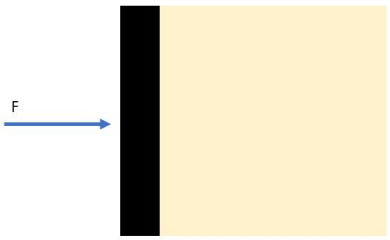

Figure 2.19: Simplified passive Rankine's lateral earth theory

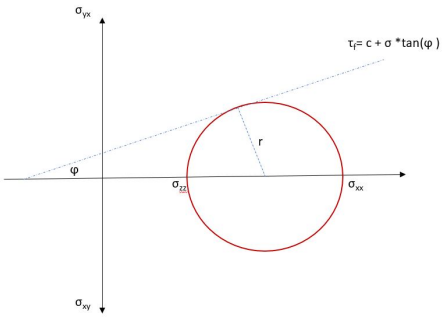

Figure 2.20: Mohr's circle applied to Rankine's theory

It is possible to determine σ'_{zz} by the weight of the soil. The radius for this Mohr circle is $\frac{1}{2}(\sigma'_{xx} - \sigma'_{zz})$, and the distance from the origin to the center is $\frac{1}{2}(\sigma'_{xx} + \sigma'_{zz})$. With that knowledge, equation 2.32 can be drawn up, which can be simplified to formula 2.33.

$$\sin\phi = \frac{\frac{1}{2}(\sigma'_{xx} - \sigma'_{zz})}{\frac{1}{2}(\sigma'_{xx} + \sigma'_{zz}) + c\cot\phi} \tag{2.32}$$

$$\sigma'_{xx} = \frac{1+\sin\phi}{1-\sin\phi}\sigma'_{zz} - 2c\frac{\cos\phi}{1-\sin\phi} \tag{2.33}$$

From that last equation, the passive earth pressure coefficient K_p can be determined, $K_p = \frac{\sigma'_{xx}}{\sigma'_{yy}} = \frac{1+\sin\phi}{1-\sin\phi}$. This coefficient gives the ratio between the horizontal and vertical principal stresses. The vertical stress can be calculated through equation 2.34.

$$\sigma'_{zz} = \gamma' * z \tag{2.34}$$

The equation for the horizontal stress becomes:

$$\sigma'_{xx} = K_p\gamma' z - 2c\sqrt{K_p} \tag{2.35}$$

The horizontal force, F, can be calculated if the height of the wall is known. F is the integration over the depth z from z=0 to z=h. This gives equation 2.36.

$$F = \frac{1}{2}K_p\gamma' h^2 - 2ch\sqrt{K_p} \tag{2.36}$$

2.3.3. Shallow foundation bearing capacity

The bearing capacity is the maximum average contact pressure between the foundation and the soil before shear failure occurs. The tracks of a subsea tracked trencher could be approximated as a shallow foundation. This will be elaborated in another chapter, but the basic theory will be discussed here. A Load is applied to the foundation and, from the foundation, worn out to the soil. If the bearing capacity of the soil is large enough, no shearing will occur. In some cases, there will be large settlements without shear failure. These cases are governed by the maximum settlement, rather than the bearing capacity. Three types of shear failure limit the bearing capacity and are shown in Figure 2.21: general shear failure, local shear failure and punching shear failure. The first method to calculate the bearing capacity was proposed by Terzaghi in 1943. In this research, Meyerhof's method is used. Meyerhof based his method on Terzaghi's but introduces shape coefficients and inclination factors, which makes it more suitable for foundations with eccentric loads (Lambe and Whitman, 1969). The tracks will fail in the plane with the smallest length. In case of the tracks this length will be the width. Meyerhof's equation for vertical loads is shown in equation 2.37 (Meyerhof, 1953).

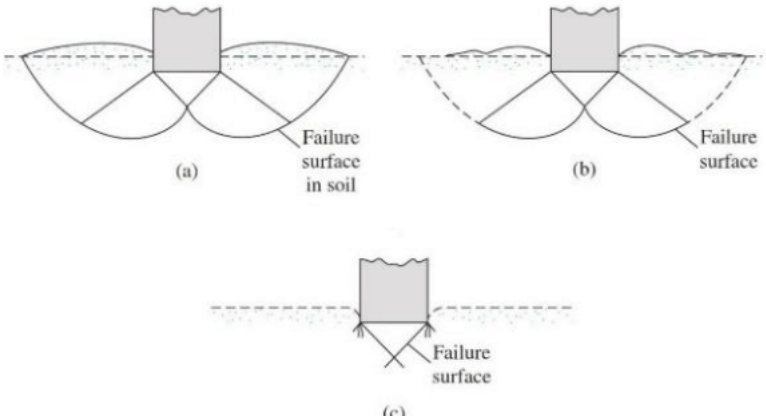

Figure 2.21: a) General Shear Failure, (b) Local Shear Failure. (c) Punching Shear

$$Q_b = cN_c i_c S_c d_c + q_0 \, N_q \, i_q S_q d_q + 0.5\gamma' B' N_\gamma i_\gamma S_\gamma d_\gamma \tag{2.37}$$

Where:

Q_b	Bearing capacity[kPa]
c	Cohesion[kPa]
$N_{c,q,\gamma}$	Bearing capacity factors[-]
$i_{c,q,\gamma}$	Inclination factors[-] (=1 assumed)
$S_{c,q,\gamma}$	Shape factors[-]
$d_{c,q,\gamma}$	Depth factors[-]
q_0	Overburden pressure[kPa]
γ	Soil unit weight [kPa]
B'	Effective width of track [m]

N_c, N_q and N_r are Meyerhof's bearing capacity factors. These factors depend on the internal friction angle, as shown in equations 2.38, 2.39 and 2.40 (Shill and Hoque, 2015).

$$N_q = \tan^2\left(\frac{\pi}{4} + \frac{\phi}{2}\right) \exp(\pi \tan(\phi)) \tag{2.38}$$

$$N_c = \left(N_q - 1\right) \cot\phi \tag{2.39}$$

$$N_\gamma = \left(N_q - 1\right) \tan(1.4\phi) \tag{2.40}$$

S_c, S_q and S_r are Meyerhof's shape factors. These factors depend on the Rankine passive-pressure coefficient, the internal friction angle and the width-to-length ratio, as shown in table 2.4 (Shill and Hoque, 2015).

ϕ	S_γ	S_c	S_q
0	1	$\left(1 + 0.2K_p \frac{B'}{L'}\right)$	1
$> 10°$	$\left(1 + 0.1K_p \frac{B'}{L'}\right)$	$\left(1 + 0.2K_p \frac{B'}{L'}\right)$	$\left(1 + 0.1K_p \frac{B'}{L'}\right)$

Table 2.4: Shape factors

When there is also a moment load on the foundation, the load will be eccentric. This means that the resulting vertical load will not be in the middle of the foundation. The eccentricity parameter, e, is a measure to represent this distance numerical. The eccentricity could work either one or two axis and can be calculated with the help of equation 2.41. To take the eccentricity into account for the bearing-capacity calculations, the effective length and the effective width should be used. Meyerhof proposed the effective width in 1953 to consider the detachment of the foundation due to the overturning moment.

The effective width and length are determined in such a way that the resultant force will be exactly in the middle of the effective area. An example of two-way eccentricity is shown in Figure 2.22 (Feng et al., 2019).

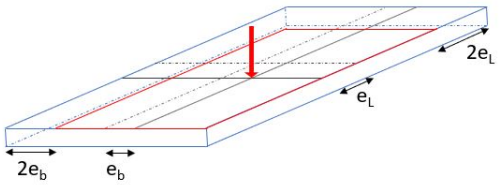

Figure 2.22: Two-way eccentricity

These effective parameters can be calculated using equation 2.42 and 2.43. One important note is that the effective width should always be smaller than the effective length (Feng et al., 2019). Otherwise, failure would change its axes and the effective length become its width in Meyerhof's bearing capacity and vice versa.

$$e = \frac{M}{V} \tag{2.41}$$

Where:

e	Eccentricity parameter[m]
M	Momental force [kNm]
V	Vertical resultant force [kN]

$$L_{eff} = L - 2e_L \tag{2.42}$$

$$B_{eff} = B - 2e_b \tag{2.43}$$

For granular soils, a drained approach is assumed here. In the case of the trencher, however, this is not always the case. In some cases contractancy or dilatancy will occur with an increase or decrease of the shear strength.

2.4. Summary

Using the three theories mentioned in this chapter: the Mohr-coulomb theory, Rankine's passive earth theory and the effective Meyerhof method, the stability of the trencher can be well approximated. However, it must be taken into account that these theories all work in the 2D-plane. This will cause small differences in the end, although most of the load will be brought back to a 2D situation. Another important conclusion is that there are many different soil parameters, several of which influence each other. There are also several processes about which little is known or which will be soil specific. It is important to take these parameters into account in the modelling and to approximate them where possible.

3

Subsea tracked trenchers

After looking at the basic principles in the previous chapter, this chapter seeks to translate these principles to the trencher. The goal of this study is to provide an algorithm to predict the mobility of different subsea tracked trenchers. There are many different trenchers, all with their own specifications and specialties. All three trenchers currently owned by Boskalis are different in terms of weight, height, types of tracks and many more specs. The figures below show the three different trenchers. Since every trencher is different, the algorithm should be easily adjustable to various types of trenchers. In order to achieve this, a simplified model of a general trencher will be used retaining the key parameters for mobility.

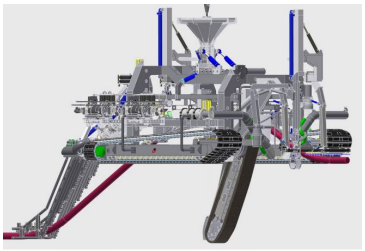

Figure 3.1: CBT2400

Figure 3.2: ROV-Trencher

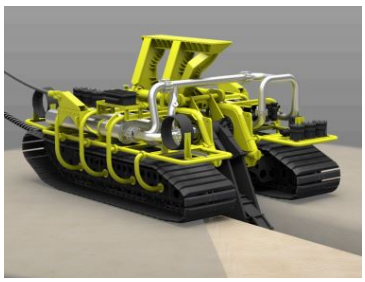

Figure 3.3: Trenchformer

Each trencher can ultimately be reduced to three essential components that influence its mobility: the tracks, the cutting tool and the core vehicle. It is important to understand what these components consist of and how they affect mobility. Once this is clear, the trencher can be simplified. The purpose of this is to be able to use the model for a wide variety of trenchers and other tracked vehicles, but also to make the model precise enough to give an exact representation of reality

3.1. Tracks

The tracks of the trencher are the contact points of the trencher with the soil and therefore have a great impact on mobility. The tracks of Boskalis' trenchers are shown in the figures below.

Figure 3.4: CBT2400 - Tracks

Figure 3.5: ROV-Trencher - Tracks

Figure 3.6: Trenchformer - Tracks

Firstly, the tracks can be divided into two major groups: flexible track belts and rigid track belts. Flexible tracks are often made of rubber and are, as the name suggests, flexible rather than rigid. The belt is often made out of one piece. This type of track is shown in figure 3.5. Benefits of the flexible tracks include less expected wear and lower weight. Figure 3.7 shows a simplified version of a system with a flexible track belt (Wong, 2001).

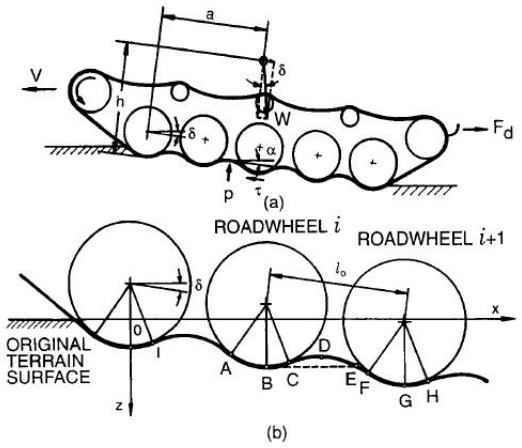

Figure 3.7: Geometry of a flexible track system in contact with a deformable terrain (Wong, 2001).

The other group of tracks are the rigid belt tracks. The belt consists of rigid links in the form of a steel chain connected with pins. On the outside of a chain link, a track shoe is attached. The rigid belt tracks are for low-speed tracked vehicles, like the trenchformer and CBT, see Figures 3.6 and 3.4. An advantage of the rigid links is that they cause the ground pressure to be evenly distributed. Figure 3.8 presents a schematic view of a rigid-track system (Wong, 2001).

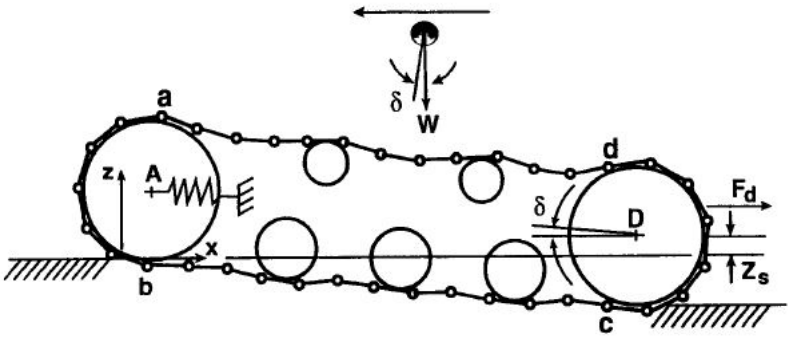

Figure 3.8: A schematic of a track system with long-pitch rigid links (Wong, 2001)

Both tracks consist of the same components for the most part. Important parts found in both types are:

- Sprockets
- Roadwheels
- Vehicle frame
- Supporting rollers
- Idlers

The track belt is the largest difference between the two sorts of tracks. Two components of the tracks directly influence the mobility of the trencher: The track's roadwheels influence the pressure distribution to the soil (Wong, 2001). Besides, the track shoe influences the shearing mechanism under the tracks and thus the traction.

As said before, the roadwheel rollers influence the pressure distribution under the tracks. Wong researched the influence of the number of rollers, their size and their spacing, as shown in Figure 3.9. The main conclusion from this study is that, with an increase in rollers and a decrease in distance and size, the pressure under the tracks is more evenly distributed (Wong, 2001).

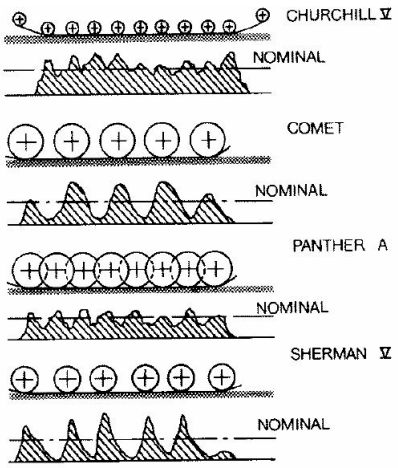

Figure 3.9: Measured normal pressure distributions 23 cm below the soil surface for various tracked vehicles (Wong, 2001)

The form of track belt is another important factor for the mobility of the trencher. The track belt's form can again be divided into two categories: belts equipped with grousers or flat belts. Flat belts consist of a chain with mounted plastic or steel pads. The pads are flat and without cut-outs for extra grip, resembling the Trenchformer's, shown in Figure 3.6. The important traction force is created by adhesion in cohesive soils and friction in granular soils, also called track-soil shearing interaction. The track belt with grousers is intended to cause shear planes in the soil under the trencher, which causes soil-soil shear interaction. Tracks with grousers exist in many forms but differ from the flat belt by the vertical cutouts, visible in Figures 3.4 and 3.5. The traction of track belts with grousers is influenced by soil-soil interaction and track-soil shearing interaction. Figures 3.10 and 3.11 show a schematic representation of the two different types of track belt.

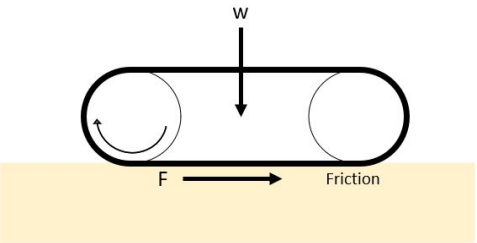

Figure 3.10: Flat track belt

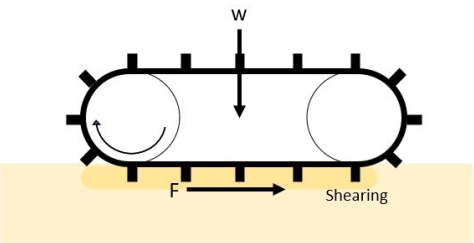

Figure 3.11: Grouser track belt

The size and the area of the grousers are a major influence on traction. The track shoes can be single-grouser shoes but also multi-grouser shoes. Besides the kind of tracks, the contact area is very important. This, of course, mostly depends on the length and width of each track.

The tracks are simplified to a track system where yhe pressure under the tracks will be uniform. This means that the roadwheel rollers themselves and the spacing between them will be small. The track belt can be equipped with track shoes with or without grousers.

3.2. Cutting tool

The main function of a subsea tracked trencher is to dig trenches to bury cables and pipes. To dig the trenches, two different cutting tools can be used: a jetting sword and a chain cutter. The two different tools are shown in the figures below.

Figure 3.12: CBT 2400 - Chain cutter

Figure 3.13: CBT 2400 - Jet sword

It is beyond the scope of this research to go deeper into the mechanics of the cutter tools. Note, however, that the cutting tools have a major influence on mobility. During the cutting process, a large horizontal force is created, which works in the opposite direction of the driving direction. This is one of the larger forces that the tracks have to overcome to drive forward. The force on the cutting tool can change with cutting depth, soil conditions and progress speed. Generally the forces on jet swords are limited in sand. In clay, however, these swords act like knives, whereby both the horizontal and vertical forces can increase significantly. Besides, cutting tools can be heavy, which should also be taken into account. The placing of the cutting tool is also of importance, since the tool is quite large and can change position in different setups and at different trench depths. Therefore, the forces working on and the placement of the cutting tool will be simplified to a 3-dimensional placing and resultant forces.

3.3. Core vehicle

The core vehicle of the trenchers has many important functions. For the mobility of the trencher, two features are particularly important: first of all, the weight and center of gravity. Since weight is one of the largest force components, it is important to take it into account as precisely as possible. Besides the weight, the overall dimensions are also important. In open waters, currents can occur, potentially

causing a force in all directions. Therefore, the frontal surface area is important, as well as the surface areas on the other sides. Since the surface areas are not fully covered, a drag coefficient should also be included for the core vehicle.

3.4. Simplified vehicle

The model should be applicable to a wide variety of trenchers. Therefore, the sample trencher should be simplified without losing the key characteristics that impact its mobility. Figure 3.14 presents a side view of the simplified vehicle, while a front view is provided in Figure 3.15. Besides the fact that all length and width dimensions can be adjusted in the 3-axle system, the core vehicle will have a water drag coefficient of CD. The tracks can be divided into several elements. One element runs from one grouser to the next. The track's grousers are also simplified to a straight block with a height and a length. Here it is important that the shearing surfaces remain the same as far as possible.

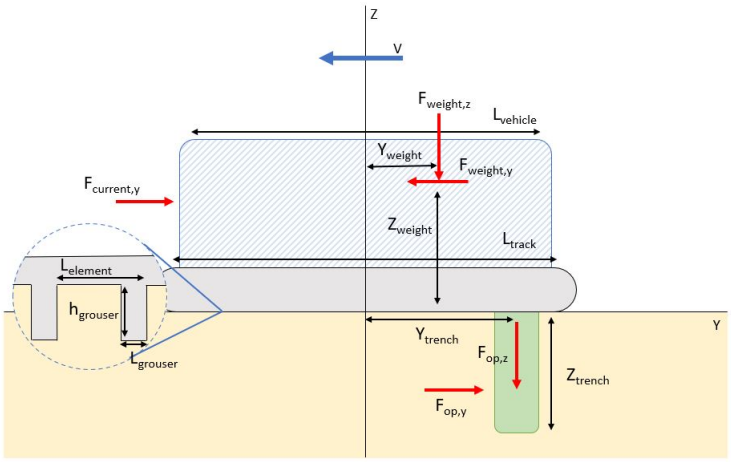

Figure 3.14: Side-view of simplified trencher

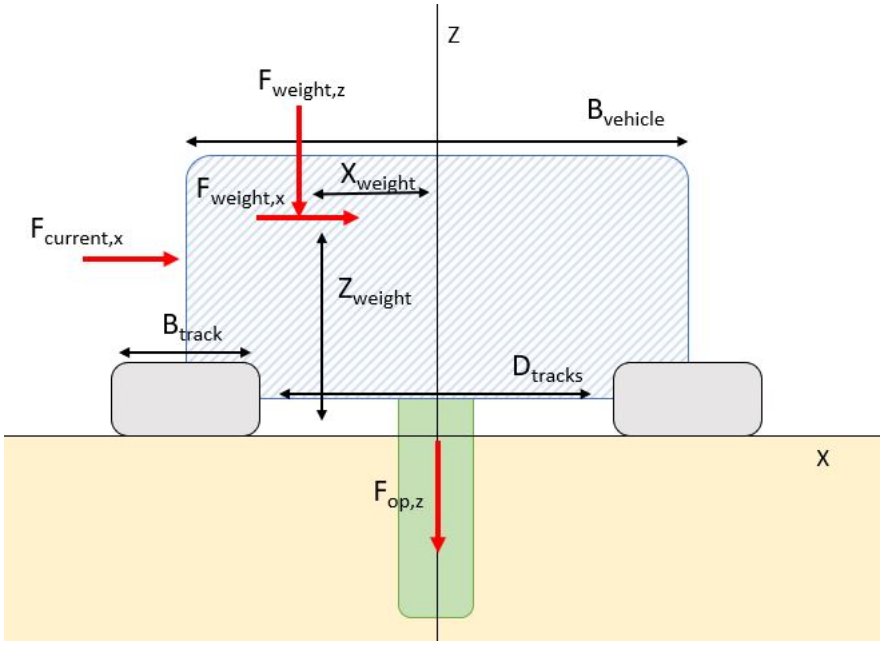

Figure 3.15: Front-view of simplified trencher

3.5. Summary

A trencher can always be reduced to three standard components: the core vehicle, the cutting tools and the track. Of these three components, the track is the most important for the interaction with the soil. However, the shape, dimensions and material can vary from track to track. Therefore, these will have to be simplified. The core vehicle should be simplified to a block with certain dimensions, a certain weight and a certain drag coefficient. Finally, the forces on the cutting tools will be used as input values for this research. In addition, the cutting tools will also be given a certain distance to the centre of the tracks.

4

Mobility of trencher

In the previous chapter, the simplification of the trencher was discussed. The first part of this chapter discusses which external factors are influential and how. In addition, the concept of mobility will be further explained, and, finally, vertical stability will be discussed. Mobility is considered from two points of view: on the one hand it concerns the circumstances in which the trencher should operate. The other point of view takes a soil perspective: when is the soil stable/strong enough and when is it not? Figure 4.1, shows the trencher's mobility scheme used in this research, based on the evaluation of terrain-vehicle systems described by Sohne (1976). First, trenching operations will be discussed, and subsequently soil strength and stability will be explored.

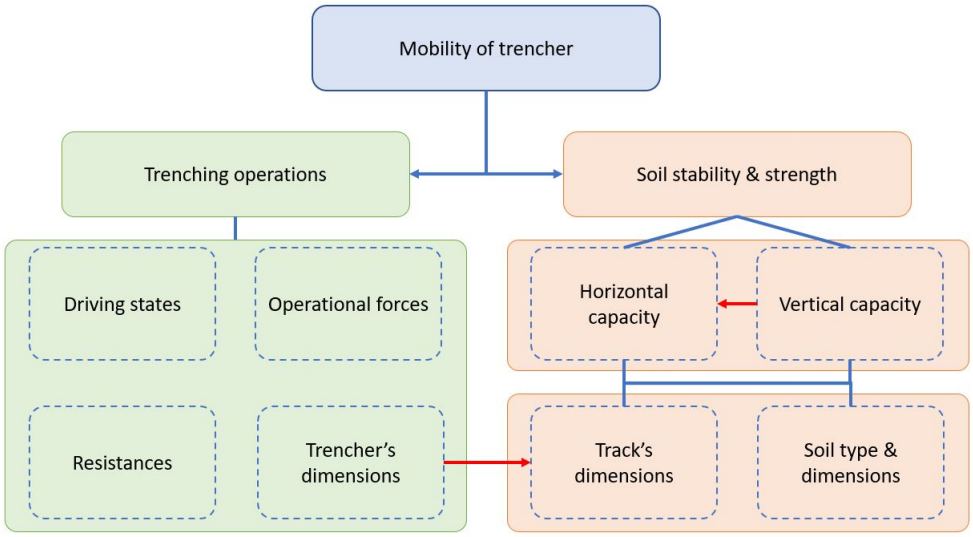

Figure 4.1: Mobility scheme

4.1. Trenching operations

4.1.1. Driving states

The trencher will have to be able to operate in different driving states, one of which is the resting state. This state is initially when the trencher has just been placed before trenching. This state is always important to check, since the trencher must always be able to fall back to this state. During this state, no cutting force will act on the jet sword or cutter. This state is thus governed by the gravitational forces. Therefore, it is important to take into account the vertical balance. However, due to the influence of a slope in the sea bottom, there can also be a horizontal force. In this state, the most important factors become bearing capacity, sinkage and ground pressure.

Another important state is the driving state. In this state the cutting forces should be included. The cutting forces are an important horizontal force that must be overcome by the traction. Note for now that this is not the only force acting on the trencher, which will be elaborated on later. In this state, both the vertical and the horizontal balances should be checked since the surroundings will determine which of the two is governing.

Besides the driving and resting state, roll and pitch play a important role in the mobility of the trencher. Pitch will be a slope over the y-axis, and roll is a slope over the x-axis, shown in Figures 4.2 and 4.3. Pitch and roll will cause a redistribution of the forces. In the mobility model, the axes will be based on the vehicle, meaning that the axes will change with changing pitch and rolls. Therefore the forces and momentum will be divided into components along the driving direction and perpendicular to the driving direction.

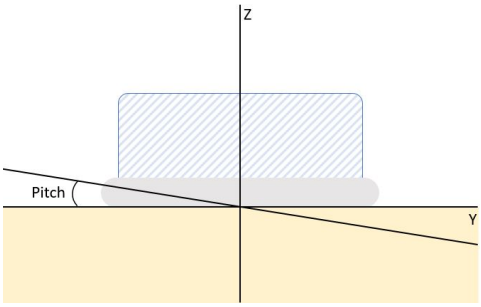

Figure 4.2: Pitch

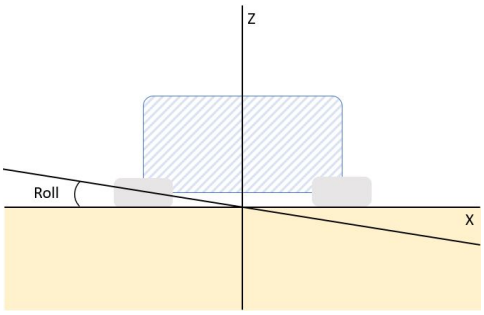

Figure 4.3: Roll

4.1.2. Trencher's dimensions

Most of the trenchers's dimensions are discussed in the earlier section of this paper. The most important dimensions are the length and width of the tracks since they make up the surface area. The length and the height of the grousers are important since they influence the shearing areas. The length of each element in the track belt is important since it determines the number of elements in each track and thus the number of shearing areas. The simplified track element is shown in Figure 4.4. The weight and center of gravity are important since they influence almost every process regarding mobility. Lastly the placement of the cutting and/or jetting sword is important.

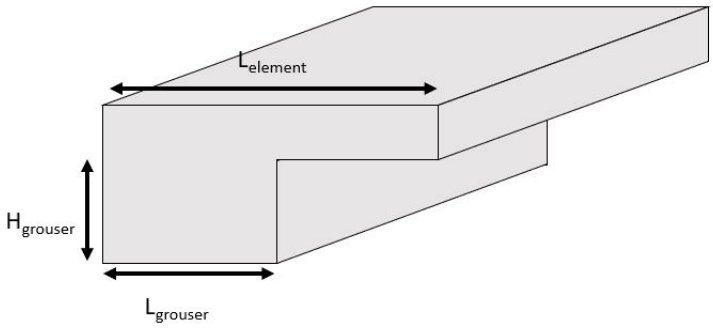

Figure 4.4: Simplified track element

4.1.3. Operational forces

The operational forces are different for every trencher, and every trencher has different configurations with yet different operational forces. Therefore the cutting forces are simplified to resulting forces in the direction of the axes. These resulting forces will be assigned to a point of engagement in the 3-dimensional coordinate system. If the forces are not well known, they can be estimated using the formulas below.

$$F_{cut,hor} = A_{trench} N_c S_u \tag{4.1}$$

Where:

$F_{cut,hor}$	Horizontal cutting force[kN]
A_{trench}	Area of cutting sword [m^3]
N_c	Cutting factor [-] (5-10)

$$F_{cut,ver} = F_{cut,hor} f_{vert} \tag{4.2}$$

Where:

$F_{cut,ver}$	Vertical cutting force[kN]
f_{vert}	Vertical cutting factor [-] (-0.5-0.5)

Besides the forces on the cutting or jetting sword, forces due to the subsea currents are also assumed to be operational forces. These forces are due to the drag of the vehicle. For the calculations of the drag force, it is assumed that the different components of the vehicle are close enough together to form a full surface area. These forces can be calculated using equation 4.3 and equation 4.4. Since the currents can come from each and any direction, the flow velocity and the angle of impact will be used (Journée et al., 2015). These formulas are valid when the current velocity is way larger as the progress speed, otherwise the progress speed should be also taken into account. The angle theta is shown in Figure 4.5.

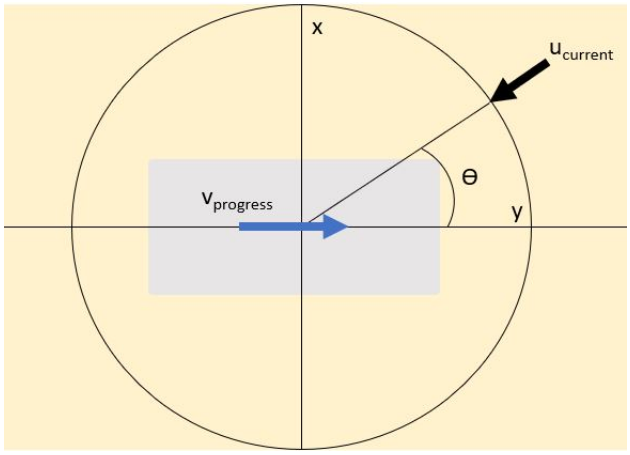

Figure 4.5: Impact angle current with vehicle

$$F_{current,x} = 0.5 \cdot H_{trencher} \cdot B_{trencher} \cdot cd \cdot u_{current}^2 \cdot \rho_w \cdot \cos(\theta_{current}) \tag{4.3}$$

$$F_{current,y} = 0.5 \cdot H_{trencher} \cdot L_{trencher} \cdot cd \cdot u_{current}^2 \cdot \rho_w \cdot \sin(\theta_{current}) \tag{4.4}$$

Where:

$F_{current,y,x}$	Current force[kN]
$H_{trencher}$	Height trencher [m]
$B_{trencher}$	Width trencher [m]
cd	Drag coefficient[-]
$u_{current}$	Current velocity [m/s]
$\theta_{current}$	Impact angle current [°]

4.1.4. Resistances

When a tracked trencher passes over a soil, there is always some formation of ruts. Ruts are formed because the tracks sink slightly into the ground. Part of this sinking is due to the elastic sinking of the soil. This is because it is assumed that trenchers will not remain stationary in the same place for too long and therefore no further static settlements will occur. Also, additional subsidence may occur, which can be seen in real life in that the rear end is often positioned lower. These two different sinkings cause three different resistances.

Two of these resistances are due to the compaction of the soil. Compaction resistances occur because it costs power for the track to compact the soil. Both resistors therefore work in the opposite direction to the direction of travel. The compaction resistances can be determined with the work done principle, assuming that the rut its volume created is $B_{track} * L_{track} * z_{total}$. This principle is shown in equation 4.5 (Baek et al., 2020).

$$R_c L_{track} = B_{track} L_{track} \int_0^{z_t} (F_{z,res} / B_{track} L_{track}) dz \tag{4.5}$$

Where:

R_c	Compaction resistance force [kN]
$F_{z,res}$	Resultant vertical force on single track [kN]

The two different resistances are determined through the two different sinkages. The static sinkage can be determined with the elastic settlement of the tracks shown in equation 4.6 (Budhu, 2011).

$$z_0 = \frac{F_{z,res}}{E_u \cdot 0.5 \cdot L_{track}} \cdot \left(1 - v_u^2\right) \cdot \mu_s \cdot \mu_{emb} \cdot \mu_{wall} \tag{4.6}$$

Where:

z_0	Elastic settlement [m]
E_u	Undrained elastic modulus [kPa] (E' in case of granular soils)
v_u	Poisson's ratio undrained condition (0.3-0.45)[-] (v' in case of granular soils(0.2-0.455))
μ_s	Shape factor (=B_{track}/L_{track}) [-]
μ_{emb}	Embedment factor [-] (=1 assumed)
μ_{wall}	Side wall factor [-] (=1 assumed)

For cohesive soils, it is important to express the undrained modulus of elasticity as the undrained shear strength. With Figure 4.6 the undrained elasticity modulus correlation factor can be determined. With this factor known the undrained modulus of elasticity can be determined using Equation 4.7 (Das, 2011). For granular soils the elastic modulus, E', is between 10 MPa for loose uniform sand to 80 MPa for dense uniform sand. Gravel and well-graded sandy soils could be as large as 320 MPa(Obrzud, 2010) (Kézdi and Rétháti, 1974) (Prat et al., 1995). It should be taken into account that the greater the Young's modulus the smaller the influence will be of the static sinkage.

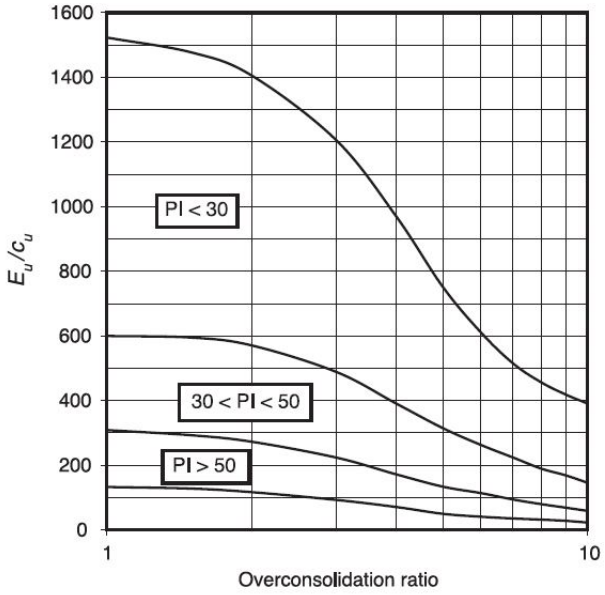

Figure 4.6: E_u/c_u values (Das, 2011)

$$E_u = kc * S_u \tag{4.7}$$

Where:

kc	undrained elasticity modulus correlation factor [-]

The slip sinkage can be determined using equation 4.8, which calculates the additional sinkage due to horizontal deformation (Wang et al., 2016).

$$z_i = \frac{h_{grouser} \cdot i}{1 - i} \tag{4.8}$$

Where:

z_i	Dynamic settlement [m]
$h_{grouser}$	Grouser height [m]
i	Slip ratio [-]

The third resistance is caused by the sinking at the front of the track. There the sinking is equal to the elastic settlement z_0. This resistance is called the bulldozing resistance and is caused by the small bump in front of the tracks that must be overcome. This resistance can be approached by the rankine passive earth theory, previously discussed in chapter 2. The resistance can be calculated with the help of equation 4.9 (Baek et al., 2020).

$$R_b = 2B_{track} \int_0^{z_0} \left(\gamma' K_p z_0 + 2c\sqrt{K_p} \right) dz \tag{4.9}$$

Where:

R_b	Bulldozing resistance [kN]
K_p	Passive earth coefficient [kN]

4.2. Vertical soil strength and stability

A single track of a trencher has two states: standing still or driving forward. A tracked trencher steers by driving one track faster then the other track. Therefore the mobility of the trencher is only determined

by vertical and horizontal stability. The horizontal and vertical axes change with the driving pitch and roll of the trencher, and therefore the two angles influence the forces on the trencher but not the plane of stability. In this section, vertical soil strength and stability will be discussed.

The vertical stability of a tracked trencher can be simplified to the vertical stability of a shallow rectangular footing(Morgan et al., 2007). This is due to the assumption that all trenchers drive a track belt with enough small roadwheel rollers with small spacing between them. The vertical stability depends on the soil pressure, the bearing capacity of the soil and the sinkage. In addition, whether a track is equipped with or without grousers will affect the vertical stability. The eccentricity of the load will also have an influence. In the first instance, centric loading will be discussed, which will then be extended to eccentric loading. It is important to realise that each track can fail independently of the other. Therefore, it is important to calculate from the whole system back to a single track, which will be discussed further in the modelling section.

4.2.1. Ground pressure distribution under centric loading

The ground pressure distribution under a footing is a function over a certain distance under the track. For a centric loading, the function will consist of a horizontal line over the entire track. A track equipped with grousers will have two phases of horizontal stability. The purpose of the grousers is to sink in the ground to create shearing planes for horizontal traction. After the sinking of the grousers, the second phase starts. The pressure distribution for this first phase can be determined through equation 4.10.

$$P = \frac{F_{z,res}}{\sum A_{grouser}} = \frac{F_{z,res}}{n_{grousers} \cdot L_{grouser} \cdot B_{track}} \tag{4.10}$$

Figure 4.7 shows a schematic view of the pressure distribution for the track with grousers in the first phase. Although the two different belt distributions with grousers are called phase 1 and phase 2, it is not certain that phase 2 always occurs. This phenomenon will be discussed later.

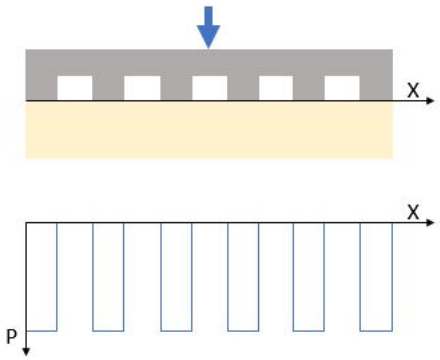

Figure 4.7: Pressure distribution for track with grousers in the first phase

The pressure distribution in the second phase for the track equipped with grousers is the same as the pressure distribution for a track without grousers. Equation 4.11 can be used for the determination of the pressure distribution in these two other situations.

$$P = \frac{F_{z,res}}{A_{track}} = \frac{F_{z,res}}{L_{track} \cdot B_{track}} \tag{4.11}$$

Figure 4.8 shows a schematic view of the pressure distribution in the second phase for the track with grousers or the pressure distribution for a flat-track belt.

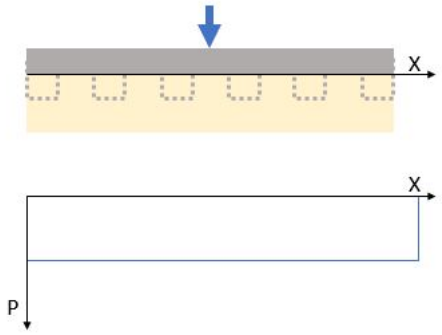

Figure 4.8: Pressure distribution for the second phase or a track without grousers

4.2.2. Ground pressure distribution under eccentric loading

In reality, the situation with the centric load hardly ever occurs. In almost all cases there will be an eccentric charge, simply because the centre of gravity is often not placed in the centre. For these kinds of loadings, the pressure distribution is not a horizontal line but a linear decreasing or increasing line. The eccentricity will be simplified to a resultant vertical force and a moment. For the loading with eccentricity, there are several loading stages, depending on the degree of eccentricity. The eccentricity parameter can be calculated using equation 2.41.

Three different cases can be distinguished for both the belts with and without grousers. First, the situation for the belt without grousers and the second phase of the belt with grousers will be discussed. The moment of inertia is needed and can be calculated through equation 4.12 for the second phase. The moment of inertia over the x axis is shown in 4.13. These two moments of inertia pertain to a double-track system.

$$I_y = \frac{(2B_{track}) * L_{track}^3}{12} \tag{4.12}$$

$$I_x = \frac{L_{track} * (D_{tracks} + B_{track})^3}{12} - \frac{L_{track} * (D_{tracks} - B_{track})^3}{12} \tag{4.13}$$

For the a single-track system, the following moment of inertia should be used:

$$I_y = \frac{(B_{track}) * L_{track}^3}{12} \tag{4.14}$$

$$I_x = \frac{L_{track} * B_{track}^3}{12} \tag{4.15}$$

e	P_{max}	P_{min}
$< \frac{1}{6} \cdot L$	$\frac{F}{L_{track}B_{track}} + \frac{M*L_{track}/2}{I}$	$\frac{F}{L_{track}B_{track}} - \frac{M*L_{track}/2}{I}$
$= \frac{1}{6} \cdot L$	$\frac{2F}{B_{track}*L_{track}}$	0
$> \frac{1}{6} \cdot L$	$\frac{2F}{3(0.5L_{track}-e)B_{track}}$	0

Table 4.1: Pressures in three different situations, belt without grousers (Budhu, 2011)

Depending on how the moment is positioned, the maximum pressure is at the front or the back of the track. The eccentricity grows as the moment grows relative to the vertical force. As soon as the eccentricity is greater than 1/6 in length, there would actually be a pulling force at part of the footing. Since we are assuming that the ground cannot absorb any tensile forces, the ground will have to compensate extra in the pressure area. The length over which the pressure is applied depends on the

track's length and the eccentricity. The three different pressure distributions for a belt without grousers and the second phase of a belt with grousers are shown in Figure 4.9. The fourth figure shows the situation where the soil will locally collapse but will not fail. This situation is approached with the effective Meyerhof method to calculate the minimum soil strength eventually. Here the pressure graph will have the shape of a block.

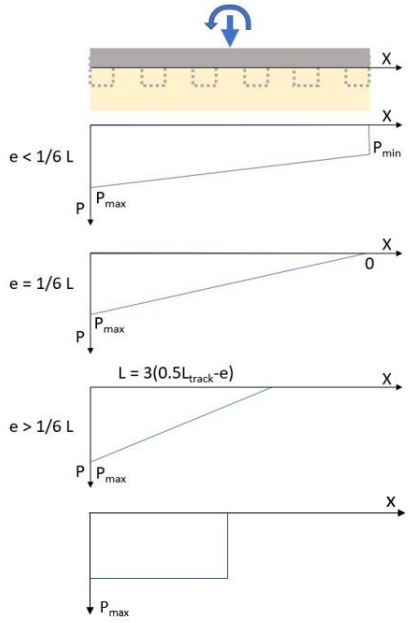

Figure 4.9: Four different pressure distributions

The first phase of the track belt with grousers is a bit different. The main difference again lies in the surface area that is smaller and in the change in moment of inertia. The new moment of inertia is an extensive formula since it depends on the number of grousers, as shown in equation 4.16. For the situation where the eccentricity is larger than 1/6 of the length, the maximum pressure is calculated by dividing it by the ratio of grousers per element. The pressure distribution calculations are shown in table 4.2.

$$I_{grousers} = \frac{B_{track}}{12}\left(\sum_{k=1}^{n_{grousers}} ((L_{track} - (k-1)L_{element})^3 - (L_{track} - (k-1)L_{element} - (k)L_{grouser})^3)\right) \tag{4.16}$$

e	P_{max}	P_{min}
$< \frac{1}{6} \cdot L$	$\frac{F}{n_{grousers} \cdot L_{grouser} \cdot B_{track}} + \frac{M * L_{track}/2}{I}$	$\frac{F}{n_{grousers} \cdot L_{grouser} \cdot B_{track}} - \frac{M * L_{track}/2}{I}$
$= \frac{1}{6} \cdot L$	$\frac{2F}{n_{grousers} \cdot L_{grouser} \cdot B_{track}}$	0
$> \frac{1}{6} \cdot L$	$\frac{2F}{3(0.5L_{track} - e)B_{track}/(L_{grouser}/L_{element})}$	0

Table 4.2: Pressures in three different situations, belt with grousers

Figure 4.10 shows a schematic view of the pressure distributions in the first phase for a track belt equipped with grousers.

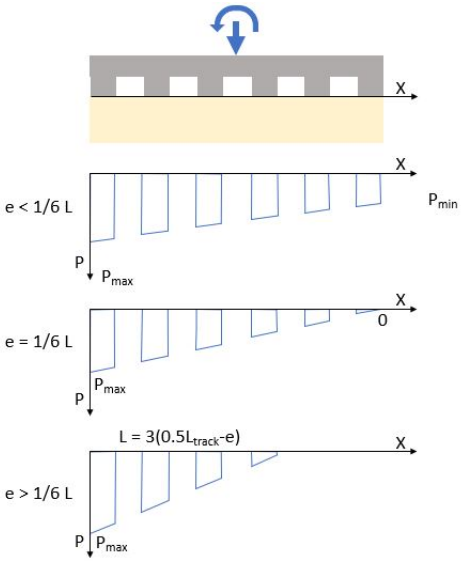

Figure 4.10: Three different pressure distributions with increasing eccentricity, belt with grousers

In order to ultimately compare these pressure distributions with the load-bearing capacity of the soil, they must be converted to an equivalent parallel distribution across the track. In the second phase with grousers and for the belt without grousers, the eccentricity will be taken into account. This is done by using the effective length and width as described in the effective Meyerhof method. Since the moment over a single grouser will be smaller and therefore the eccentricity has less influence on this, the average pressure over each grouser will be taken. Both the equivalent horizontal distributions will be shown in Figure 4.11.

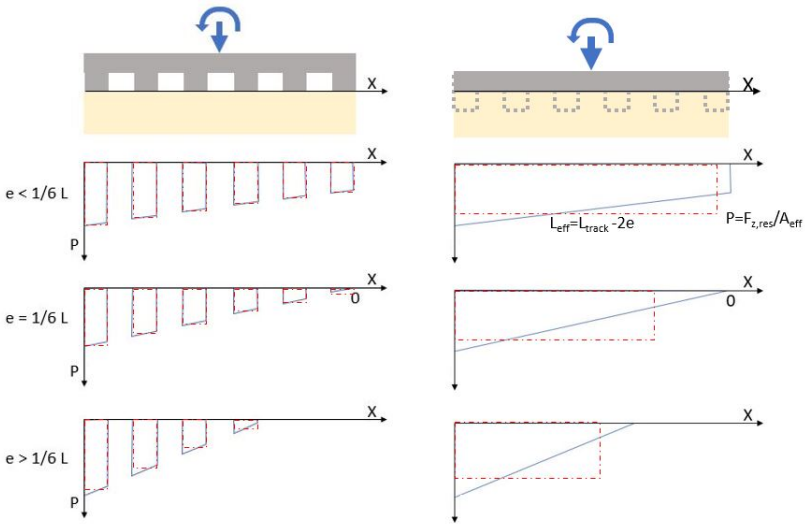

Figure 4.11: Equivalent horizontal distributions

4.2.3. Bearing capacity

As mentioned in previous sections, the second phase of the track belt with grousers and the track belt without grousers can be assumed to be a shallow foundation, where the length is the length of the track and the width is the width of the track. To calculate the bearing capacity in clay as well as in sand of a shallow foundation loaded with an eccentric load, it is common to use Meyerhof's bearing capacity method together with Meyerhof's effective area method, whereby the effective length and width should be used as inputs. The effective length and width can be calculated through equations 4.17 and 4.18.

$$L_{eff} = L_{track} - 2\frac{M_y}{F_z} \tag{4.17}$$

$$B_{eff} = B_{track} - 2\frac{M_x}{F_z} \tag{4.18}$$

With the effective length and width known, it is possible to determine the shape and bearing capacity factors. From there, the bearing capacity can be calculated using equation 4.19. The width of the track is assumed to be smaller than the length. If, exceptionally, the length is less than the width, the length must be taken as the width and vice versa. The depth should be zero since it is not desirable for the trencher to sink too deep as this will negatively impact horizontal stability.

$$\mathrm{q_b} = \mathrm{cN}_c\mathrm{S}_c + \gamma' D_f\ \mathrm{N_q S_q} + 0.5\gamma'\mathrm{B'_{track}N}_\gamma\mathrm{S}_\gamma \tag{4.19}$$

The first phase of the track belt with grousers requires a different approach, in that the bearing capacity for a single grouser should be used. Therefore, the length is the width of the track and the width is the length of the grouser. What should be taken into account is that the bearing capacity of a single track is determined. However, when two shallow foundations are placed closely together, the ultimate bearing pressure, increases substantially in the presence of another footing in granular soils. While in cohesive soils, the interference does almost not influence the bearing capacity (Alwalan, 2018).

4.2.4. Initial settlement

In the end, the equivalent soil pressure distribution will be compared with Meyerhof's bearing capacity. Should the pressure distribution be greater than the bearing capacity at a depth of zero, then the trencher will sink until a balance is achieved between the bearing capacity and pressure distribution. This is also called initial settlement. With Equation 4.19 rewritten the initial settlement by soil failure can be calculated using equation 4.20.

$$\left(\frac{\mathrm{F}_{z,res}}{\mathrm{L}_{eff}\mathrm{B}_{eff}} - \mathrm{cN}_c\mathrm{S}_c - 0.5\gamma'\mathrm{B'_{track}N}_\gamma\mathrm{S}_\gamma\right)\frac{1}{\mathrm{N_q S_q}} = \gamma' D_f \tag{4.20}$$

4.3. Summary

The mobility of the trencher can thus be viewed in two directions: vertically and horizontally. In addition, it is important to include pitch and roll angles. Current and operational forces can also influence its mobility. In addition, there will also be motion resistances acting opposite to the direction of travel. The vertical balance can be divided into two phases: one when the trencher is standing on the grousers and one when the grousers have subsided or the trencher has no grousers. In the first phase, the calculation of initial subsidence, section 4.2.2, can be used to determine whether each grouser will sink completely into the ground. The second phase will ultimately be decisive for the vertical balance. If there is eccentric loading, the pressure distribution in 4.2.2. can be used to calculate back the forces and moments acting on a single track. This is important as there can be large differences between the two tracks, when flowing from the side or a roll angle. Finally, the stability can be calculated using the effective area method for a single track. This method can be used for both granular and cohesive material.

5

Horizontal Traction Model

Now that the vertical balance is known, the horizontal balance will be examined. What we take away from the previous chapter is that not every grouser sinks to the same depth. Horizontal stability is a more complicated process as it depends on many parameters. The problem is divided into the traction of the track and the resistance forces. This section will provide a generic model of the horizontal stability. The next chapter will offer a more in-depth calculation of the traction. The traction forces for cohesive soils and granular soils both depend on different processes, shown in the table below. Also, the type of tracks will influence the traction process: a flat track belt will be governed by soil-track interaction, while the track belt with grousers depends on soil-track and soil-soil interaction. For the flat track belt, the shearing area is easily defined. For the track belt with grousers, the shear area for soil-track interaction and the shear area for soil-soil interaction depend on the dimensions of the grousers and the penetration depth of each grouser.

	Internal friction	External friction	Pore pressure	Cohesion	Adhesion
Granular soils - Flat track belt		x			
Granular soils - Track belt with grousers	x	x	x		
Cohesive soils - Flat track belt				x	x
Cohesive soils - Track belt with grousers				x	x

Table 5.1: Shear strength influence by soil type and track belt type

5.1. Flat track belt - Granular soils

The traction of the flat track belt operating in a granular soil is determined by track-soil interaction. This means that the main force is friction. The external shear strength depends on the external friction angle and the normal pressure on the interaction plane. The shear strength can be calculated using Coulomb's shear stress calculation, shown in equation 5.1. The normal pressure on the track-soil shear plane is determined in the vertical stability calculations. Depending on the moment, the vertical pressure on the track is not evenly distributed. As a result, the maximum friction shear strength is also different per location. Figure 5.1 shows a schematic sample distribution.

$$\tau_{t-s,max} = \sigma' \cdot \tan(\delta) \tag{5.1}$$

Where:

$\tau_{t-s,max}$	Shear strength track-soil [kPa]
σ'	Effective stress [kPa]

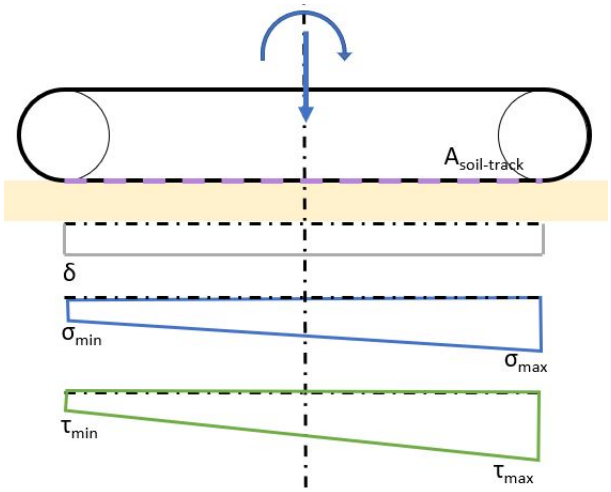

Figure 5.1: Traction of a flat track belt on a granular soil

To determine the total traction of the track, track-soil maximum shear strength should be integrated over the surface area of the track. Equation 5.2, shows the formula for the entire track.

$$F_{traction} = \int_{l_0}^{l_{end}} B_{track} \tau_{a,max} dL \tag{5.2}$$

5.2. Flat track belt - Cohesive soils

The traction of a flat track belt on cohesive soil is determined exclusively by the track-soil interaction. The maximum shear strength of track-soil shearing is constant over the entire track and depends on the adhesive factor and the undrained shear strength. The maximum shear strength is calculated using equation 5.3. The shear strength is independent of the place under the tracks and is thus evenly distributed, as shown in Figure 5.2. The sensitivity should also be taken into account. This means that the point from which the soil has been fully remolded should be determined. From that point, the remolded shear strength is governing.

$$\tau_{t-s,max} = \alpha S_u \tag{5.3}$$

$$\tau_{t-s,res} = \alpha S_u / S_t \tag{5.4}$$

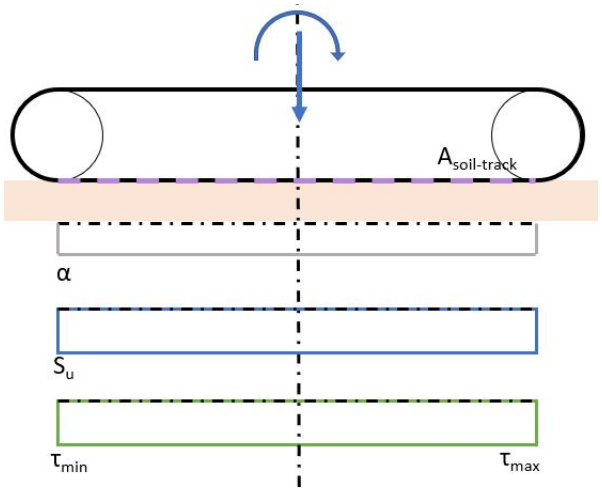

Figure 5.2: Traction of a flat track belt on a cohesive soil

The total traction can be calculated by integrating the shear strength over the area. Since the shear strength is independent over the length or the width, the integral will end in formula 5.5.

$$F_{traction} = B_{track} L_{track} \tau_{f.max} \tag{5.5}$$

5.3. Entire track belt with grousers - Granular soils

The track belt with grousers on a granular soil is also governed by track-soil and soil-soil shearing. For granular soils, the shear strength can be calculated using equation 5.6 and 5.7. Both shear strengths depend on the normal stress. The normal pressure distribution depends on the resultant vertical force as well as the moment and is a function of track length. A schematic example is shown in Figure 5.3. Both the soil-soil and track-soil shear strengths exhibit the same slope, but the track-soil strength is a fraction of the soil-soil shear strength.

$$\tau_{t-s,max} = \sigma' \cdot \tan(\delta) \tag{5.6}$$

$$\tau_{s-s,max} = \sigma' \cdot \tan(\phi) \tag{5.7}$$

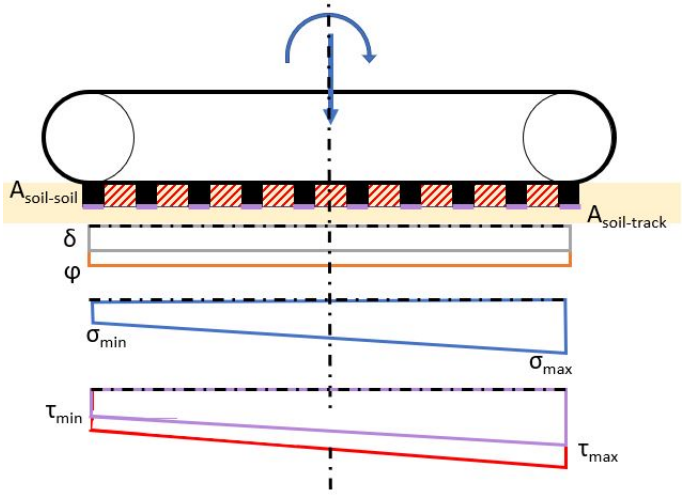

Figure 5.3: Traction of a grouser track belt on a granular soil

The total traction is the integral of the shear strength, but only over the area where the certain shear sort is happening. So, the track-soil traction force is the integral of the track-soil shear strength over the area of the grousers. The soil-soil traction force is the integral over the shearing area between the grousers. The shearing area between the grousers consists of one plane at the bottom and two on the sides. These shearing surfaces do not have to be rectangular but also depend on the penetration depth of the grousers (Mocera et al., 2020). These different surfaces, and thus different shearing modes, will be discussed in the next section. The normal pressures on the side planes are the vertical pressure times the passive earth coefficient of Rankine, shown in equation 5.8. The traction force is shown in equation 5.9 (Baek et al., 2018). In granular soil, it is important to also take into account the water pressure differences that can occur through dilatation or contractancy.

$$\tau_{s-s,maxside} = K_p \sigma \cdot \tan(\phi) \tag{5.8}$$

$$F_{traction} = \sum^{n_{tracks}} \tau_{t-s,max} L_{grouser} B_{track} + \tau_{s-s,max} \sum A_{s-s,bottomshearplane} + \tau_{s-s,maxside} \sum A_{s-s,sideshearplane} \tag{5.9}$$

5.4. Single track element traction - Granular soils

In granular soils, the traction force of a track belt with grousers is determined by the internal friction, the external friction and the pore pressure. For the traction force of single elements, four different soil-soil

failure mechanisms can be distinguished. When the grouser has fully penetrated, it is assumed that the granular soil fails like the cohesive soil. This means that it can fail as a block or as a wedge (Baek et al., 2019). When the grouser has partially penetrated, the soil will fail following Rankine's passive earth theory (Mocera et al., 2020), and, finally, the grouser may not penetrate at all. In this last situation, the traction only depends on the friction. Figure 5.4 shows the four different scenarios.

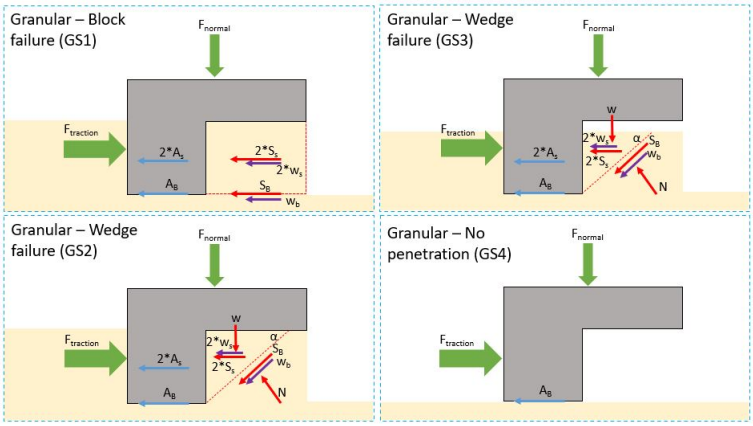

Figure 5.4: Single-track failure mechanisms in granular soils

If these different failure mechanisms are considered in a chain of connected elements, it can be concluded that failure mechanism GS2 cannot occur: The soil moving upward would have to push the element and the rest of the chain upwards, which is unlikely. Shearing mode GS2 is therefore disregarded in the traction calculation of the track belt.

5.4.1. Granular soil 1 (GS1)

The traction force can be identified with the help of the equilibrium of forces on the soil cut. Figure 5.5, shows a schematic view of the sheared soil in combination with the single track element. The soil will have three soil-soil shear planes: one at the bottom of the soil block and one on each side of the soil block. These three shear planes all represent soil-soil interaction. The element will also have three track-soil shear planes around the grouser: one at the bottom and two on the sides of the grouser. The formation of the shear layers will also lead to water underpressure, which will in turn impact the horizontal equilibrium. An overview of the forces is given in Figure 5.5.

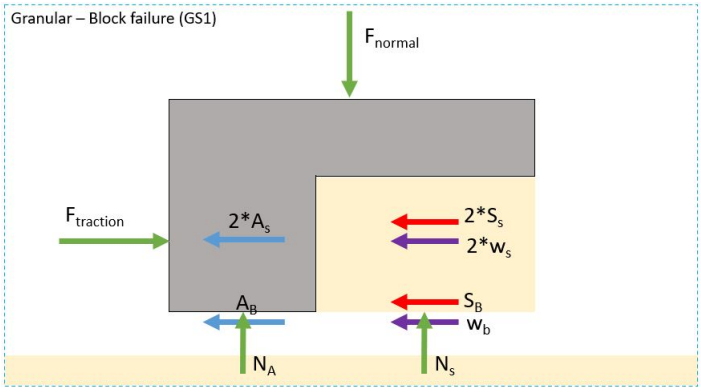

Figure 5.5: GS - Block failure by fully penetrated grousers

The forces acting on the GS1 cut are:

- A normal force acting on the soil-soil shear surface $N_S = A_s \sigma'_v \tan(\phi)$.
- A normal force acting on the track-soil shear surface $N_A = A_a \sigma'_v \tan(\phi)$.

- A bottom shear force A_B as a result of track-soil friction $N_A * \tan(\delta)$.
- Two side shear forces A_S as a result of track-soil friction $K_p * N_A * \tan(\delta)$.
- A bottom shear force S_B as a result of soil-soil internal friction $N_S * \tan(\phi)$.
- Two side shear forces S_S as a result of soil-soil internal friction $K_p * N_S * \tan(\phi)$.
- A force as a result of water underpressure in the bottom shear plane W_b (Al-Karni, 2011).
- Two forces as a result of water underpressure in the bottom shear plane W_s.

The normal forces on the shear areas can be determined by using the vertical equilibrium of forces. This equilibrium is shown below.

$$\sum F_v = 0 = F_{normal} - N_A - N_S \tag{5.10}$$

The ratio between the N_A and the N_S force is determined by the area over which the forces work. The derivation of the ratio is shown below. With the help of the ratio and the normal force N_A and N_s can be determined.

$$\frac{N_A}{L_{grouser}B_{track}} = \frac{N_s}{(L_{element} - L_{grouser})B_{track}} \tag{5.11}$$

$$N_A \frac{(L_{element} - L_{grouser})}{L_{grouser}} = N_s \tag{5.12}$$

The shear forces in granular soils are dependent on the normal forces on the shear planes. With the normal forces determined, the horizontal force equilibrium can be set up. Two forces in the equilibrium are still undetermined: the forces caused by the water underpressure. The horizontal equilibrium is shown below.

$$\sum F_H = 0 = F_{traction} - 2K_p \frac{1}{2} N_A \tan(\delta) - N_A \tan(\delta) - 2K_p \frac{1}{2} N_S \tan(\phi) - N_S \tan(\phi) - 2w_s - w_b \tag{5.13}$$

In the above formula, all forces are known except for the forces caused by the water underpressure in the shear layer. Due to dilatation, there will be an increase in pore volume, causing underpressure. The water underpressure will persist until enough water will have flowed to the shearing surface. The formulas below are used to determine the pressure difference. Because it is unclear how fast the water will actually flow, an average pressure difference will be used that will decrease with the progress of the single element under the track. The thickness of the shear layer can be determined with the help of equation 5.14. This equation is based on the research presented in figure 5.6.

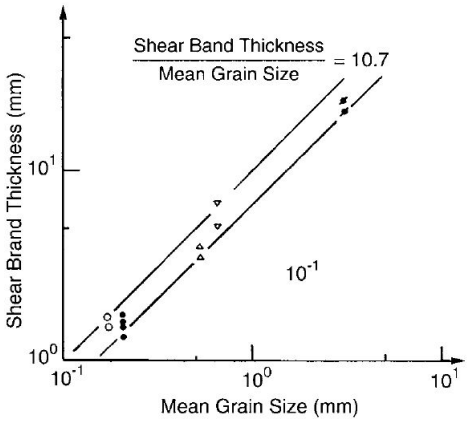

Figure 5.6: Thickness of shear band as a function of particle size (Mitchell and Soga, 2005, after Oda and Iwashita, 1999)

$$Th_{shear} = 10.7 * d_{50} \tag{5.14}$$

Where:

Th_{shear}	Shear plane thickness [m]
d_{50}	Median soil particle size [kPa]

With the thickness of the shear band known, the shear layer can be determined through the equation below.

$$V_{shear} = Th_{shear} A_{shear} \tag{5.15}$$

Where:

V_{shear}	Shear volume [m^3]
A_{shear}	Shear area [m^2]

With the total shear volume known, the average flow rate can be determined through equation 5.16.

$$Q_{avg,shear} = \frac{\delta\eta V_{shear} * L_{track}}{v_{progress}} \tag{5.16}$$

Where:

$Q_{avg,shear}$	Average flow rate [m^3/s]
$v_{progress}$	Progress speed track [m/s]
$\delta\eta$	Porosity difference [-]

With the law of Darcy, the pressure difference can be determined, as shown in equations 5.17 and 5.18.

$$\delta h_{avg} = \frac{Q_{shear}}{k_w * A_{shear}} * l_{flow} \tag{5.17}$$

Where:

δh_{avg}	Head pressure difference [m]
k_w	Soil permeability [-]
l_{flow}	Average flow length [m]

$$\delta P_{avg} = \rho_w g \delta h_{avg} \tag{5.18}$$

Where:

δP_{avg}	Pressure difference [kPa]

The flow length can be determined by drawing flow lines to the shear planes. The flow net is shown in Figure 5.7. The flow length is the average of the longest and the shortest flow line. For the bottom shear layer, this results in equation 5.19, and for the shear planes on the sides, equation 5.20 is used.

$$l_{b,avg} = (\frac{1}{4}\pi 2 h_{grouser} + \frac{1}{4}\pi 2(h_{grouser} + \frac{1}{2}B_{track}) + \frac{1}{4}\pi B_{track})/2 \tag{5.19}$$

$$l_{s,avg} = (\frac{1}{4}\pi 2 h_{grouser})/2 \tag{5.20}$$

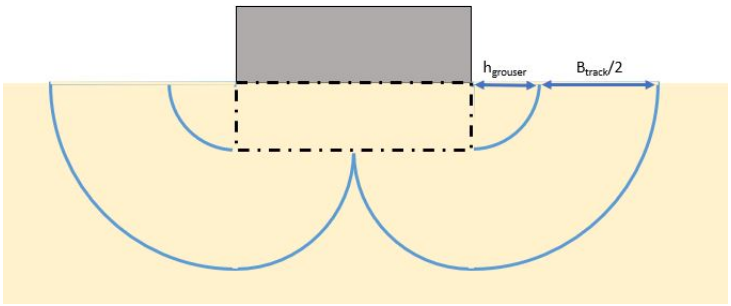

Figure 5.7: Flow net for GS1

Now that the pressure difference is known, the forces due to the water pressure differences can be calculated. The water pressure causes an increase or decrease of the normal force on the shear plane. Therefore, the additional force can be calculated using equation 5.21. This force can be negative and positive.

$$w_{avg} = \delta P_{avg} * \tan(\phi) \tag{5.21}$$

5.4.2. Granular soil 3 (GS3)

In shear mode GS3, the vertical normal force is not large enough to penetrate the grouser entirely. Since the grouser is not penetrated entirely, the horizontal part of the track element is not in contact with the soil between the grousers. Since no vertical force is being applied to the soil block between the grousers, it will fail in accordance with the Rankine passive earth theory. Following this theory, the sheared soil chunk will look like a wedge rather than a block. This means that the shear plane will work in an angle, which causes the two equilibria to change with it. The angle of shear is not known but will normally form to the angle of least resistance. An assumption made in this research is that the soil will fail, following Rankine's passive earth theory, which means that the angle will be $45 + \phi/2$. The difference between this theory and the real situation is that this theory is about an infinitely long slice of soil. This assumption is made because the length of this ground slice (= width track) is much larger than the height (< height grouser) of the same slice. Figure 5.13 shows the forces working on the soil wedge and the track element.

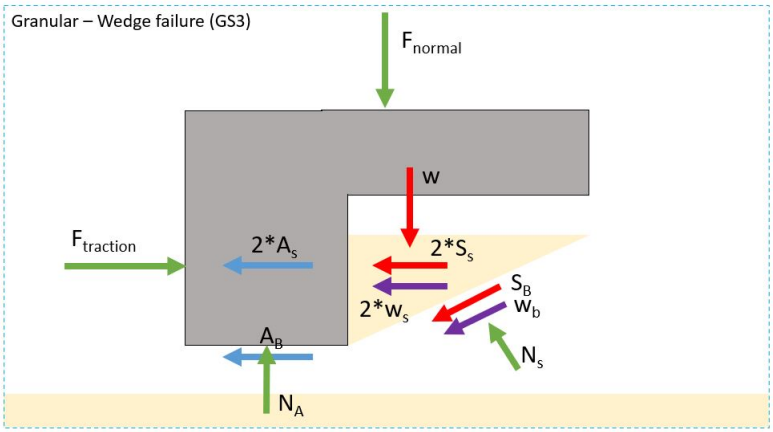

Figure 5.8: GS - Wedge failure by partially penetrated grousers

The forces working on the GS3 cut are:

- A normal force acting on the soil-soil shear surface N_S.
- A normal force acting on the track-soil shear surface N_A.

- A weight force of the soil cut on the shear plane W.
- A bottom shear force A_B as a result of track-soil friction $N_A * \tan(\delta)$.
- Two side shear forces A_S as a result of track-soil friction $K_p * N_A * \tan(\delta)$.
- A bottom shear force S_B as a result of soil-soil internal friction $N_S * \tan(\phi)$.
- Two side shear forces S_S as a result of soil-soil internal friction $K_p * N_S * \tan(\phi)$.
- A force as a result of water underpressure in the bottom shear plane W_b.
- Two forces as a result of water underpressure in the bottom shear plane W_s.

The vertical equilibrium can be divided into two free body diagrams: one for the track element and one for the soil chunk. The vertical force equilibrium for the track element is shown in equation 5.22. From there, the normal force acting on the two track-soil shearing planes will be known.

$$\sum F_{v,trackelement} = 0 = F_{normal} - N_A \tag{5.22}$$

The second vertical equilibrium is made up around the soil wedge. Bear in mind that the shear force S_B depends on the normal force N_s. When the forces caused by the water pressures are known, the normal force N_s can be determined. Equation 5.23 shows the vertical equilibrium.

$$\sum F_{v,soilwedge} = 0 = W + S_b \sin(45 + \phi/2) + w_b \sin(45 + \phi/2) - N_s * \cos(45 + \phi/2) \tag{5.23}$$

The traction force is determined from the horizontal equilibrium shown in equation 5.24. The last two unknowns to solve these series of equations are the forces due to the water pressure.

$$\sum F_h = 0 = F_{traction} - 2A_s - A_B - 2S_s - 2w_s - S_B \cos(45+\phi/2) - w_b \cos(45+\phi/2) - N_s \sin(45+\phi/2) \tag{5.24}$$

Again, the change in water pressure can be solved through equations 5.14 till 5.18. The difference in water pressure calculation in this shearing mode, compared with shearing mode GS1, is flow length. Since the side shearing planes are triangular in shape, the average flow lengths in shearing mode GS3 are half those determined in GS1. In addition, the depth of the penetration determines one distance rather than the height of the grouser. The formulas are shown in equations 5.25 and 5.26.

$$l_{b,avg} = (\frac{1}{4}\pi 2 d_{grouser} + \frac{1}{4}\pi 2(d_{grouser} + \frac{1}{2}B_{track}) + \frac{1}{4}\pi B_{track})/4 \tag{5.25}$$

$$l_{s,avg} = (\frac{1}{4}\pi 2 d_{grouser})/4 \tag{5.26}$$

5.4.3. Granular soil 4 (GS4)

In this last granular shearing mode, the normal force on the track element is too small for any penetration of the grouser. This will cause only the bottom of the grouser to be in contact with the soil, leading to only one track-soil shearing plane. Figure 5.9, shows the forces working in this shearing mode.

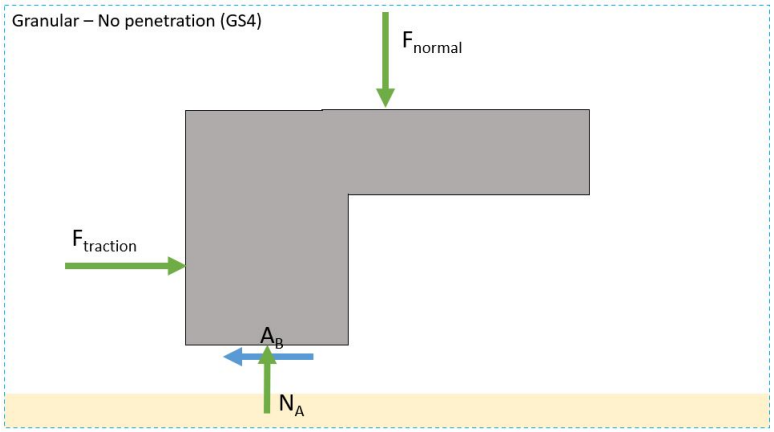

Figure 5.9: GS - Friction failure by no penetration

The forces working in this mode are:

- A normal force acting on the track-soil shear surface N_A.
- A bottom shear force A_B as a result of track-soil friction $N_A * \tan(\delta)$.

The vertical and horizontal equilibria are shown in equations 5.27 and 5.28. Since the normal force is too small to cause penetration of the grouser and the shear force also depends on the normal force, it can be assumed that the influence of this shearing mode on overall traction will be small compared to that of the other shearing modes.

$$\sum F_{vertical} = F_{normal} - N_A \tag{5.27}$$

$$\sum F_{horizontal} = F_{traction} - A_B \tag{5.28}$$

5.5. Entire track belt with grousers - Cohesive soils

The track belt with grousers on a cohesive soil depends on track-soil shearing interaction as well as soil-soil shearing interaction. The shear strength under the track therefore depends on the type of shearing. The soil-soil shear strength can be calculated using equation 5.29, and the track-soil shear strength can be calculated using equation 5.31. The shear strength under the tracks is shown in Figure 5.10. The sensitivity should also be taken into account. Therefore, the point from which the soil has been fully remolded should be determined. From that point the remolded shear strength is governing.

$$\tau_{s-s,max} = S_u \tag{5.29}$$

$$\tau_{s-s,res} = S_u / S_t \tag{5.30}$$

$$\tau_{t-s,max} = \alpha S_u \tag{5.31}$$

$$\tau_{t-s,res} = \alpha S_u / S_t \tag{5.32}$$

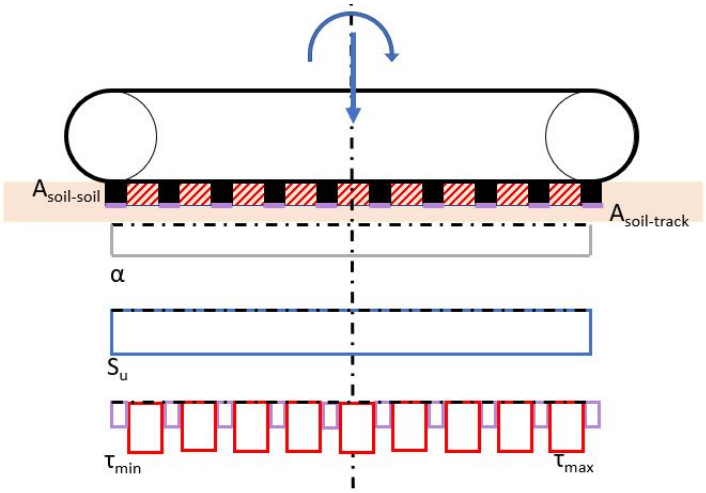

Figure 5.10: Traction of a grouser track belt on a cohesive soil

The total traction can be calculated by integrating the track-soil shear strength over its shearing area and by integrating the soil-soil shear strength over its own area. The track-soil area is determined by the grouser area. The soil-soil area depends on the shear planes between the grousers. There will be a soil-soil shear plane at the bottom and at the sides between the grousers. The shear planes between the grousers can take different forms; these different options will be discussed in the next section. The general formula is provided in equation 5.33.

$$F_{traction} = \sum^{n_{tracks}} \tau_{a,max} L_{grouser} B_{track} + \tau_{c,max} \sum A_{s-s,shearplane} \tag{5.33}$$

5.6. Single track element traction - Cohesive soils

In cohesive soils, the traction force is determined by the cohesion and the adhesion of the soil. Cohesion plays a part at the soil-soil shear planes, and adhesion governs the track-soil shear planes. When a single element is loaded, four different failure situations can be distinguished. When the grouser is fully penetrated the soil can fail as a block or as a wedge (Baek et al., 2019). However, as with granular soil, the wedge failure mechanism can be disregarded. Due to the rising soil, the track element will be pushed up. While this would be possible for a single element, a track belt links multiple elements, probably making the lifting force insufficient. In the event of a partially penetrated grouser, the traction force could be determined using Rankine's passive earth theory. In the situation where no penetration occurs at all, the traction is governed by the adhesion. Figure 5.11 shows the different shearing modes for cohesive soils.

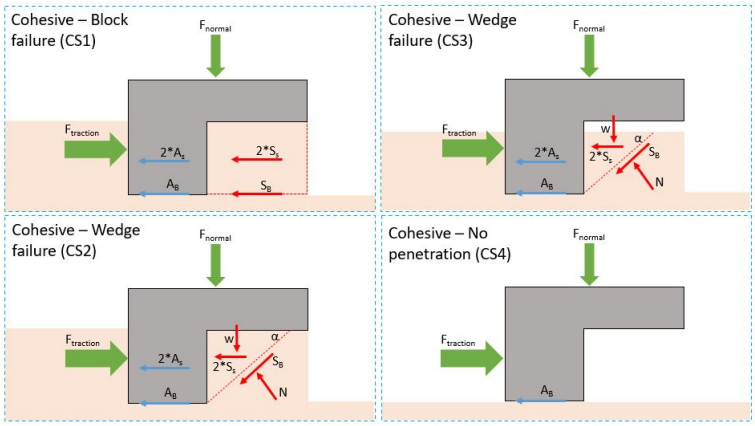

Figure 5.11: Single-track failure mechanisms in cohesive soils

5.6.1. Cohesive soil 1 (CS1)

In cohesive soils, cohesion governs the soil-soil interaction and adhesion governs the track-soil interaction. The largest difference between granular soils and cohesive soils is that the shearing forces in cohesive soils are independent of the normal forces working on the shear planes. This is due to the assumption that the friction angles in cohesive soils are zero. Therefore, only the horizontal force equilibria must be known in order to determine the traction force. The forces working in the CS1 shearing mode are shown in Figure 5.12.

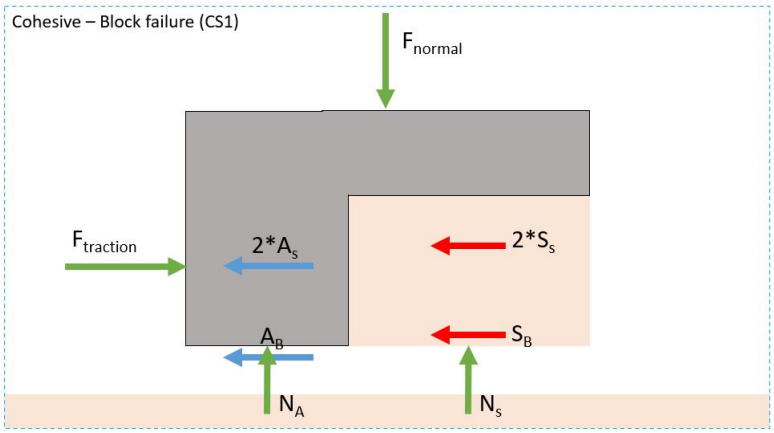

Figure 5.12: CS - Block failure by fully penetrated grousers

The forces working on the CS1 cut are:

- A normal force acting on the soil-soil shear surface N_S.
- A normal force acting on the track-soil shear surface N_A.
- A bottom shear force A_B as a result of track-soil friction $A_{b,grouser} * \alpha Su$.
- Two side shear forces A_S as a result of track-soil friction $A_{s,grouser} * \alpha Su$.
- A bottom shear force S_B as a result of soil-soil internal friction $A_{b,soil} * Su$.
- Two side shear forces S_S as a result of soil-soil internal friction $A_{s,soil} * Su$.

The horizontal force equilibrium can be calculated once the dimensions of the track element and the undrained shear strength are known, as per equation 5.34.

$$\sum F_{horizontal} = 0 = F_{traction} - A_{b,grouser}\alpha Su - A_{s,grouser}\alpha Su - A_{b,soil}Su - A_{s,soil}Su \tag{5.34}$$

5.6.2. Cohesive soil 3 (CS3)

In shearing mode CS3, the grouser has not fully penetrated the soil. In this mode, the track element does not apply a vertical force to the soil between the grousers, which causes the soil to fail as per Rankine's passive earth theory, i.e. shear like a wedge. Here, the same assumption is made as in GS3, i.e. that the angle of the shear plane for cohesive soils is $45°$. Figure 5.13 shows the forces working on the shear planes.

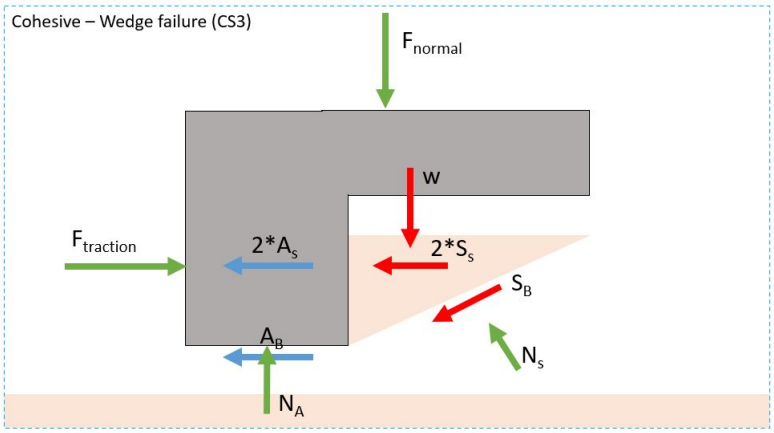

Figure 5.13: CS - Wedge failure by partially penetrated grousers

The forces working on this soil cut are:

- A normal force acting on the soil-soil shear surface N_S.
- A normal force acting on the track-soil shear surface N_A.
- A weight force working on the soil wedge W.
- A bottom shear force A_B as a result of track-soil friction $A_{b,grouser} * \alpha Su$.
- Two side shear forces A_S as a result of track-soil friction $A_{s,grouser} * \alpha Su$.
- A bottom shear force S_B as a result of soil-soil internal friction $A_{b,soil} * Su$.
- Two side shear forces S_S as a result of soil-soil internal friction $A_{s,soil} * Su$.

The traction force can be determined with the horizontal equilibrium, as per equation 5.35. The normal force N_s is one of the unknowns in the horizontal equilibrium. This force can be determined with the help of the vertical equilibrium of the soil wedge, as per equation 5.36. With the normal force known, the traction can be calculated.

$$\sum F_{horizontal} = 0 = F_{traction} - A_{b,grouser}\alpha Su - A_{s,grouser}\alpha Su - A_{b,soil} Su \sin(45) - A_{s,soil} Su - N_s \cos(45) \tag{5.35}$$

$$\sum F_{vertical,soil} = 0 = W + A_{b,soil} Su \cos(45) - N_s \sin(45) \tag{5.36}$$

5.6.3. Cohesive soil 4 (CS4)

In the last shearing mode for cohesive soils, the track element has again failed to penetrate the soil at all. This means that only the bottom of the grouser is in contact with the soil and the only shear plane is a track-soil shear plane, the strength of which is determined by the adhesive strength of the soil. The forces in this shearing mode are shown in Figure 5.14.

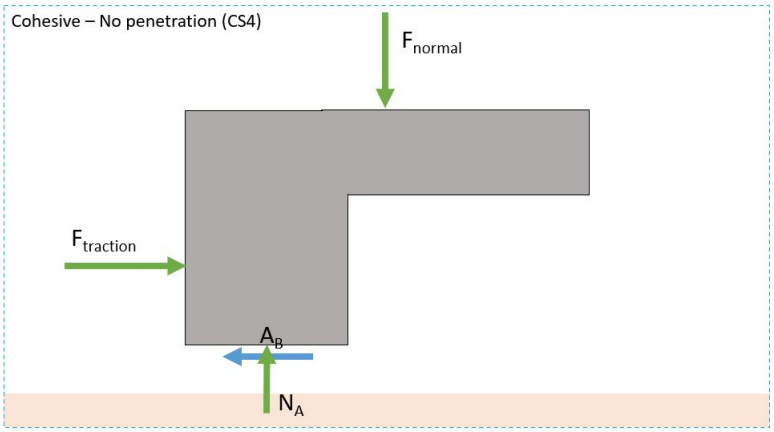

Figure 5.14: CS - Adhesion failure by no penetration

The forces working on this soil cut are:

- A normal force acting on the track-soil shear surface N_A.
- A bottom shear force A_B as a result of track-soil friction $A_{b,grouser} * \alpha Su$.

The traction force is determined only by the horizontal equilibrium, as shown in equation 5.37. The traction force is determined only by the undrained shear strength of the soil and the bottom area of the grouser.

$$\sum F_{horizontal} = 0 = F_{traction} - A_{b,grouser} * \alpha Su \tag{5.37}$$

5.7. Effective driving force

The effective driving force is a force that does not actually exist but is used to determine whether or not traction is sufficient in the calculation model. The effective driving force can be explained as the difference in force between traction and resistance as well as other operational forces. It is therefore an important threshold for the trencher's mobility. If the effective force is less than or equal to zero, the trencher will not be able to operate in those conditions. The equation below shows the formula for the effective driving force.

$$F_{eff} = F_{traction} - \sum F_{resistances} - \sum F_{operational} \tag{5.38}$$

5.8. Summary

A shearing mode can be determined from the immersion depth per grouser. There are three shearing modes that can occur in a continuous chain. With granular material, it is important to take permeability into account because this can cause dilatancy and contractancy. The vertical pressure also influences the horizontal force. With cohesive material, it is mainly the undrained shear strength that is of influence. In addition, the shear planes depend on the shear mode and the simplified parameters of the tracks. Ultimately, the horizontal force will be expressed as an effective force. This force does not actually exist, but makes it easy to set limits, i.e. where the effective force is zero.

6

Modelling

This chapter discusses the model created as part of this research, incorporating the theoretical knowledge from the previous chapters. This means that the influences of different processes on each other will be defined. Furthermore, it will be discussed how the created model solves the mobility problem and what its inputs and outputs should be. This chapter does not re-write all calculation formulas but shows the relationships between the different formulas. The model is written in python.

6.1. Overview of modelling scheme

The deployability of a subsea tracked trencher depends on the trafficability of the soil and the mobility of the trencher. In order to be able to estimate the deployability, the horizontal and vertical stability of the ground must be checked. In the model, it was decided to calculate these two stabilities through separate equations. In Figure 6.1, a simplified representation of the model is given; in Appendix **??** the extended diagram can be seen. The trafficability of a soil is the ability of a soil to support mobility.

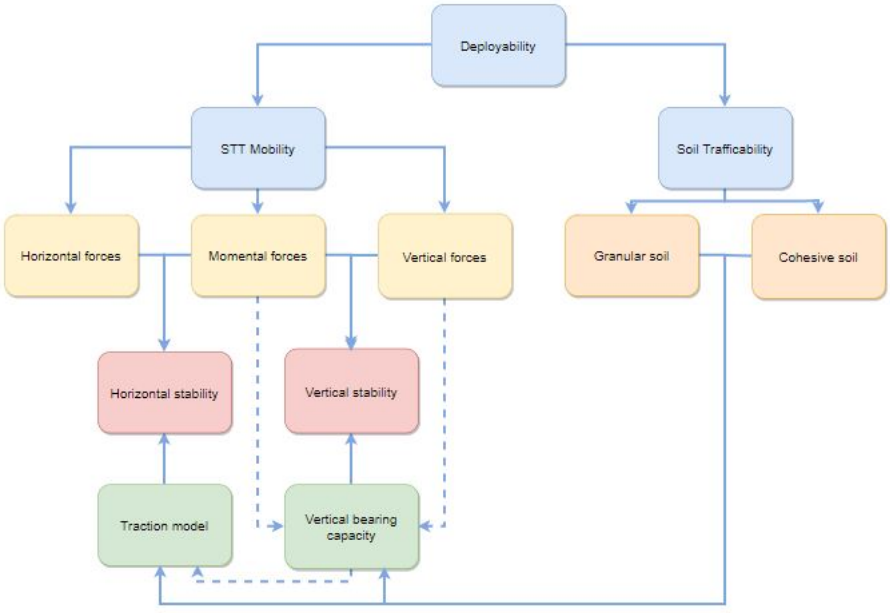

Figure 6.1: Simplified model scheme

The model ultimately revolves around the vertical and horizontal balance between the trencher applying the forces and the soil, which must be strong enough to absorb these forces. The model starts with the input. As input to the model, the soil parameters, external factors and dimensions of the trencher must

be given. From here, the simplified trencher is built and the resultant forces are computed. The resultant forces are the first input of the stability calculations. On the other hand, soil parameters should be inserted to calculate the soil strengths using the traction model and the vertical bearing capacity model. From the soil type, the governing shear strength parameters should be determined. After the governing shear strength is known, the traction model and vertical bearing capacity model are used to determine the horizontal and vertical strength forces of the soil. The vertical bearing capacity model is influenced by the soil shear strength, but also by the momental and vertical forces that work on the trencher. These forces determine the effective area of the tracks that is used for the bearing capacity. For the traction model, the penetration depth of each grouser should be known, in order to determine each element's shearing mode. From the shearing modes, the traction forces of the elements are summed. This total force is the traction force of a single track. The stability of the soil is sufficient if the strength forces are larger than the opposing applied force. In the next sections, a more in-depth analysis of the different building blocks will be discussed.

6.2. Load calculation

All the model parts start with an input and work towards certain outputs. The first part in the model is the load calculation. This section of the model aims to calculate the loads that should be overcome for the stability: the equivalent pressure distribution and the resultant horizontal force. Besides these two outputs, a third output is needed for the traction calculation: the linear pressure distribution per track. The entire algorithm for the load calculation is shown in Figure 6.2. The red squares are input values, the blue squares are calculation steps, yellow are values used from other parts of the code, and the green squares are output values for this particular section of the code. The dashed lines should be seen as influencing parameters, while the solid lines can be interpreted as calculation steps.

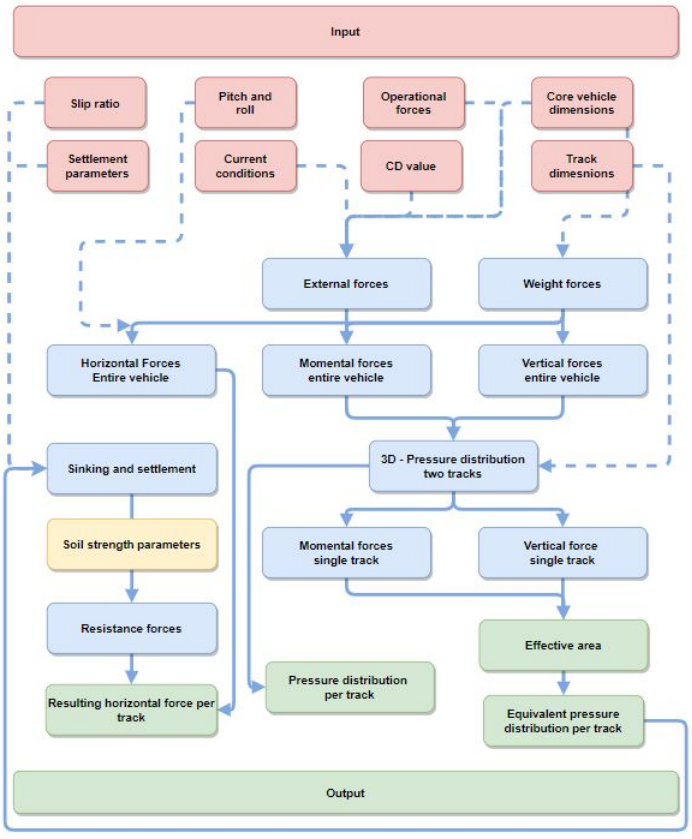

Figure 6.2: Model scheme of the load calculation

As stated earlier, to predict the mobility of the trencher, prior knowledge is needed on some of the parameters. In order to determine the loads on the soil, the following input values are required:

- Maximum slip ratio, i [-]
- Pitch & Roll, [°]
- Operational forces [kN]
- Core vehicle dimensions:
  - Length of track, L_{track} [m]
  - Width of track, B_{track} [m]
  - Length core vehicle, $L_{trencher}$ [m]
  - Height core vehicle, $H_{trencher}$ [m]
  - Width between tracks, dTracks [m]
  - Submerged weight of trencher [Ton]
  - Y-distance weight to center track, y_{weight} [m]
  - Z-distance weight to soil, z_{weight} [m]
- CD-value, CD [-]
- Track dimensions:
  - Height of grouser, $h_{grouser}$ [m]
  - Length of grouser, $L_{grouser}$ [m]
  - Length of single element, $L_{element}$ [m]
- Current conditions:
  - Current velocity, $u_{current}$ [m/s]
  - Angle with front, $\theta_{current}$ [°]
- Settlement parameters:
  - Poisson's ratio, ν [-]
  - Elasticity modulus, E [kPa]

Most of the input values are trencher-specific dimensions. Most dimensions should be known, but if they are not, they should be estimated as accurately as possible. Especially the dimensions of the tracks are important since they will have a major influence on the model. The other input parameters are soil-related parameters or environment-related parameters and should be tested or estimated.

As can be seen in Figure 6.2, the first step is to determine all of the external forces and weight forces on the trencher. Most of these forces are input values and therefore do not need to be calculated. Others, like the current force, should be calculated. In this step, it is important that each force has a clear point of engagement, a direction and a magnitude. Once these are known, the model will convert everything to resultant forces with a single point of application in the centre of the trencher. These resultant forces consist of a horizontal, a vertical and two momental forces over the x and y axes. These forces are in relation to the horizontal and vertical axes which, in turn, rotate with the soil slopes. The pitch and roll input should therefore also be taken into account by determining the resultant forces. With the resulting forces on the vehicle known, the pressure distribution for the double-track system can be determined. If the moment about the y-axis is greater than zero, it means that the vertical forces will be distributed disproportionately over the two tracks. Since each track can fail independently, it is important to take into account the redistribution of the vertical force. Besides the vertical force per track, the momental force over the x-axis per track is also very important. The momental force over the x-axis can be calculated by taking half the momental force over the double-track system. Now the single-track system is known, Meyerhof's effective area method is used to determine the equivalent area over which

a horizontal pressure distribution works. When the effective area is known, the equivalent pressure distribution per track can be determined. From the 3D - pressure distribution of the two tracks, the other pressure output, the pressure distribution per single track, can be calculated.

The last loop is to determine the three resistance forces. Together with the horizontal opposing force per track, these three resistance forces form the total opposing force that needs to be overcome by the traction. The resistance forces depend on the sinking that the trencher experiences. The sinking depends on the initial failure of the tracks, the elastic settlement and the settlement due to the slipping of the grousers. The initial failure happens when the bearing capacity is not high enough. Then the track sinks further into the ground to find more bearing capacity. The two compaction resistances depend on the total sinking of the tracks. Because the distribution per track is different, the total sinking per track will also be different. As a result, the resistances must be calculated for each track. The third resistance is the bulldozing resistance, which depends on Rankine's lateral earth pressure exerted by the sand heap in front of the tracks. This sand heap is determined by the initial failure and the initial settlement. Sinking due to skidding of the grousers only comes into play at the back of the tracks. Another initial calculation step must be taken: the shear strength of the soil is needed to calculate the soil capacities. This calculation will be discussed in the next section.

6.3. Shear strength

The model to calculate the shear strength of the soil is related to the calculation of the loads because the resistances depend on the shear strength, and the shear strength of granular soil in turn depends on the normal pressure acting on the shear plane. The color scheme of the flow chart is similar to the previous scheme. The output of this part of the model is shear strength. An overview of the model for cohesive soils is shown in Figure 6.3 and for granular soils in Figure 6.4.

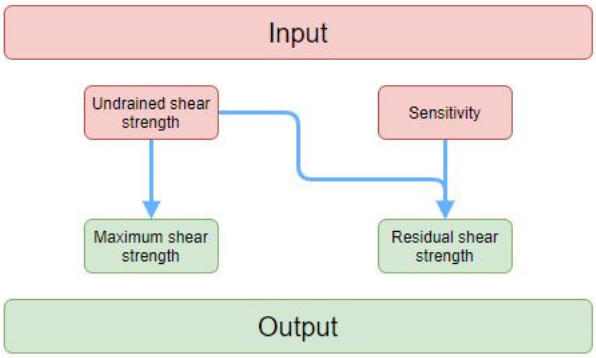

Figure 6.3: Model scheme of the shear strength calculation cohesive soils

In order to determine the shear strength, the inputs that must be known are:

- Initial porosity, η_i [-]
- Critical shear porosity, η_{cs} [-]
- Relative Density, RD [-] (from which the internal friction angle is determined)
- Effective particle size, d_{10} [m]
- Median particle size, d_{50} [m]
- Undrained shear strength, S_u [kPa]
- Sensitivity, S_t [-]

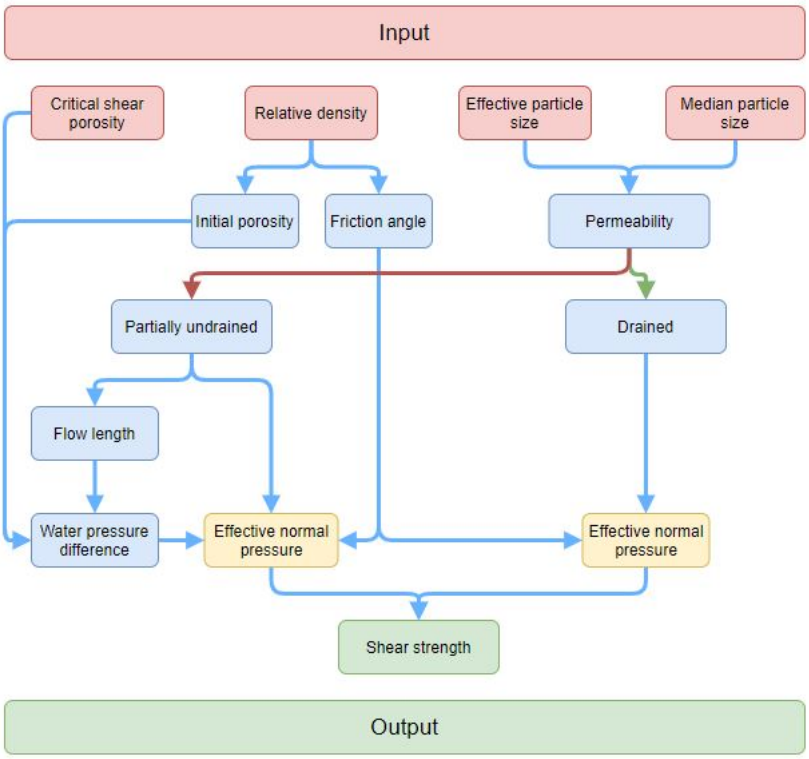

Figure 6.4: Model scheme of the shear strength calculation granular soils

The shear strength calculation can be divided into two parts: one for cohesive soils and the other for granular soils. The shear strength for cohesive soils actually only depends on the undrained shear strength and the sensitivity. Since the undrained shear strength is one of the inputs for this model, the maximum shear strength follows directly from its value. The residual shear strength is also important and follows from the undrained shear strength and the sensitivity. The second calculation is for granular soils. Here, again, a split can be made between drained conditions and partially drained conditions. In both conditions, the shear strength depends on the friction angles, derived from the relative density. But, the shear strength of partially drained soil also depends on the water overpressures or underpressures that arise when the soil is shearing. The extent to which the soil is considered drained or partially undrained is determined by its permeability, and thus by the effective particle size. When the effective particle size is smaller, the soil becomes less permeable, and it will take longer for the shear layer to drain. Besides the water pressure differences, the normal pressure on the shear planes is also important for the shear strength of granular soils. When the normal pressure is higher, shear strength will also grow. Since the exact orientation of the shear planes is not determined yet, the output shear strength for granular soils will be an equation depending on the normal pressures. These pressures follow from the load calculations in combination with the penetration depth of the grousers. When the shear strength is known, the traction model and the bearing-capacity model should be used to calculate the traction, soil strength and bearing capacity.

6.4. Soil strengths

The part of the code from which the soil strength follows is the last part before two stability checks are performed. The loads on the soil and the shear strength of the soil are known. In order to make the soil strength calculations, no additional input values are required, other than those already used in the previous sections. This part is governed by two different models: the vertical bearing capacity model and the horizontal traction model. First the vertical bearing capacity model will be discussed. After that, the steps of the traction model will be reviewed. An overview of the bearing capacity model is provided in Figure 6.5. The overview for the traction model is shown in Figure 6.6.

The vertical bearing capacity model starts with the effective dimensions of a single track, as determined by Meyerhof's effective area method. Using these dimensions, Meyerhof's shape factors and bearing-capacity factors are determined. When these six factors are known, Meyerhof's bearing-capacity method to determine the vertical bearing capacity per track will be known. Since the forces per track are different, the effective area will vary as well, resulting in different bearing capacities. This means that the trencher can fail per track, so that the weakest bearing capacity will govern.

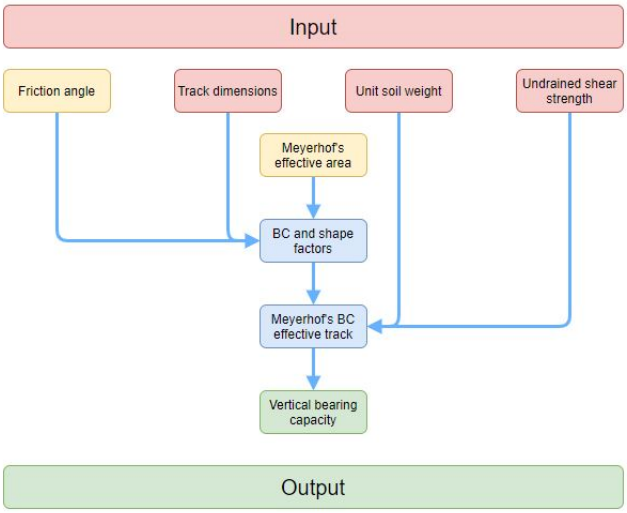

Figure 6.5: Model scheme of the bearing capacity soil-strength calculation

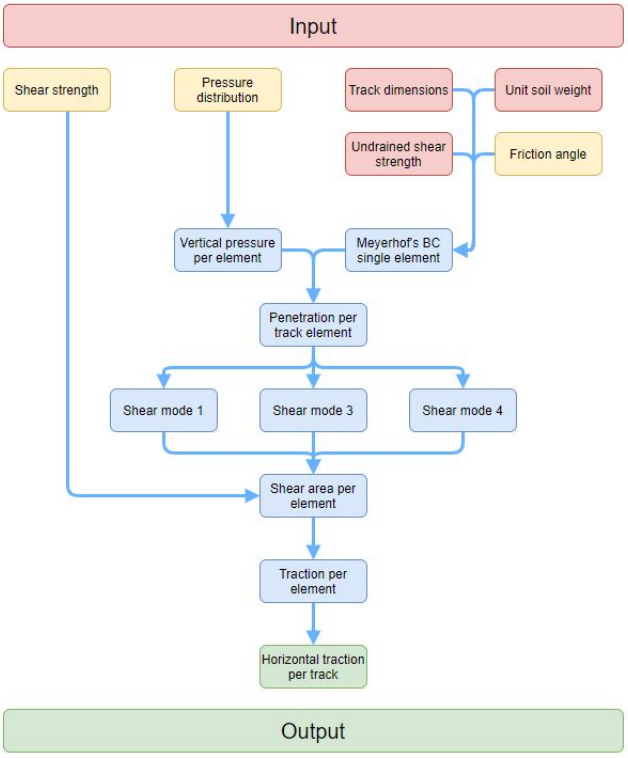

Figure 6.6: Model scheme of the traction soil-strength calculation

The horizontal traction model starts with the Meyerhof's bearing-capacity calculation for a single grouser. Equating the vertical pressure per track element with Meyerhof's bearing capacity per grouser determines the penetration depth per element. When the penetration depth is known, the shearing mode per element can be used to calculate the horizontal traction force per element. The model loops through the different elements. Within this loop the sensitivity and the change in pore pressures are included, in order to determine the governing shearing strength for each element. The iteration for every element in the traction model for granular soils is shown in Figure 6.7 and for cohesive soils in Figure 6.8. When the traction force per element is known, the traction over a single track can be calculated. Again, the penetration depths and shearing modes can vary between both tracks, so, again, the lowest traction force per track will govern. With the traction force per track and the bearing capacity per track known, the stability checks can be executed.

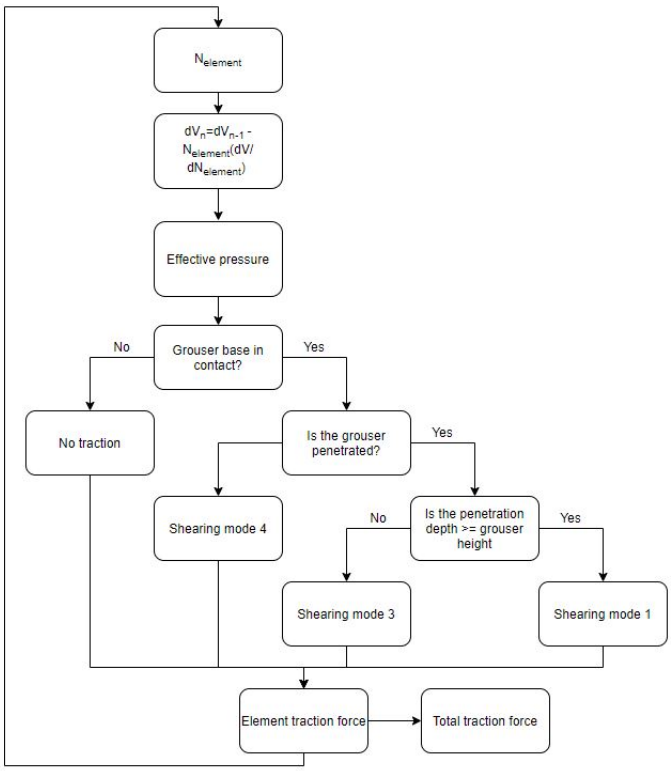

Figure 6.7: The traction model in granular soils

6.5. Stability check

The execution of the stability check is again done in two parts; both horizontal and vertical stability should be achieved, and if one of these is not achieved, the trencher's mobility will be insufficient. An overview of the stability check is provided in Figure 6.9. The stability check indicates whether and, if so, which failure would occur. In both cases (vertical and horizontal), this check is performed using the effective force. If the effective force is positive, soil strength is sufficient. If it is negative, soil strength is insufficient. When the entire model is looped through more parameters, the effective force will behave like a curve. The intersections of this curve with the x-axis will be the tipping points of mobility. From the theory behind soil-strength calculations, it can be concluded that bearing capacity will give a minimum soil strength, whereas, in many cases, the horizontal traction force will give a maximum and a minimum. This will be discussed in the next section and visualised in the CBT 2400 case study in chapter 7.

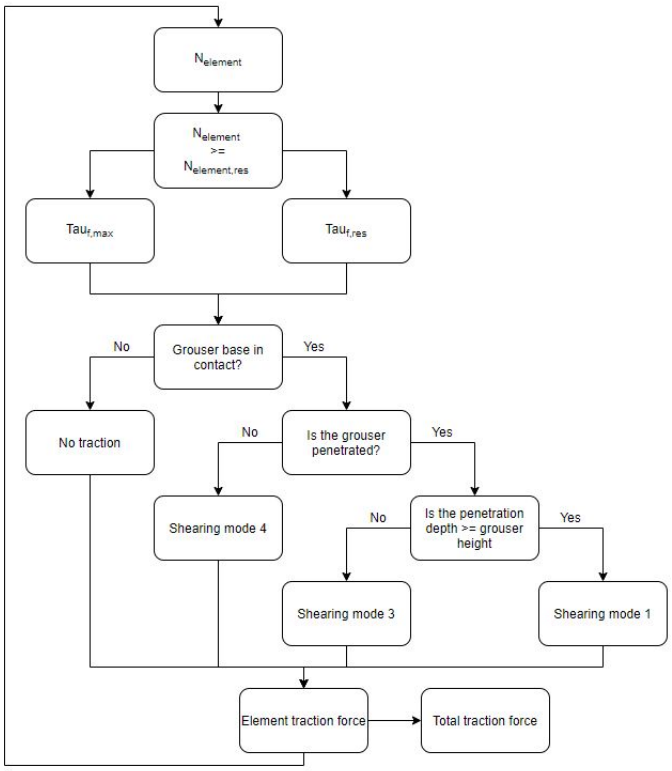

Figure 6.8: The traction model in cohesive soils

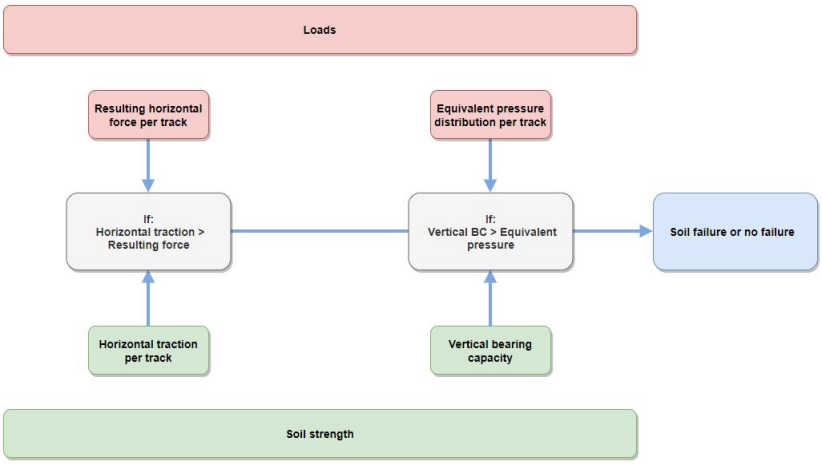

Figure 6.9: Model scheme of the stability check

6.6. Iteration

The final step that has been added to the model is the ability to iterate through different parameters. Sometimes, not all parameters are known prior to the tendering phase. Also, certain limits of external facilitation of mobility may need to be determined. This can be done with the help of these iterations. To provide a comprehensive picture, an iteration step for the important soil parameters, such as relativity density or undrained shear strength, has been modelled. Also, an iteration step was included to determine the limits of an external factor such as the pitch angle or the force on the jet sword. An overview of how these iteration steps relate to the rest of the model is provided in Figure 6.10.

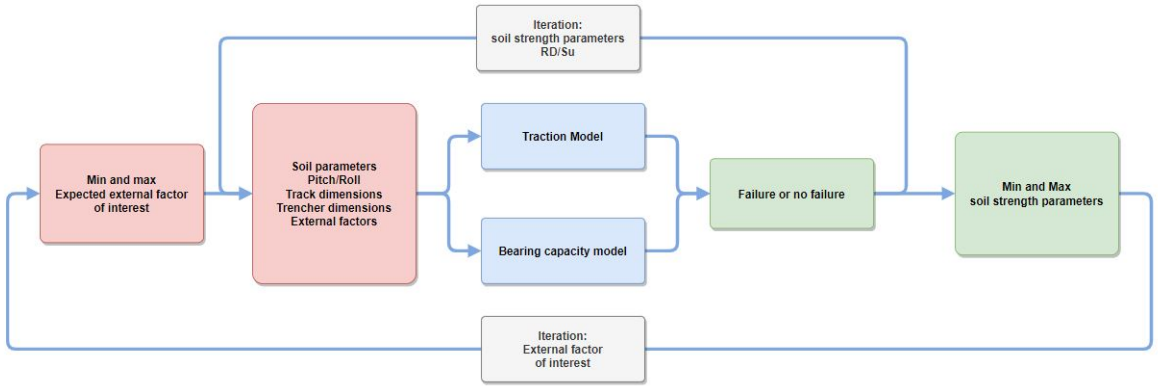

Figure 6.10: Schematic view of the double iterations

6.7. Summary

The model is thus divided into two parts: a vertical model and a horizontal model. The stability check is ultimately carried out using these two models. To perform this check as well as possible, input values must be given about the trencher itself, the external forces and the soil parameters. The input values about the trencher can all be determined using the simplifications outlined earlier in this study. The soil-specific input values should follow from an investigation of the soil. If this is not the case, they would have to be estimated, which would of course introduce additional uncertainty in the model. The external factors may vary from one moment to the next. Hence it is important to consider different cases. The model is constructed such that values can be easily looped. This makes it possible to gain insight into several parameters in one graph. The operating range will eventually consist of a lower and upper limit within which the trencher can operate. The lower limit is determined by either the vertical or horizontal stability while the upper limit is determined by the horizontal model.

7

Case study - CBT 2400

In this chapter, a case study will be carried out for the trencher CBT 2400. Multiple simulations will be performed to determine the limits of its operational circumstances. Eventually, the work area resulting from the case study will be compared with data from the field to validate the model.

7.1. Cases

7.1.1. Cohesive soils

The basic case uses the most standard values in order to be able to compare it with the other cases. In this case, for example, no sensitivity is included, there will be no roll angle and no flow either. In Table 7.1 the input values are given, next to the simplifications of the trenchers and the above soil relations.

Input parameters			
Roll [deg]	0	Sensitivity [-]	1
$\theta_{current}$ [deg]	0	$J_{residual}$ [m]	0.02
$u_{current}$ [m/s]	0	i_{sr} [-]	0.2
z_{trench} [m]	3.3	$N_{element,res}$	1
Cd [-]	2	kc [-]	500
γ' [kN/m^3]	6.5	ν [-]	0.3

Table 7.1: CS - Base case input parameters

Figure 7.3, shows the results of the cohesive soil base case. The x and y axes show the pitch and the needed undrained shear strength, respectively. From the vertical stability follows a lower limit. When this lower limit is not governing, it is shown with a yellow dotted line. When vertical stability is not met, the trencher will sink into the soil. From the horizontal stability, a lower and an upper limit follows. The lower limit of the horizontal stability is, when not governing, represented by a blue dotted line. When the trencher fails, by this limit, the grousers are in many cases penetrated, but the soil is not strong enough for operation. This means that the trencher will dig itself in. The upper limit is always ruling since it is the only upper limit, and the result shows this limit with the green line. The upper limit can be seen as a trencher on ice, where the tracks will slide across the ice without shearing the soil: the undrained shear strength is too great for the grousers to sink, and adhesion is insufficient to give the trencher the necessary traction.

The results show that, between zero and -20 degrees, pitch will sink if the undrained shear strength is less than about 10 kPa. From 0 to 10 degrees and from -20 to -30, the lower limit is determined by the horizontal model, and the soil will therefore fail by digging itself in. If the gradient is larger than 10 degrees or the gradient is less than 30 degrees, no mobility is possible anyway. At a slope of -10 degrees, the upper limit is determined by the limit of the model: 110 kPa. With a larger or smaller slope, the upper limit will decrease. If there is no slope during the operation, a minimum undrained soil strength of 10 kPa and a maximum undrained soil strength of 85 kPa are required. At a pitch of 5

degrees, a minimum soil strength of 15 kPa and a maximum soil strength of 70 kPa are required. At a pitch of -5 degrees, a minimum soil strength of 10 kPa and a maximum soil strength of 95 kPa are required.

In order to clearly show the difference in the area of operation with a numerical value, the ratio of the area between the graphs to the total area is given. The total area is the area under a horizontal line at 110 kPa, from -40 till 40 degree pitch. For the base case, this percentage is 31.0 %. The largest part of the trencher's operation can be expected to be between pitches of -15 and 15 degrees if the trencher can operate under every condition between those pitch angles. Outside these boundaries, the trencher cannot operate as the ratio of the total operating area would be small. However, the trencher would still be of great value and deployable in almost every contract. Therefore, it is important to take this ratio into consideration as well. This area ratio is also known as the effective operation area ratio. The effective operation area ratio in the base case is 54.4%. The key results are provided in table 7.2. The graphical representation of both parameters is shown in the pictures below. Where finally the purple surface is divided by the red surface. In addition to these two ratios, the maximum values at zero, minus five and five degrees are also given. More can be done with these values than the ratio values in practice.

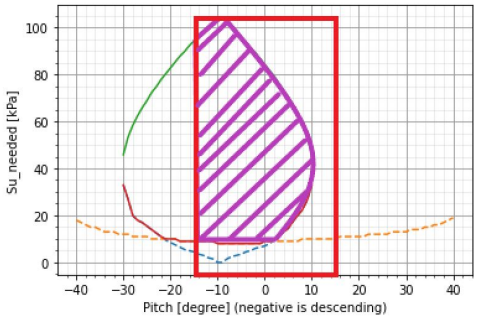

Figure 7.1: Effective operation area ratio

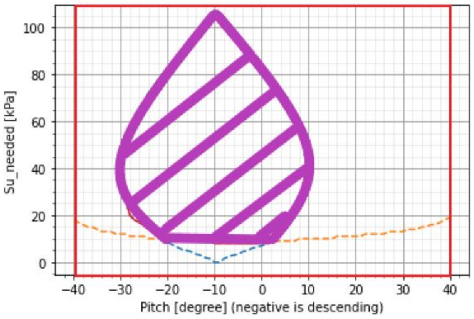

Figure 7.2: Total operation area ratio

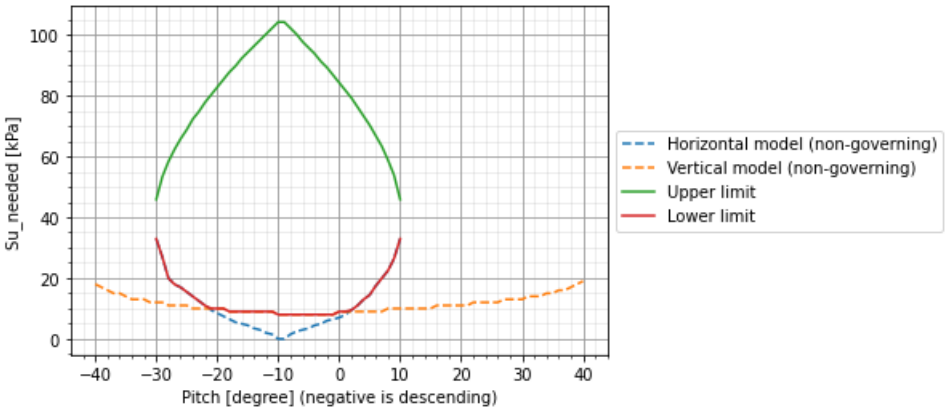

Figure 7.3: Cohesive soils (CS) - Base case

CS - Roll

The trencher's operation area will change little at small roll angles, as shown in the figures below. The total operation area ratio for a 5-degree roll is 30.8 %, and the effective operation area ratio is 54.0 %. For a 10-degree roll, the ratio's are 30.7 % for the total and 54.0 % for the effective ratio. For a 20-degree roll, the total operation area ratio is 30.2 % and the effective ratio is 54.0 %. This means that the change constitutes a decrease of 0.8 % in the total operation area ratio and 0.4 % in the effective operational area. By increasing roll, changes in the operational areas are limited but present. The most notable difference with the base case is in vertical stability, where the two boundaries for vertical stability are

	BC
Maximum pitch [°]	10
Minimum pitch [°]	-30
Total operation area ratio [%]	31.0
Effective operation area ratio (Pitch < +/-15) [%]	54.4
Su_{needed} min-max (0°) [kPa]	10-85
Su_{needed} min-max (5°) [kPa]	15-70
Su_{needed} min-max (-5°) [kPa]	9-95

Table 7.2: CS - Base case results

moving inwards. However, this change is largely not normative as this process only becomes governing at a roll angle of 20 degrees, as shown in Figure 7.6. In this event, the trencher will sink rather than dig itself in at a pitch larger than 27 degrees, with a maximum. As roll angles increase, the boundaries will move to the center of the area, thus decreasing the maximum and minimum pitch angles. Alongside a change in vertical stability, smaller differences can be observed in the lower limit of horizontal stability. Here the limit is more incremental: at a pitch of 5 degrees, the minimum kPa of the lower limit is slightly higher. The most important results are offered in table 7.3. This table again shows the small differences caused by the roll angle.

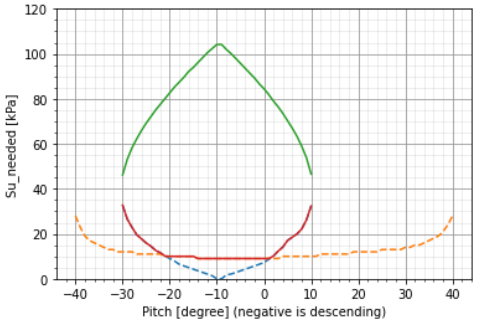

Figure 7.4: CS - Roll=5

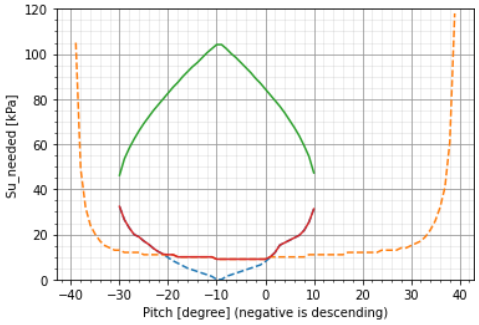

Figure 7.5: CS - Roll=10

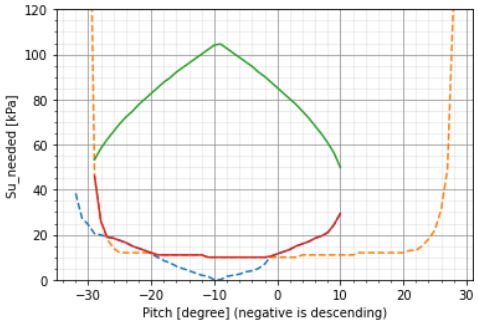

Figure 7.6: CS - Roll=20

CS - Current conditions

The first three pictures show the influence of a current straight ahead. The total operation area ratio grows with increasing flow velocity. For a velocity of 0.5 [m/s], the percentage is 31.2 %; for a velocity of 1.0 [m/s], the percentage is 31.4 %; and for a velocity of 1.5 [m/s], the percentage is 32.0 %. In contrast, the effective operation area decreases with increasing flow rates. The effective operation area percentage for the 0.5 [m/s] flow is 51.9 %, which further decreases to 43.8 % at a flow rate of 1.0 [m/s]. With a flow rate of 1.5 [m/s], the ratio is even smaller, reaching an effective percentage of 29.6 %. This decrease can be explained by the reduction of the maximum pitch. The pitch decreases to

	BC	roll=5	roll=10	roll=20
Maximum pitch [°]	10	10	10	10
Minimum pitch [°]	-30	-30	-30	-29
Total operation area ratio [%]	31.0	30.8	30.7	30.2
Effective operation area ratio (Pitch < +/-15)[%]	54.4	54.0	54.0	54.0
Su_{needed} min-max (0°) [kPa]	10-85	10-85	10-85	10-85
Su_{needed} min-max (5°) [kPa]	15-70	18-70	18-70	18-70
Su_{needed} min-max (-5°) [kPa]	9-95	10-95	10-95	10-96

Table 7.3: CS - Roll case results

even a maximum of 0 degrees at a flow of 0.5 [m/s]. The increase in total area is small and therefore difficult to observe. Small differences can be observed in the slopes of both the upper and lower limits, the most important of which can be found in table 7.4.

	BC	U_c=0.5	U_c=1.0	U_c=1.5
Maximum pitch [°]	10	9	5	0
Minimum pitch [°]	-30	-31	-35	-40
Total operation area ratio [%]	31.0	31.2	31.4	32.0
Effective operation area ratio (Pitch < +/-15)[%]	54.4	51.9	43.8	29.6
Su_{needed} min-max (0°) [kPa]	10-85	10-82	17-72	30-50
Su_{needed} min-max (5°) [kPa]	15-70	18-67	30-50	-
Su_{needed} min-max (-5°) [kPa]	9-95	9-92	10-87	15-73

Table 7.4: CS - Frontal current conditions

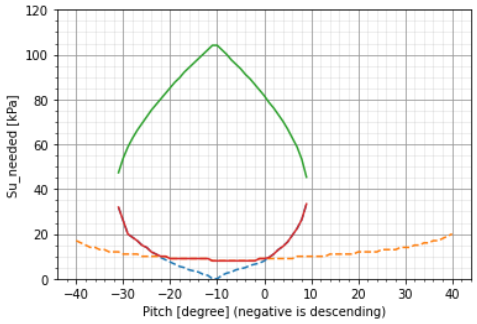

Figure 7.7: CS - $u_{current}$=0.5

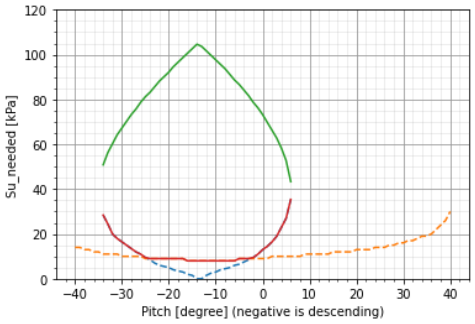

Figure 7.8: CS - $u_{current}$=1.0

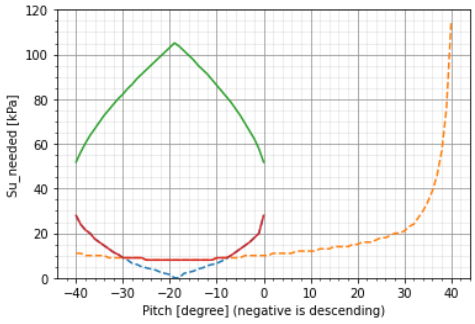

Figure 7.9: CS - $u_{current}$=1.5

The results of the roll angles show that a change in perpendicularity to the driving direction of the trencher has little influence in cohesive soils. Therefore, only the condition of a 1.5 [m/s] current will be

considered for perpendicular impact on the trencher. In this condition, the total working area is reduced to 30.6 %. The effective operation area ratio is 53.6 %. In both results, the low impact can be seen. When combining a flow from the side with a roll angle, the impact is greater: the total operation area decreases to 27.7 % while the effective ratio remains unchanged at 53.6 %. The working areas are displayed in the figures below, and the results are presented in Table 7.5.

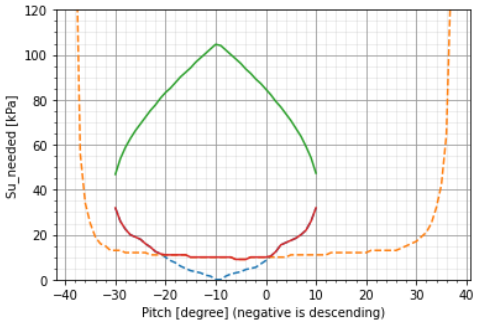

Figure 7.10: CS - $u_{current}$=1.5, θ_c = 90

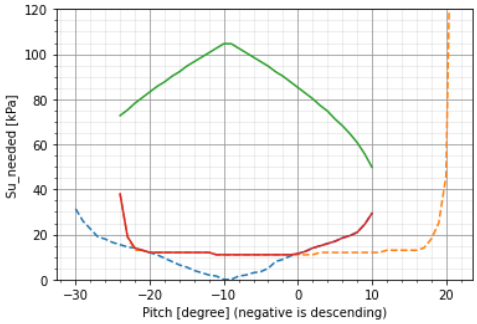

Figure 7.11: CS - $u_{current}$=1.5, θ_c = 90, roll=15

	BC	U_c=1.5, θ=90	U_c=1.5, θ=90, roll=15
Maximum pitch [°]	10	10	10
Minimum pitch [°]	-30	-30	-24
Total operation area ratio [%]	31.0	30.6	27.7
Effective operation area ratio (Pitch < +/-15)[%]	54.4	53.6	53.6
Su_{needed} min-max (0°) [kPa]	10-85	10-85	10-85
Su_{needed} min-max (5°) [kPa]	15-70	17-70	17-70
Su_{needed} min-max (-5°) [kPa]	9-95	9-95	11-97

Table 7.5: CS - Perpendicular current conditions

An impact angle of 45 degrees on the trencher leads to a combination of a frontal and a perpendicular force. As the flow is split between these two forces, it has less impact than either of the two separate flows. This can be seen in the pictures below and in table 7.6, where the key outcomes can be found.

	BC	U_c=0.5, θ=45	U_c=1.0, θ=45	U_c=1.5, θ=45
Maximum pitch [°]	10	9	7	3
Minimum pitch [°]	-30	-31	-33	-37
Total operation area ratio [%]	31.0	31.0	31.1	31.3
Effective operation area ratio (Pitch < +/-15)[%]	54.4	52.5	46.7	36.4
Su_{needed} min-max (0°) [kPa]	10-85	10-82	12-76	20-65
Su_{needed} min-max (5°) [kPa]	15-70	17-67	22-60	-
Su_{needed} min-max (-5°) [kPa]	9-95	9-95	10-90	11-82

Table 7.6: CS - 45° current conditions

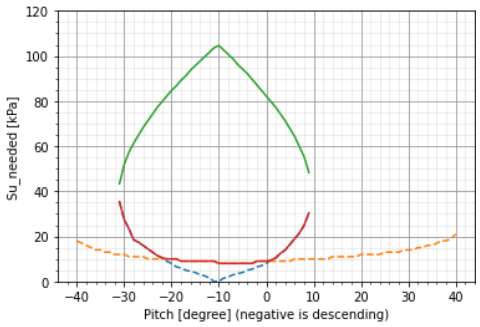

Figure 7.12: CS - $u_{current}$=0.5, $\theta_{current}$ = 45

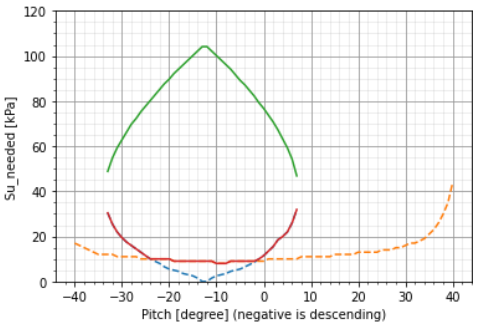

Figure 7.13: CS - $u_{current}$=1.0, $\theta_{current}$ = 45

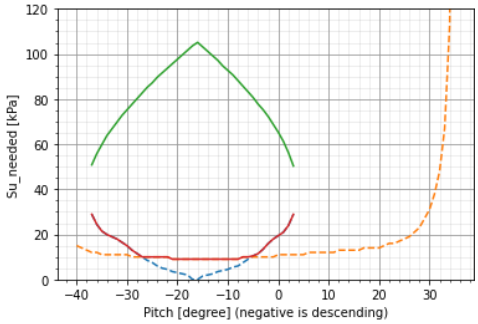

Figure 7.14: CS - $u_{current}$=1.5, $\theta_{current}$ = 45

When the currents impact the vehicle from behind, the influence on its mobility will be the opposite from that of the frontal impact. The mobility envelopes can be seen in the figures below. The most important outcomes are gathered in Table 7.7. The total operation area ratio decreases slightly whereas the effective operation area ratio increases, due to a greater maximum pitch angle.

	BC	U_c=0.5, θ=180	U_c=1, θ=180
Maximum pitch [°]	10	11	14
Minimum pitch [°]	-30	-29	-25
Total operation area ratio [%]	31.0	31.0	30.8
Effective operation area ratio (Pitch < +/-15)[%]	54.4	56.9	64
Su_{needed} min-max (0°) [kPa]	10-85	10-87	10-93
Su_{needed} min-max (5°) [kPa]	15-70	13-72	10-80
Su_{needed} min-max (-5°) [kPa]	9-95	9-97	9-105

Table 7.7: CS - 180° current conditions

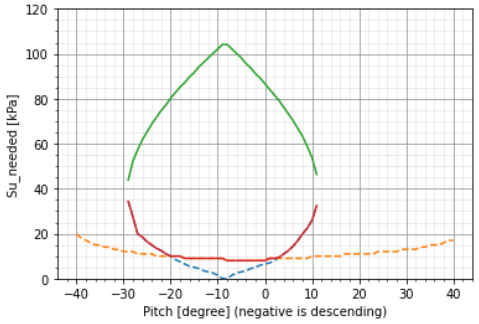

Figure 7.15: CS - $u_{current}$=0.5, $\theta_{current}$ = 180

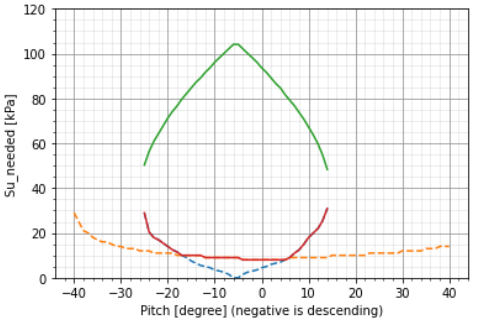

Figure 7.16: CS - $u_{current}$=1, $\theta_{current}$ = 180

CS - Drag coefficient
Since the drag coefficient of the trencher is estimated, it could vary. In order to determine the sensitivity of this estimated parameter, the frontal current is investigated using a drag coefficient of 1, which equals that of a solid cube. A reduction of the drag coefficient leads to a smaller change rate. This process can be observed in Table 7.8 and the figures below.

	BC	U_c=0.5, CD=1	U_c=1, CD=1
Maximum pitch [°]	10	9	8
Minimum pitch [°]	-30	-30	-32
Total operation area ratio [%]	31.0	31.0	31.2
Effective operation area ratio (Pitch < +/-15)[%]	54.4	49.2	64
Su_{needed} min-max (0°) [kPa]	10-85	10-82	11-77
Su_{needed} min-max (5°) [kPa]	15-70	16-68	20-62
Su_{needed} min-max (-5°) [kPa]	9-95	9-95	9-91

Table 7.8: CS - 180° current conditions

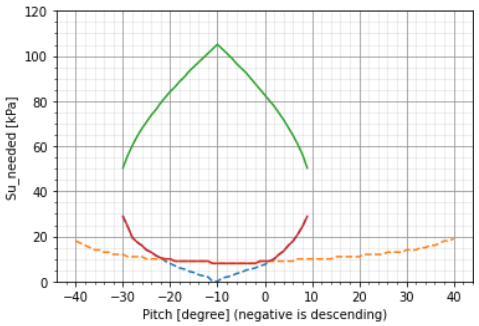

Figure 7.17: CS - $u_{current}$=0.5, Cd= 1.0

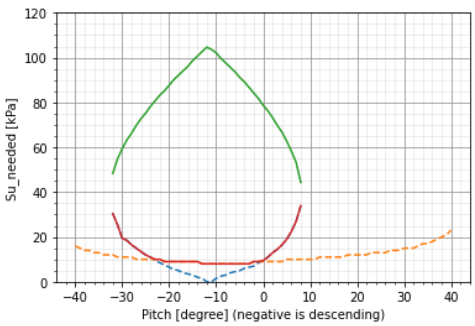

Figure 7.18: CS - $u_{current}$=1.0, Cd= 1.0

CS - Sensitivity
The sensitivity of the soil affects it in two ways: On the one hand, the absolute value of the sensitivity influences the residual shear strength. In addition, it is also important to identify the moment when the residual shear strength kicks in, i.e. when the tracks have shifted so much that that this strength becomes relevant. This moment can be expressed as the position of the element in the link. For example, it may occur already at the second element or not until the 15th element. As previously described, this again depends on the slip ratio and the shear displacement required to achieve the residual shear strength. When there is a shear-displacement graph it can be interpreted with the figure below. The sensitivity is the ratio between the maximum and residual shear strength. The slip ratio cannot be determined before operation. An analysis will have to be made of what is maximally acceptable. The literature gives a value of 0.2, as already explained in chapter 2. However, this means that over a track of 6 metres, 1.2 metres of slip is acceptable.

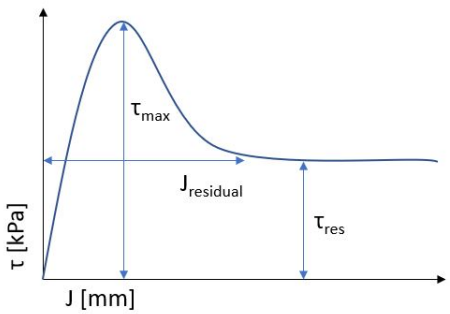

Figure 7.19: Shear-displacement graph interpretation

The results of the influence of sensitivity when only one element has peak shear strength can be seen in the images below. They show that, with increasing sensitivity, the mobility envelope changes. At a sensitivity of 2, the total and effective area ratio increases. At even larger sensitivities, the areas decrease. The increase is due to the greater adhesion forces caused by smaller undrained shear strengths. As a result, the trencher is more mobile in stronger cohesive soils. The exact values are shown in Table 7.9.

	BC	S=2, n_e=1	S=4, n_e=1	S=8, n_e=1	S=16, n_e=1
Maximum pitch [°]	10	9	7	0	-6
Minimum pitch [°]	-30	-29	-27	-19	-13
Total operation area ratio [%]	31.0	36.9	25.5	11.7	4.2
Effective operation area ratio[%]	54.4	63.4	47.9	27.3	11.0
Su_{needed} min-max (0°) [kPa]	10-85	23-110	51-110	107-110	-
Su_{needed} min-max (5°) [kPa]	15-70	35-110	75-110	-	-
Su_{needed} min-max (-5°) [kPa]	9-95	10-110	25-110	55-110	-

Table 7.9: CS - Sensitivity

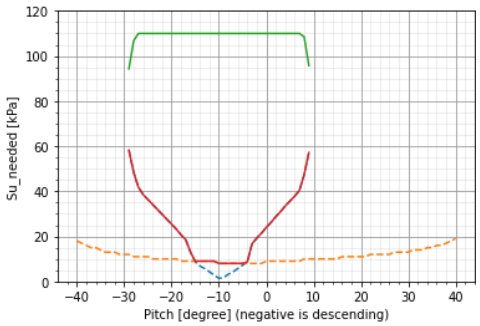

Figure 7.20: CS - S=2

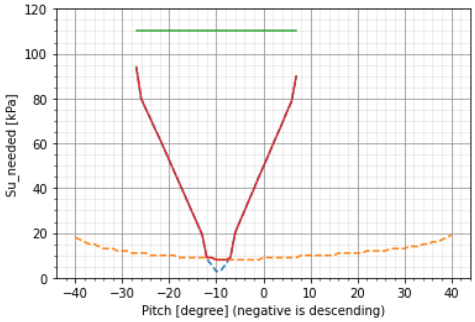

Figure 7.21: CS - S=4

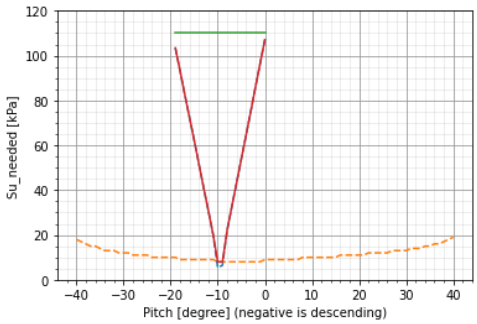

Figure 7.22: CS - S=8

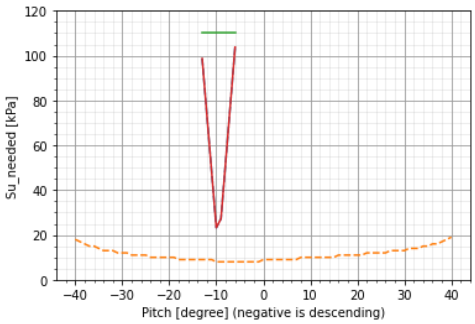

Figure 7.23: CS - S=16

When the residual shear strength enters at a higher element, the changes are in a similar direction but at lower rates. The areas become larger at a higher element. The values can be found in Table 7.10. The figures below show the mobility envelopes.

	BC	S=4, n_e=7	S=4, n_e=15	S=4, n_e=22
Maximum pitch [°]	10	5	4	6
Minimum pitch [°]	-30	-24	-24	-26
Total operation area ratio [%]	31.0	26.5	28.0	29.2
Effective operation area ratio[%]	54.4	50.3	51.9	53.3
Su_{needed} min-max (0°) [kPa]	10-85	40-110	20-102	15-90
Su_{needed} min-max (5°) [kPa]	15-70	77-90	45-75	25-68
Su_{needed} min-max (-5°) [kPa]	9-95	15-110	9-110	9-105

Table 7.10: CS - Sensitivity, $n_{element}$

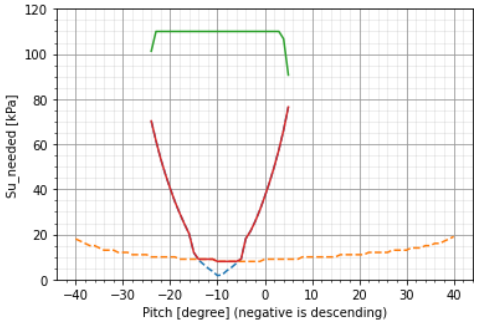

Figure 7.24: CS - S=4, $n_{element,res}$=7

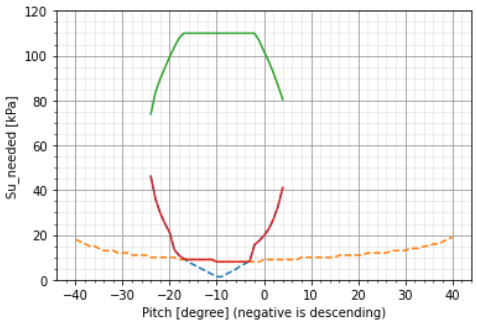

Figure 7.25: CS - S=4, $n_{element,res}$=15

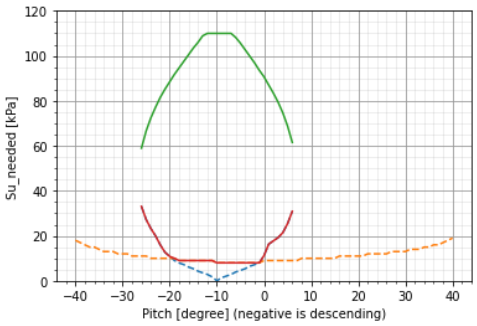

Figure 7.26: CS - S=4, $n_{element,res}$=22

CS - Slip ratio

Here, the influence of the slip ratio is considered. Soil sensitivity is set at 1, so that the changes in slip ratio only affect the dynamic sinking of the trencher. Table 7.11 shows the results, and the mobility envelopes are shown in the figures below.

	BC	i_{sr}=0.3	i_{sr}=0.1	i_{sr}=0.05
Maximum pitch [°]	10	9	10	10
Minimum pitch [°]	-30	-29	-30	-30
Total operation area ratio [%]	31.0	29.6	32.1	32.6
Effective operation area ratio (Pitch < +/-15)[%]	54.4	52.2	56.1	56.8
Su_{needed} min-max (0°) [kPa]	10-85	10-82	10-85	10-86
Su_{needed} min-max (5°) [kPa]	15-70	15-68	15-72	15-73
Su_{needed} min-max (-5°) [kPa]	9-95	9-93	9-97	9-98

Table 7.11: CS - Slip ratio

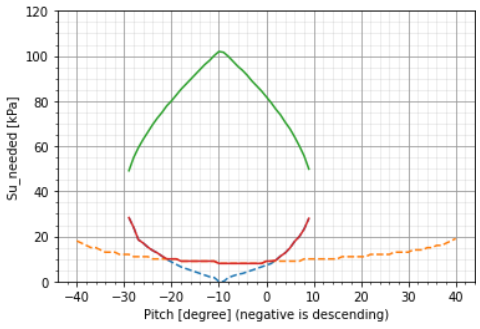

Figure 7.27: CS - i_{sr}=0.3

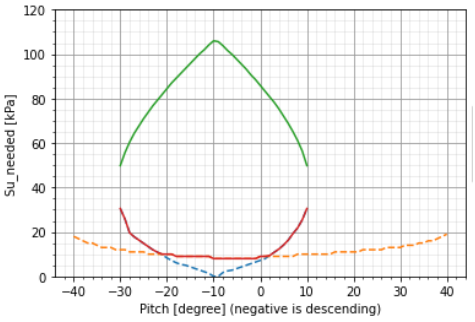

Figure 7.28: CS - i_{sr}=0.1

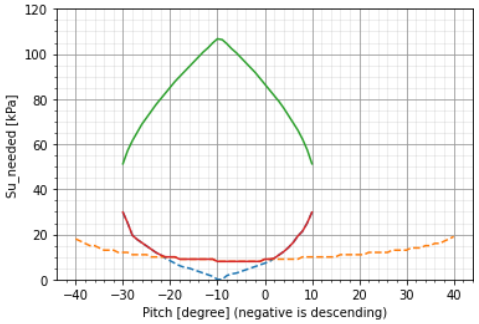

Figure 7.29: CS - i_{sr}=0.05

CS - Elasticity

When the modulus of elasticity changes, the initial settlement will change. This in turn affects the bulldozing and static compaction resistance. As can be seen from Figures and Table 7.12, the soil has a negative influence as it becomes less stiff (more elastic) and a positive influence as it becomes stiffer. Note that, as with the slip ratio, the change rate is quite small.

	BC	kc=100, i=0.05	kc=500, i=0.05	kc=1000, i=0.05
Maximum pitch [°]	10	8	10	11
Minimum pitch [°]	-30	-28	-30	-31
Total operation area ratio [%]	31.0	28.2	32.6	33.2
Effective operation area ratio[%]	54.4	50.4	56.8	57.6
Su_{needed} min-max (0°) [kPa]	10-85	10-82	10-86	10-86
Su_{needed} min-max (5°) [kPa]	15-70	20-65	15-73	15-73
Su_{needed} min-max (-5°) [kPa]	9-95	9-93	9-98	9-100

Table 7.12: CS - Elasticity

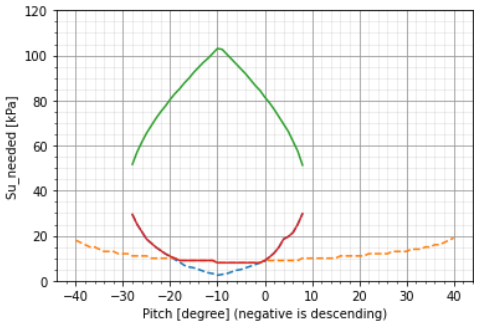

Figure 7.30: CS - kc=100, i=0.05

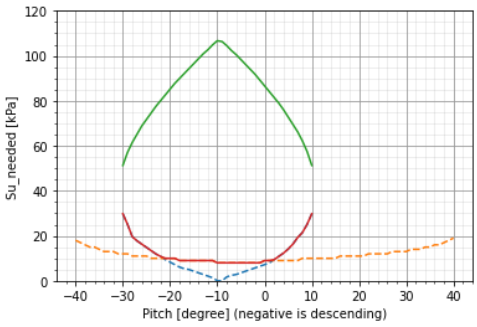

Figure 7.31: CS - kc=500, i=0.05

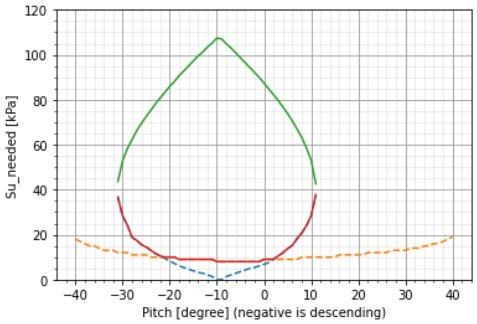

Figure 7.32: CS - kc=1000, i=0.05

7.1.2. Granular soils

The input values for the base case for granular soils are shown in table 7.13. As with the cohesive soils, the base case is without flow and a roll angle. The median particle size is 0.0003 m, and the grading of the particle size is five. The relation between the internal friction angle and the relative density that is used is shown in the equation below.

$$\phi = 25 + 0.25 * RD \tag{7.1}$$

Input parameters			
Roll [deg]	0	d_{50} [m]	0.00025
$\theta_{current}$ [deg]	0	$\frac{d_{50}}{d_{10}}$ [-]	1.5
$u_{current}$ [m/s]	0	i_{sr} [-]	0.2
z_{trench} [m]	3.3	$v_{progress}$ [m/s]	0.27
Cd [-]	2	E' [kPa]	25000
γ' $[kN/m^3]$	8	ν [-]	0.3

Table 7.13: GS - Base case input parameters

Figure 7.33 shows the mobility envelope of the CBT2400 trencher in the base case. The base case mobility in granular soils is larger than in cohesive soils. The total operation area ratio of the base case is 52.7 %, and the effective operation area ratio is 74.3 %. For pitch angles between the -30 and 10 degrees, the lower limit is determined by vertical stability. If this limit is not met, the trencher will sink. The limit for this region is between an RD of 20 % at a pitch of -6 degrees and an RD of 30% at a pitch of -30 and 12 degrees. Outside these borders, the trencher will dig itself in and requires an RD of over 30 %. The maximum pitch that the trencher can drive is 25 degrees. The upper limit is not decisive at almost any pitch. A relative density of 100 is a theoretical and practical limit that cannot be broken. The most important outcomes are shown in Table 7.14. From an angle of 15 degrees a lowering of the upper limit can be seen. It moves with a small jump which means that the traction force between a relative density of 90% and 100% is almost the same. The reason for this is that the grousers no

longer penetrate, which causes a lowering in traction force, and from there the traction force increases less since it is depending on the external friction angle.

	BC
Maximum pitch [°]	25
Minimum pitch [°]	-40
Total operation area ratio [%]	52.6
Effective operation area ratio [%]	74.3
RD_{needed} min-max (0°) [%]	23-100
RD_{needed} min-max (5°) [%]	25-100
RD_{needed} min-max (-5°) [%]	20-100

Table 7.14: GS - Base case results

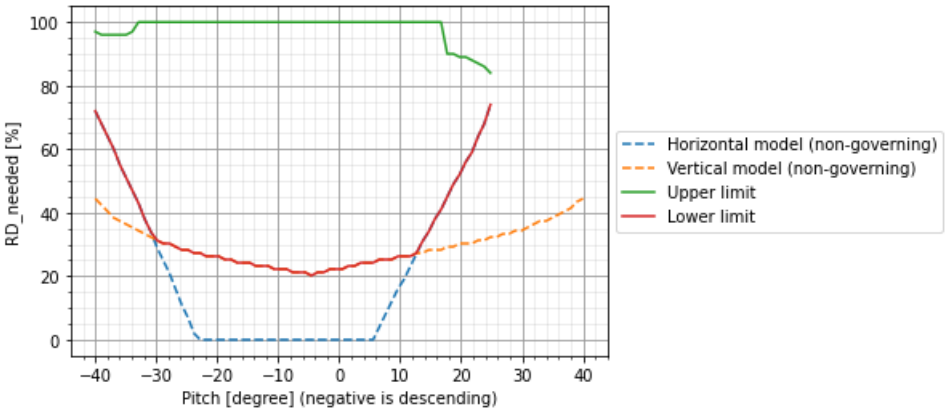

Figure 7.33: Base case granular soil

GS - Roll

Both operational area ratios decrease with increasing roll angles. With a roll angle of 5 degrees the total operation area ratio decreases with 5.9% compared with the base case. The effective operation area ratio decreases with 3.3% compared with the base case. This is caused by the steeper horizontal lower limit borders. The maximum and minimum pitch angles decrease as well. When the roll is 10 degrees, the areas become even smaller: The total operation area ratio is 41.4 %, the effective operation area ratio 65.3 %. At a roll angle of 15 degrees, the total ratio becomes 34.1%, with an effective ratio of 55.9%. This means a total decrease of almost 30% and an effective decrease of 15%, both compared with the base case. Table 7.15 shows the outcomes.

	BC	Roll=5	Roll=10	Roll=15
Maximum pitch [°]	25	21	17	12
Minimum pitch [°]	-40	-40	-38	-34
Total operation area ratio [%]	52.6	46.7	41.4	34.1
Effective operation area ratio [%]	74.3	71.0	65.3	55.9
RD_{needed} min-max (0°) [%]	23-100	25-100	25-100	26-100
RD_{needed} min-max (5°) [%]	25-100	25-100	27-100	30-100
RD_{needed} min-max (-5°) [%]	20-100	22-100	23-100	25-100

Table 7.15: GS - Roll case results

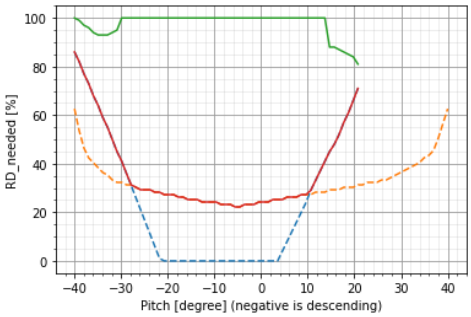

Figure 7.34: GS - Roll = 5

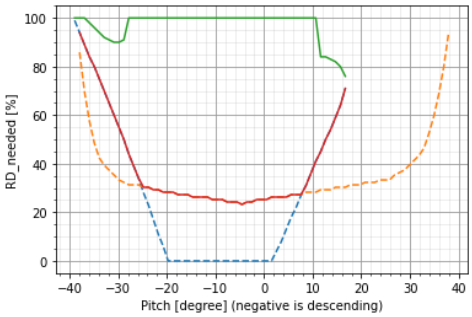

Figure 7.35: GS - Roll = 10

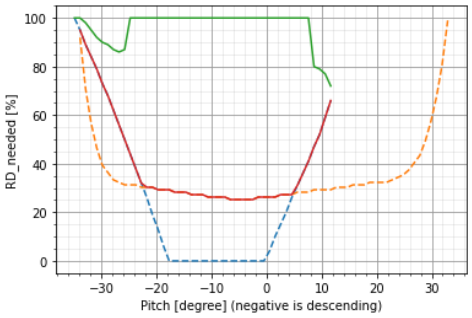

Figure 7.36: GS - Roll = 15

GS - Current

For the flow, again, different scenarios are considered. Firstly, frontal impacts for flow velocities of 0.5 m/s, 1.0 m/s and 2 m/s. As with the cohesive soils, we can see the mobility envelope move to the negative pitch angles again. The total operation area ratio decreases, as well as the effective operation area ratio. At a flow rate of 2 m/s, the total operation area ratio decreases by 6.6%, the effective ratio by 24.2%. The maximum pitch angle at a flow rate of 2 m/s is 15 degrees. The other results can be found in Table 7.4.

	BC	$U_c = 0.5$	$U_c = 1.0$	$U_c = 2.0$
Maximum pitch [°]	25	25	23	15
Minimum pitch [°]	-40	-40	-40	-40
Total operation area ratio [%]	52.6	52.4	51.6	46.0
Effective operation area ratio [%]	74.3	73.7	70.7	50.5
RD_{needed} min-max (0°) [%]	23-100	23-100	25-100	37-100
RD_{needed} min-max (5°) [%]	25-100	25-100	27-100	53-95
RD_{needed} min-max (-5°) [%]	20-100	21-100	23-100	30-100

Table 7.16: GS - Frontal current case results

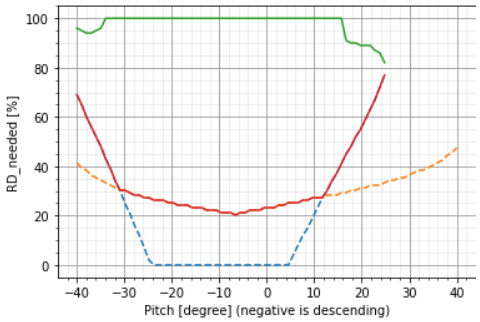

Figure 7.37: GS - $U_{current} = 0.5$

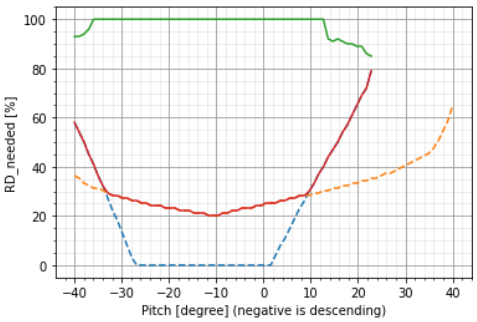

Figure 7.38: GS - $U_{current} = 1.0$

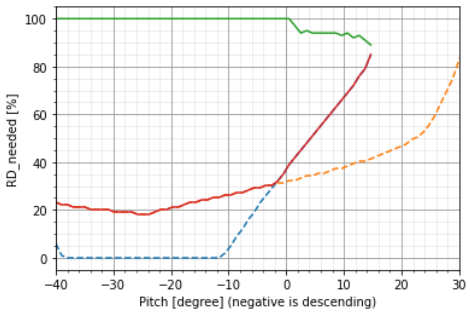

Figure 7.39: GS - $U_{current} = 2.0$

When the flow falls at an angle of 90 degrees, i.e. perpendicular to the direction of travel of the trencher, we see the same changes as with a roll angle. The mobility surfaces become more limited and the borders steeper. At a current speed of 2 m/s, the maximum pitch is only 7 degrees, and a minimum relative density of 30% is required for a horizontal seabed. The results can be found in Table 7.17, and the figures below show the mobility envelopes.

	BC	$U_c = 0.5$, θ=90	$U_c = 1.0$, θ=90	$U_c = 2.0$, θ=90
Maximum pitch [°]	25	24	21	7
Minimum pitch [°]	-40	-40	-40	-29
Total operation area ratio [%]	52.6	51.1	46.2	24.9
Effective operation area ratio [%]	74.3	73.6	70.6	44.7
RD_{needed} min-max (0°) [%]	23-100	23-100	25-100	30-100
RD_{needed} min-max (5°) [%]	25-100	25-100	26-100	57-76
RD_{needed} min-max (-5°) [%]	20-100	21-100	23-100	29-100

Table 7.17: GS - Perpendicular current case results

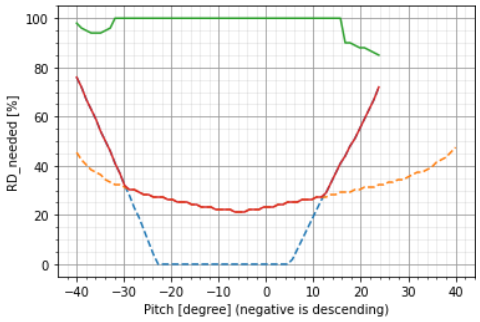

Figure 7.40: CS - $u_{current}$=0.5, θ_c = 90

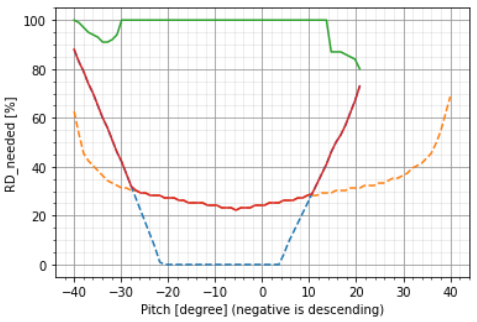

Figure 7.41: CS - $u_{current}$=1.0, θ_c = 90

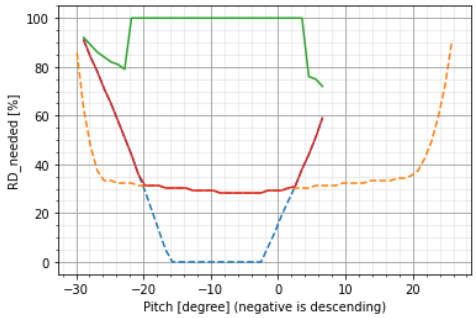

Figure 7.42: CS - $u_{current}$=2.0, θ_c = 90

When the flow makes an impact at an angle of 45 degrees, the drag force caused by the flow will be transmitted partly in a frontal direction and partly in a perpendicular direction. From the previous cases, we can deduce that the mobility envelopes will both move to the negative pitch angles and the borders will also become steeper. Both these processes have great impact on the effective operation area ratio. The results are summarised in Table 7.18, and the mobility envelopes are displayed in the figures below.

	BC	$U_c = 0.5$, θ=45	$U_c = 1.0$, θ=45	$U_c = 2.0$, θ=45
Maximum pitch [°]	25	24	20	4
Minimum pitch [°]	-40	-40	-40	-40
Total operation area ratio [%]	52.6	51.3	47.5	32.0
Effective operation area ratio [%]	74.3	73.2	68.6	31.4
RD_{needed} min-max (0°) [%]	23-100	23-100	25-100	57-85
RD_{needed} min-max (5°) [%]	25-100	25-100	27-100	-
RD_{needed} min-max (-5°) [%]	20-100	21-100	23-100	35-100

Table 7.18: GS - 45° current case results

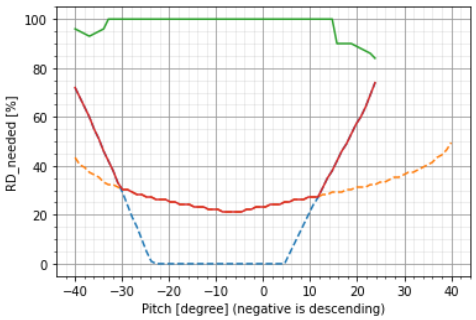

Figure 7.43: CS - $u_{current}$=0.5, θ_c = 45

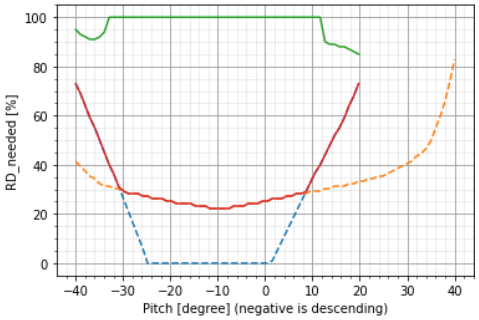

Figure 7.44: CS - $u_{current}$=1.0, θ_c = 45

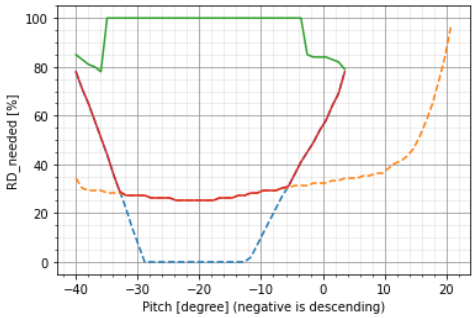

Figure 7.45: CS - $u_{current}$=2.0, θ_c = 45

GS - Elasticity modulus

With the effective elasticity modulus, the influence of the initial settlement on sandy soils can be determined. In the base case, a modulus of 25,000 kPa is used. In addition, for this case, we investigate a modulus of 10,000 kPa, 50,000 kPa and 80,000 kPa. As can be seen in both the graphs and the table with the results, the effective elasticity modulus, and thus the bulldozing and static compaction resistance, has a minor influence on the mobility of the trencher. Beyond 50,000 kPa, there is no difference in mobility anymore. With a modulus of 10,000 kPa, a small decrease in mobility can be observed.

	BC	E'=10,000	E'=50,000	E'=80,000
Maximum pitch [°]	25	24	26	26
Minimum pitch [°]	-40	-40	-40	-40
Total operation area ratio [%]	52.7	51.5	53.2	53.2
Effective operation area ratio [%]	74.3	73.8	74.3	74.3
RD_{needed} min-max (0°) [%]	23-100	23-100	23-100	23-100
RD_{needed} min-max (5°) [%]	25-100	25-100	25-100 25-100	
RD_{needed} min-max (-5°) [%]	20-100	20-100	20-100	20-100

Table 7.19: GS - Elasticity case results

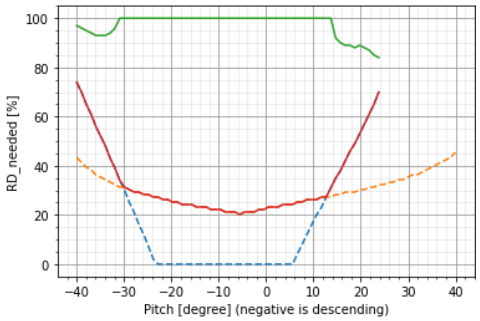

Figure 7.46: GS - E' = 10,000 kPa

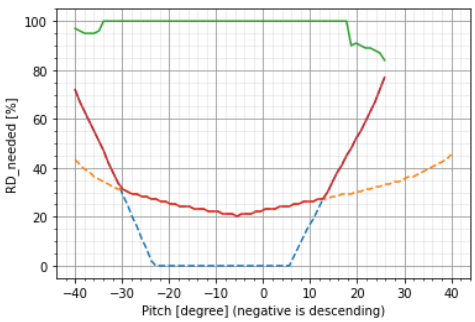

Figure 7.47: GS - E' = 50,000 kPa

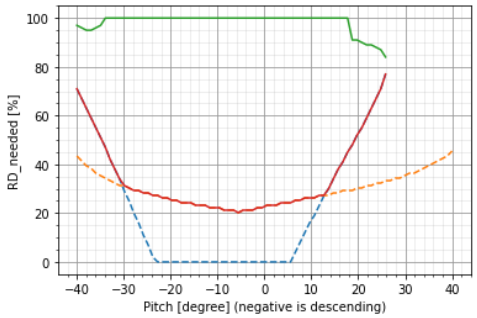

Figure 7.48: GS - E' = 80,000 kPa

GS - Median grain size

With equal grading but different median particle sizes, there is no difference at all in the mobility envelopes. The results are summarised in Table 7.20, and the relevant graphs are shown in the figures below.

	BC	d50 = 0.0001 m	d50 = 0.001 m
Maximum pitch [°]	25	25	25
Minimum pitch [°]	-40	-40	-40
Total operation area ratio [%]	52.7	52.7	52.6
Effective operation area ratio [%]	74.3	74.3	74.3
RD_{needed} min-max (0°) [%]	23-100	23-100	23-100
RD_{needed} min-max (5°) [%]	25-100	25-100	25-100
RD_{needed} min-max (-5°) [%]	20-100	20-100	20-100

Table 7.20: GS - Median particle size case results

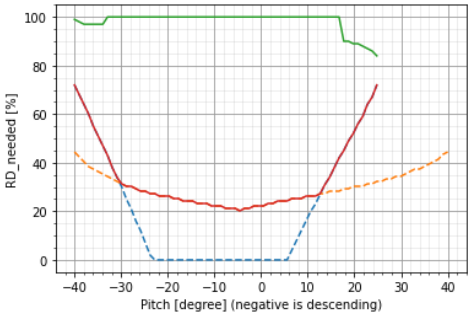

Figure 7.49: GS - d_{50} = 0.0001 m

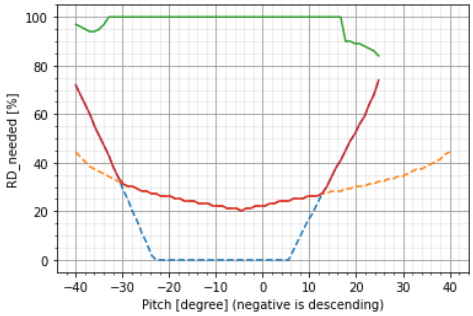

Figure 7.50: GS - d_{50} = 0.001 m

GS - Particle grading

By fluctuating the particle grading, the influence of the effective particle size can be examined. This ultimately influences permeability and thus the degree of dilatancy or contractancy. In these samples, the gradings three, seven and ten are included. The median particle size is 0.0001 m, which is already a small grain of sand. The figures for the mobility envelopes show the dilatancy and contractancy processes at gradings 7 and 10. However, in these conditions mobility will increase in higher relative densities. Nevertheless, a small decrease can be seen in the effective area ratio. This is reflected in the table with the results for this case.

	BC	$\frac{d50}{d10}$ = 3	$\frac{d50}{d10}$ = 7	$\frac{d50}{d10}$ = 10
Maximum pitch [°]	25	25	26	29
Minimum pitch [°]	-40	-40	-40	-40
Total operation area ratio [%]	52.7	52.6	53.1	53.0
Effective operation area ratio [%]	74.3	74.3	73.8	73.1
RD_{needed} min-max (0°) [%]	23-100	23-100	23-100	23-100
RD_{needed} min-max (5°) [%]	25-100	25-100	25-100	25-100
RD_{needed} min-max (-5°) [%]	20-100	20-100	20-100	20-100

Table 7.21: GS - Particle grading case results

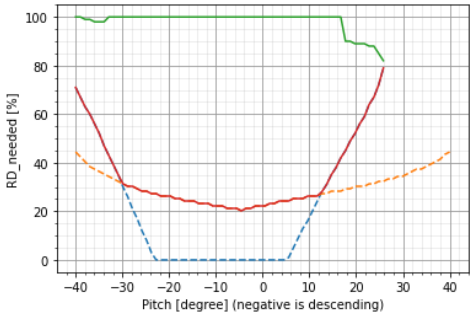

Figure 7.51: GS - d_{50} = 0.0001 m, $\frac{d_{50}}{d_{10}}$ = 3

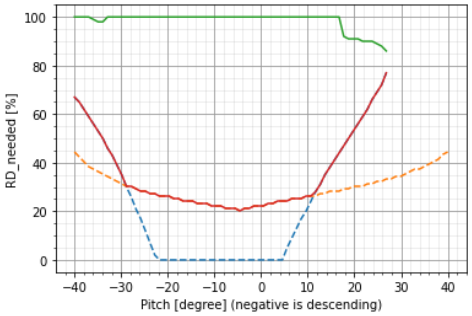

Figure 7.52: GS - d_{50} = 0.0001 m, $\frac{d_{50}}{d_{10}}$ = 7

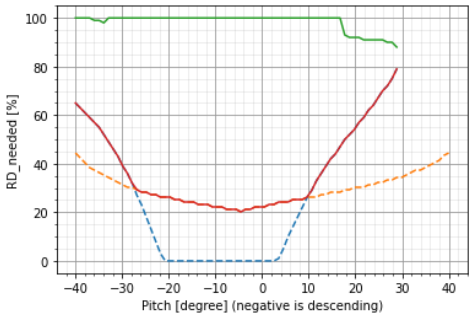

Figure 7.53: GS - d_{50} = 0.0001 m, $\frac{d_{50}}{d_{10}}$ = 10

GS - Progress velocity

The speed of progress also affects the degree of contractancy and dilatancy. In the cases above, the maximum speed of the CBT2400 was taken as an indicator. Here, we will also look at half and one fifth of the maximum speed. What follows from the mobility envelopes is that the degree of dilatancy and contractancy decreases at lower speeds, observable at the straightening of the borders. The results can be found in Table 7.22.

	BC	$v_{progress}$ = 0.028 m/s	$v_{progress}$ = 0.139 m/s
Maximum pitch [°]	29	25	26
Minimum pitch [°]	-40	-40	-40
Total operation area ratio [%]	53.0	52.9	53.1
Effective operation area ratio [%]	73.1	74.2	73.7
RD_{needed} min-max (0°) [%]	23-100	23-100	23-100
RD_{needed} min-max (5°) [%]	25-100	25-100	25-100
RD_{needed} min-max (-5°) [%]	20-100	20-100	20-100

Table 7.22: GS - Progress velocity case results

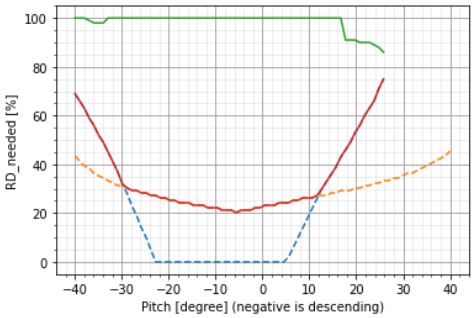

Figure 7.54: GS - v_p = 0.028 m/s,d_{50} = 0.0001 m, $\frac{d_{50}}{d_{10}}$ = 10

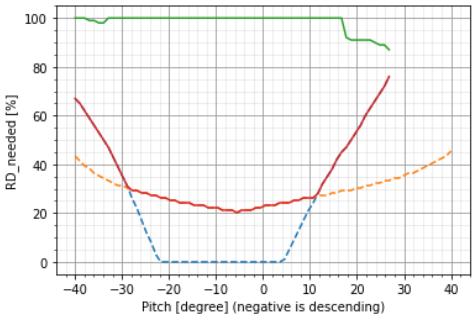

Figure 7.55: GS - v_p = 0.139 m/s,d_{50} = 0.0001 m, $\frac{d_{50}}{d_{10}}$ = 10

7.2. Trencher improvements

In this section, we will look at whether the mobility of the CBT2400 can be improved by making minor adjustments to the trencher. The dimensions of the tracks (length x width), the length of the grouser, and the moving of the centre of gravity in the longitudinal direction will be examined. Any changes will be benchmarked against the performance in the base case.

7.2.1. Track dimensions

The first two adjustments under consideration are to widen or lengthen the tracks by half a metre. Widening the tracks would be easier as it would only require the mounting of other elements on the chain. Lengthening the tracks is more cumbersome, as the whole chassis would need to be changed, but might nevertheless be worth considering.

Widening of tracks

It could be interesting to widen the tracks. Doing so will provide extra area, so that the applied pressure will decrease. In addition, it would enlarge the shearing areas in the horizontal traction model. Figure 7.56, shows the mobility envelope in cohesive soils. The total operation area ratio is 42.5 %, and the effective operation area ratio is 67.7 %. This constitutes an increase of 11.5% and 13.3%, respectively. Also, the minimum and maximum pitch angles increased with a larger width in cohesive soils. In granular soils, there is also an increase in mobility. While the maximum and minimum pitch angles show almost no change, the mobility in granular soils with lower relative density improves. This can also be seen in the operation areas. The total operation ratio increased with 7.6%, and the effective operation ratio increased with 11.3 %.

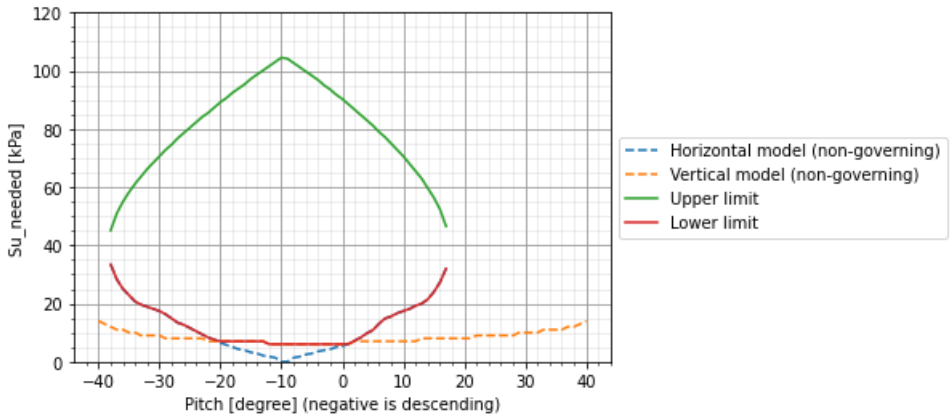

Figure 7.56: Cohesive soil - Width of track = 2.0 m

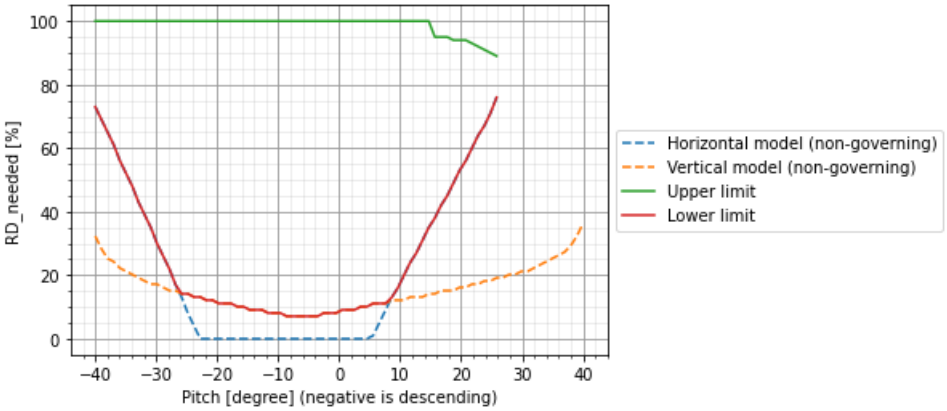

Figure 7.57: Granular soil - Width of track = 2.0 m

Length of tracks

Longer tracks also achieve an increase in the mobility of the CBT2400, although significantly smaller in both cohesive and granular soils. The total operation area ratio in cohesive soils grows with 3.6%, while the effective operation area ratio grows with 4.5%. In granular soils, the total operation area ratio grows with 2.1% and the effective operation area ratio with 2.1%. All results for granular soils are shown in Table 7.24; the results for cohesive soils are presented in Table 7.23.

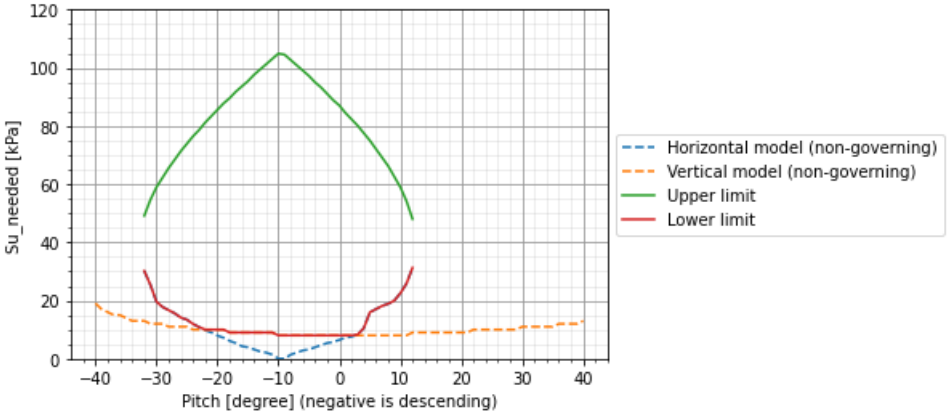

Figure 7.58: Cohesive soil - Length of track = 6.5 m

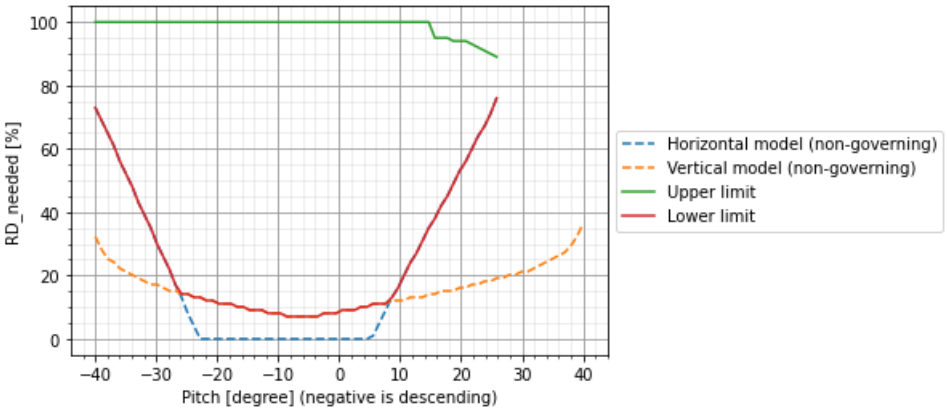

Figure 7.59: Granular soil - Length of track = 6.5 m

	BC	$B_{track} = 2$	$L_{track} = 6.5$
Maximum pitch [°]	10	17	12
Minimum pitch [°]	-30	-38	-32
Total operation area ratio [%]	31.0	42.5	34.6
Effective operation area ratio (Pitch < +/-15) [%]	54.4	67.7	59.0
Su_{needed} min-max (0°) [kPa]	10-85	6-90	10-87
Su_{needed} min-max (5°) [kPa]	15-70	12-80	17-75
Su_{needed} min-max (-5°) [kPa]	9-95	6-98	9-97

Table 7.23: Cohesive soils - Track dimensions

	BC	$B_{track} = 2$	$L_{track} = 6.5$
Maximum pitch [°]	25	26	27
Minimum pitch [°]	-40	-40	-40
Total operation area ratio [%]	52.6	60.2	54.7
Effective operation area ratio [%]	74.3	85.6	76.4
RD_{needed} min-max (0°) [%]	23-100	9-100	9-100
RD_{needed} min-max (5°) [%]	25-100	10-100	10-100
RD_{needed} min-max (-5°) [%]	20-100	7-100	7-100

Table 7.24: Granular soils - Track dimensions

7.2.2. Grouser dimensions

The grouser is an important part of the track because it determines the shear mechanisms that provide the traction. The CBT2400 now has grousers with a length of 13 cm. To investigate whether its mobility can be improved through grouser selection, two cases are examined: one without grousers, i.e. a flat track, and one with a grouser with a length of 4 cm. In theory, a grouser with a smaller length will ensure more soil-soil shear interaction, and the element will achieve full penetration faster. A flat track, on the other hand, is designed to use the entire surface in a track-soil shear interaction. The mobility envelope of the smaller grouser in cohesive soils is shown in Figure 7.60. In the lower part of the envelope, an increase can be observed, whereas the section above 50 kPa shows a significant decrease in mobility. The total operation area ratio is 21.9 %, which constitutes a decrease. The same applies to the effective area ratio, which amounts to 40.1 percent with a grouser length of 4 cm. Figure 7.61 displays the mobility envelope of the CBT2400 with a smaller grouser in granular soils. In contrast with the cohesive soils, an increase in mobility can be observed here. This is especially apparent in the total operation area ratio, which rises to 63.1 percent. The effective operation area ratio remains almost stable, only growing with 0.4 percent.

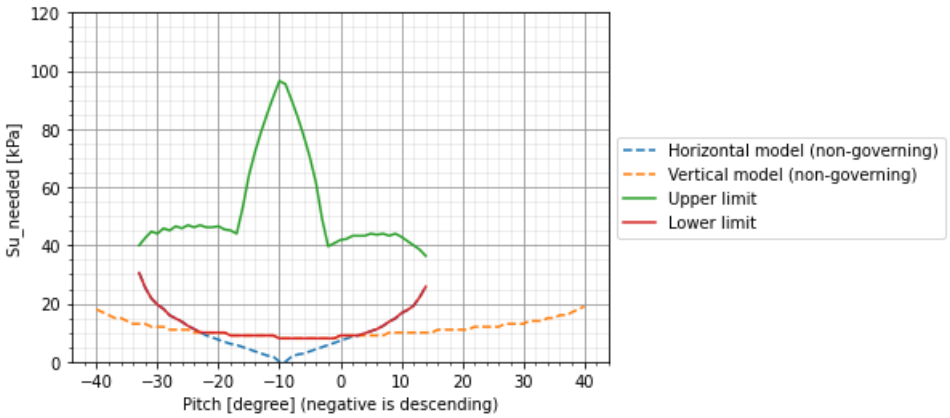

Figure 7.60: Cohesive soil - Length of grouser = 4 cm

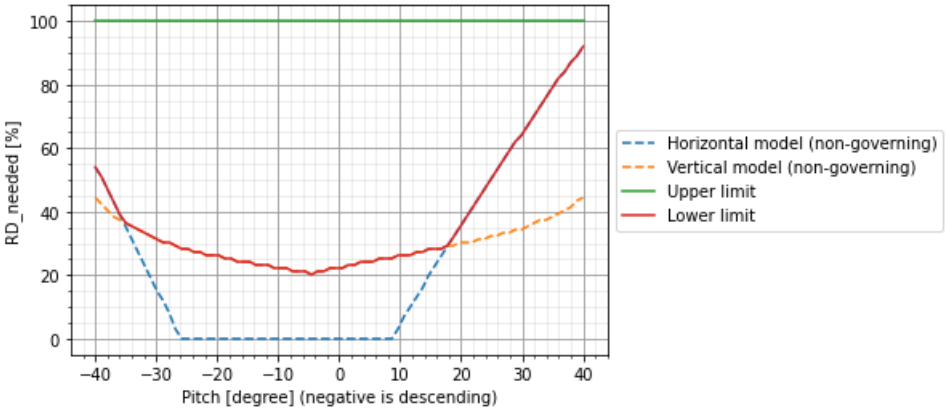

Figure 7.61: Granular soil - Length of grouser = 4 cm

In the case of a flat track, the entire surface will be used to achieve track-soil shear interaction. In this situation, the shear force depends on adhesion and friction. In Figure 7.62, the mobility envelope for a flat track belt in cohesive soils is displayed. In these soils, both the total and effective ratios increase. The total operation area becomes 51.1 %, and the effective operation area ratio becomes 73.2 percent. In granular soils, however, the mobility of the flat track belt is less than with the original track belt: the total operation area ratio with a flat track belt drops to 43.0 %, and the effective area ratio is 70.0 %. Table 7.25 shows the results for cohesive soils, and Table 7.26 shows the results for granular soils.

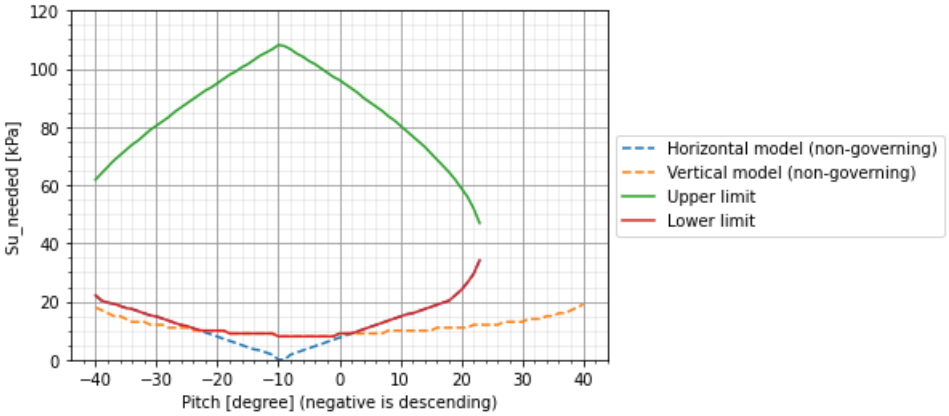

Figure 7.62: Cohesive soil - Flat track belt

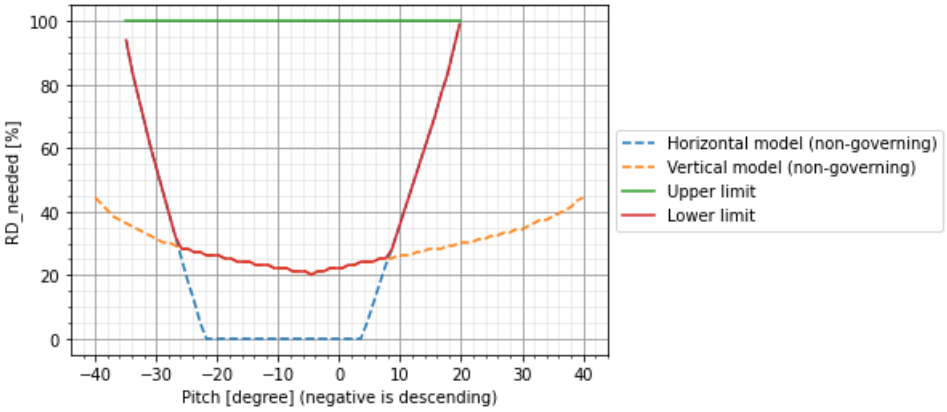

Figure 7.63: Granular soil - Flat track belt

	BC	$L_{grouser} = 0.05$	Flat track
Maximum pitch [°]	10	14	23
Minimum pitch [°]	-30	-33	-40
Total operation area ratio [%]	31.0	21.9	51.1
Effective operation area ratio (Pitch < +/-15) [%]	54.4	40.1	73.2
Su_{needed} min-max (0°) [kPa]	10-85	10-43	10-96
Su_{needed} min-max (5°) [kPa]	15-70	12-43	12-77
Su_{needed} min-max (-5°) [kPa]	9-95	9-70	9-103

Table 7.25: Cohesive soils - Track dimensions

	BC	$L_{grouser} = 0.05$	Flat track
Maximum pitch [°]	25	40	20
Minimum pitch [°]	-40	-40	-35
Total operation area ratio [%]	52.6	63.1	43.0
Effective operation area ratio [%]	74.3	74.7	70.0
RD_{needed} min-max (0°) [%]	23-100	23-100	23-100
RD_{needed} min-max (5°) [%]	25-100	25-100	25-100
RD_{needed} min-max (-5°) [%]	20-100	20-100	20-100

Table 7.26: Granular soils - Track dimensions

7.2.3. Center of gravity

In this case study, it is tested whether a shift in the centre of gravity of half a metre backwards or forwards in the longitudinal direction improves mobility. The figures below show the mobility envelopes for cohesive soils. Though the shapes of the graphs do change, the areas hardly change at all. The total operation area ratio changes with less than half a percent in both cases; the effective operation area ratio changes with less than one percent. Table 7.27, displays the results.

	BC	$y_{weight} = 0.5mfor$	$y_{weight} = 0.5mback$
Maximum pitch [°]	10	10	10
Minimum pitch [°]	-30	-31	-30
Total operation area ratio [%]	31.0	31.1	31.2
Effective operation area ratio (Pitch < +/-15) [%]	54.4	54.0	55.0
Su_{needed} min-max (0°) [kPa]	10-85	10-84	10-84
Su_{needed} min-max (5°) [kPa]	15-70	11-70	15-70
Su_{needed} min-max (-5°) [kPa]	9-95	10-95	10-95

Table 7.27: Cohesive soils - Center of gravity

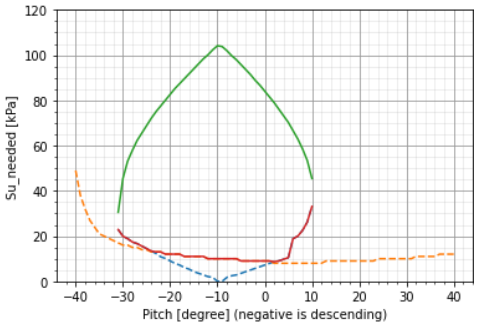

Figure 7.64: Cohesive soil - COG 0.5 m forwards

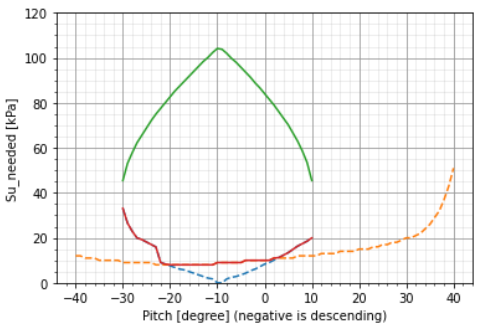

Figure 7.65: Cohesive soil - COG 0.5 m backwards

In granular soils, mobility deteriorates when the weight is moved half a metre forward. The total ratio drops by 2.5 percent, and the effective ratio drops by 0.7 percent. When the weight is shifted half a

metre backwards, the total ratio increases with 1.1 percent. However, the effective area drops with 3.1 percent. The results are shown in Table 7.28, and the mobility envelopes are shown below.

	BC	$y_{weight} = 0.5mfor$	$y_{weight} = 0.5mback$
Maximum pitch [°]	25	23	30
Minimum pitch [°]	-40	-40	-40
Total operation area ratio [%]	52.6	50.1	53.7
Effective operation area ratio [%]	74.3	73.6	71.2
RD_{needed} min-max (0°) [%]	23-100	23-100	28-100
RD_{needed} min-max (5°) [%]	25-100	20-100	30-100
RD_{needed} min-max (-5°) [%]	20-100	25-100	25-100

Table 7.28: Granular soils - Center of gravity

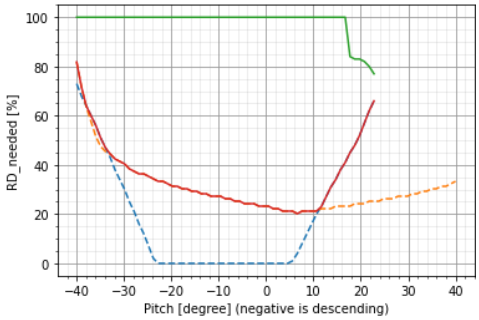

Figure 7.66: Granular soil - COG 0.5 m forwards

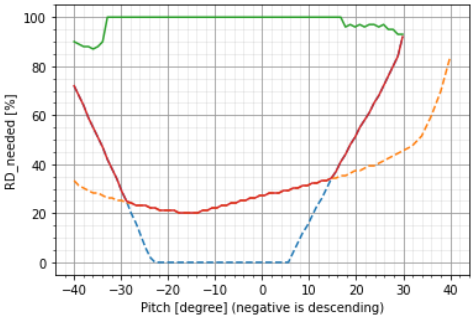

Figure 7.67: Granular soil - COG 0.5 m backwards

7.3. Validation

7.3.1. CBT2400 - Borssele case

On the project in Borssele, the trencher sank during initial placement. This means that there was no vertical stability. This can be seen in the mobility envelopes, where soil strength will be below the yellow line. In order to approach the case as accurately as possible and get a good idea of whether the model works well, the ground data must first be properly mapped out. The model will then be used to check whether the data corresponds to reality. The failure location was between KP41 and KP40 and is shown as a red square in Figure 7.68. As can be seen in the figure, the closest soil tests were carried out in two locations. The soil conditions at the failure location itself will therefore be approximated by taking the average soil conditions of those two locations.

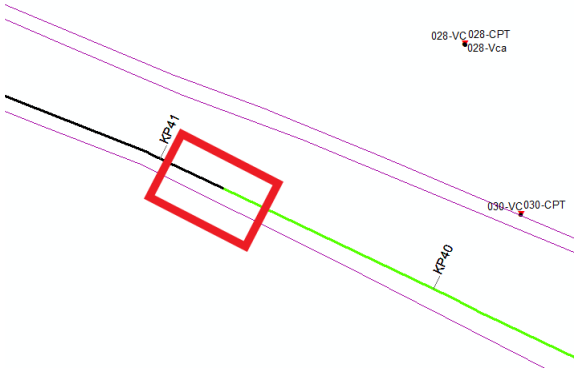

Figure 7.68: Failure location Borssele

At both test sites, a CPT test was performed, and the particle size distribution was determined. For the 030 location, the tests are shown in Figure 7.69 and Figure 7.70, and for the 028 location the tests

are shown in Figure 7.71 and Figure 7.72. The CPT tests cover the first two meters, and the particle size distribution covers the first meter. Finally, the relative density parameter is estimated by taking the average of the first half metre of the soil. The median and d_{10} directly follow from the particle distribution tests. For the relative density, the red line will be used, which is the CPT interpretation of Kulhawy & Mayne (1990). The mean relative density is 20% at location 030 and 25% at location 028. The median particle size at location 030 is 0.1 mm, and the d_{10} is 0.016 mm. At location 028, the median particle size is 0.4 mm, and the d_{10} is 0.016 mm.

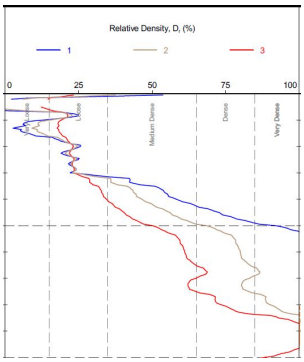

Figure 7.69: CPT Borssele - 030

PARTICLE SIZE (mm)	PERCENT PASSING
4.00	100
2.00	99
1.40	99
1.00	99
0.71	98
0.500	97
0.355	93
0.250	87
0.180	83
0.125	73
0.090	33
0.063	16
0.0450	14
0.0380	13
0.0200	11
0.0160	10
0.0020	7

Figure 7.70: PSD Borssele - 030

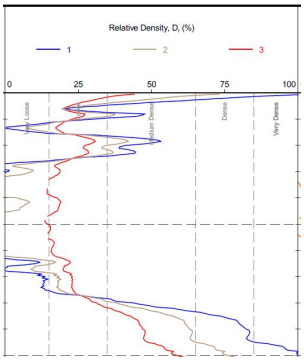

Figure 7.71: CPT Borssele - 028

PARTICLE SIZE (mm)	PERCENT PASSING
4.00	100
2.00	99
1.40	95
1.00	88
0.71	81
0.500	64
0.355	42
0.250	29
0.180	22
0.125	19
0.090	16
0.063	13
0.0450	12
0.0380	11
0.0200	11
0.0160	10
0.0020	6

Figure 7.72: PSD Borssele - 028

From the soil parameters determined earlier, and with the knowledge that the trencher failed during placement on the seabed, the input parameters can be determined. Since the bathymetry is not known, a roll angle and flow velocity of 0 are assumed. The pitch angle is less important since the model loops through that value. The progress velocity and trench depth are both zero, given that the trencher failed during placement. All input values can be found in Table 7.29.

Input parameters			
Roll [deg]	0	d_{50} [m]	0.00025
$\theta_{current}$ [deg]	0	d_{10} [m]	0.000016
$u_{current}$ [m/s]	0	i_{sr} [-]	0.2
z_{trench} [m]	0	$v_{progress}$ [m/s]	0.0
Cd [-]	2	E' [kPa]	25000
γ $[kN/m^3]$	8	ν [-]	0.3

Table 7.29: GS - Borssele input parameters

Figure 7.73, shows the mobility envelope of Borssele. The purple line represents the assumed relative density at the failure location. As can be seen, for almost all pitches, the trencher would sink in the

ground. Only around a negative pitch of 20 degrees, the trencher would not sink. However, it is unlikely for a trencher to be placed on a seabed at an angle of 20 degrees. It can be observed that the vertical stability becomes worse if there are no operational forces and the vertical stability becomes governing for the larger part of the mobility.

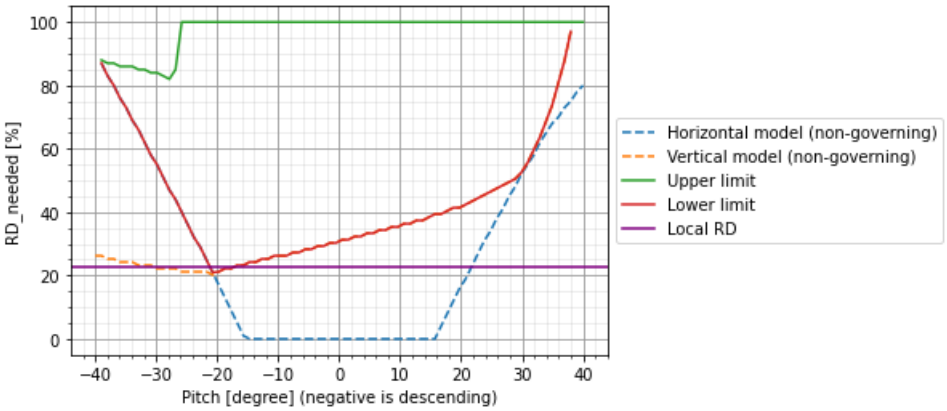

Figure 7.73: Mobility envelope - Borssele case

7.3.2. CBT2400 - Moray east case

During the Moray East case, there were two moments where the trencher slipped while both the cutter and the jet sword were operating. The slippage was measured by a different track speed between the starboard and port-side tracks. After the trencher had slipped, it drove back a bit, then followed the same trajectory without the cutter and jet sword operating. The memo produced after the trencher had slipped also mentions a soft slippery layer, which could indicate the presence of a soft clay layer. The trajectory between wind turbines OSP2 and G17 will be used as a case to validate the horizontal part of the model.

One of the difficulties in the Moray East area is that the soil conditions vary. This makes it difficult to estimate exact soil conditions at the failure location. In addition, the soil profile suggests the presence of currents, indicated by the channels visible on the depth map. When the nearest CPT is used to determine the soil conditions, the soil will certainly be strong enough to allow mobility at the failure location. However, by analysing the circumstances in which this CPT is done, it can be concluded that those are different to the circumstances at the failure location. The red cross in Figure 7.74 shows the failure location while the nearest CPT is shown with a red circle. The different shades of yellow already indicate different types of soil on the seabed: the brighter yellow is categorized as sand while the darker yellow consists of sand mixed with gravel. Note that this does not mean that the top layer consists of this type of soil throughout the entire area. When the expected top layer is thin it can be washed away by currents. Another important difference is that the failure location is in a deeper channel while the CPT is not. Because of these differences, a CPT is considered where conditions are more similar to those at the failure site.

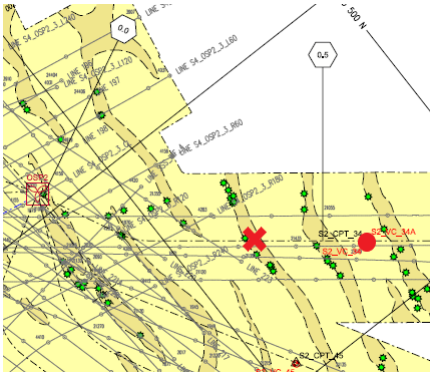

Figure 7.74: Failure location - Seabed Moray East

To get the best possible picture, the CPT test location should be carried out under the same conditions. This means in a deeper channel where, in general, there is a top layer of sand with gravel and where the boulder clay lies slightly buried under the top layer. From Figure 7.75, it can be concluded that the soil a meter under the seabed consists of boulder clay.

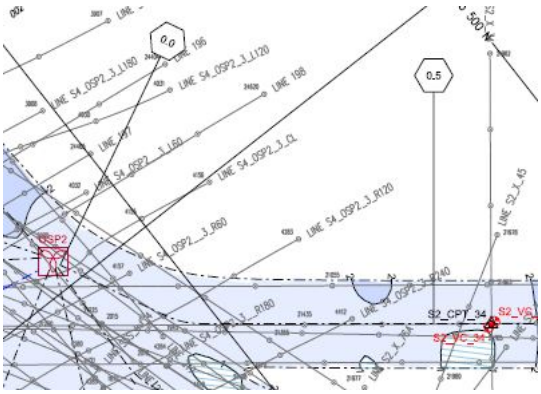

Figure 7.75: Failure location - Shallow soil Moray East

The nearest test location that has more or less the same characteristics is spot 36. The test location is positioned in a deeper channel, the seabed consists of sand and gravel and the boulder clay starts one meter under the seafloor. At this location, two CPT's are performed, the results of which are shown in Figure 7.76. These two measurements, taken in close proximity, show how variable the soil can be around Moray East. Both locations have a weaker top layer of 0.5 m, one composed of granular soil and one of cohesive soil. This difference may be due to the higher flow velocity likely to have occurred in the latter channel, causing the top layer of granular material to be swept away. The second layer, till one meter deep, consists of a dense granular soil. From one meter deep, boulder clay is found in the soil.

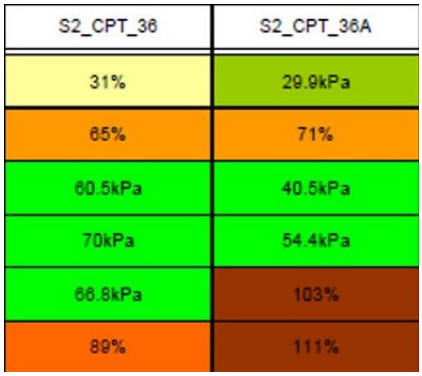

Figure 7.76: CPT's location 36

For the case study, both soil types will be investigated. Since the granular material consist of sand and gravel, the median diameter is assumed to be 1 mm, and a grading is chosen of $d_{50}/d_{10} = 3$. As can be seen in the above figure, the relative density is 31%. For the cohesive soil, the undrained shear strength is 29.9 kPa. The sensitivity of this soil is not known but will be assumed to be normally sensitive, which is a factor four. The residual shear strength will occur from the fifteenth element, this will represent an intermediate response. Both elasticity moduli are assumed to be the same as in the base case. For the external factors, assumptions will also have to be made. It is known that, in order to avoid the stronger boulder clay, the trenching depth in other parts of the trajectory was 1.3 m, and the cutter was also in operation. There is no information about the forces on the cutter. To take these forces into account, an extra horizontal force of 50 kN is assumed. This, together with the maximum cutting force of the jet sword, will give an approximation of this problem. The roll and pitch angle at failure was around one degree. All other parameters are not known and must therefore be assumed equal to those in the base cases. The input parameters for both cases are provided in the tables below.

Input parameters			
Roll [deg]	1	Sensitivity [-]	4
$\theta_{current}$ [deg]	0	$J_{residual}$ [m]	0.6
$u_{current}$ [m/s]	0	i_{sr} [-]	0.2
z_{trench} [m]	1.3	$N_{element,res}$	15
Cd [-]	2	kc [-]	500
γ [kN/m^3]	6.5	ν [-]	0.3

Table 7.30: Moray east - Possible cohesive soil

Input parameters			
Roll [deg]	1	d_{50} [m]	0.001
$\theta_{current}$ [deg]	0	$\frac{d_{50}}{d_{10}}$ [-]	5
$u_{current}$ [m/s]	0	i_{sr} [-]	0.2
z_{trench} [m]	1.3	$v_{progress}$ [m/s]	0.056
Cd [-]	2	E' [kPa]	25000
γ [kN/m^3]	8	ν [-]	0.3

Table 7.31: Moray east - Possible granular soil

The results of the two cases are presented below in four images. It can be observed that, for cohesive soils, mobility is indeed not good enough to operate with a cutter and a jet; the trencher would slip and not sink. If the cutter and jet sword were stowed, the trencher could operate. The purple cross indicates the operation as performed. This corresponds to the story in the memo. The possible presence of a granular soil indicates that the operation should have been possible with a cutter and jet. However, the operation was on the edge of the working area, and minor changes in the circumstances could still lead to failure. It can be observed that, without a cutter and jet sword, the trencher would fail. This is

due to the elimination of the counteracting moment and the upward force of the jet sword. Any failure in granular soil would be vertical failure, i.e. the trencher sinking rather than slipping. In other words, the conclusion in the memo of a soft and slippery cohesive local soil condition can be validated using the model.

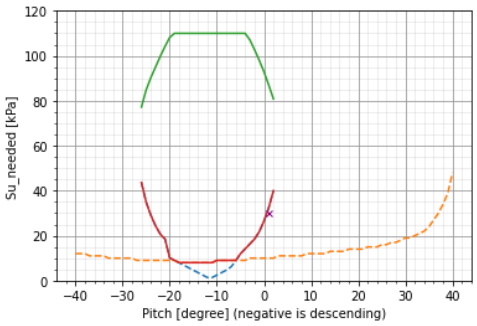

Figure 7.77: Moray east - Possible cohesive soil (cutter and jet operation)

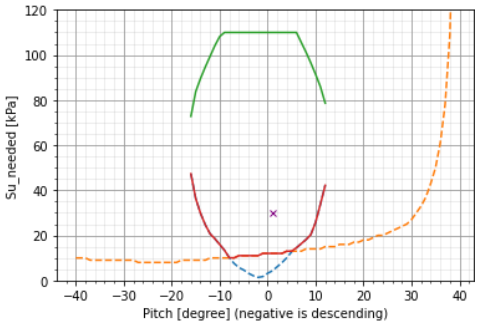

Figure 7.78: Moray east - Possible cohesive soil (no cutter and jet operation)

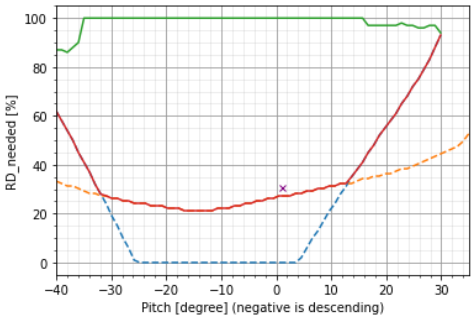

Figure 7.79: Moray east - Possible granular soil (cutter and jet operation)

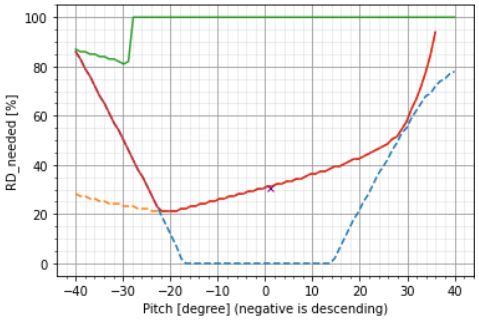

Figure 7.80: Moray east - Possible granular soil (no cutter and jet operation)

7.4. Summary

The conclusion from the case studies is that, in cohesive soils, the influence of factors working in the same direction as the driving direction exceeds that of factors working perpendicular to the driving direction. In granular soils, this is different because the roll angle and perpendicular flow also have an impact. An important parameter for cohesive soils is again the sensitivity of the soil. With granular material, the influence of contractancy and dilatancy is important as the effective particle size becomes smaller. Mobility in cohesive soils is mostly governed by the horizontal model, whereas, in granular soils, there is a greater chance of vertical failure. If the mobility of the trencher were improved, the greatest gains can be achieved by widening the tracks. Changing the grousers could also have a positive impact on the trencher's mobility but seems more contingent on the sort of operation. With the help of these two cases, Borssele and Moray East, the horizontal and vertical models are validated.

8

Discussion and conclusions

8.1. Discussion

The research revolves around the model created. Ultimately, the conclusions drawn are based on this model. Chapter 7 discusses the validity of this model using two case studies, in which both the horizontal and the vertical models are validated. The formed model seems to offer a good representation of reality in both situations, with limited soil research. This is important as the model will be used for assessing potential risks in the future. In addition, the model can be expected to produce more accurate results if the soil investigation is extended and specified on the model, which parameters and which soil research will be discussed later in this chapter. The conclusions regarding the influences of the various processes can be generalised for trenchers with the same dimensions as the CBT2400. However, the mobility envelopes are trencher specific. On the other hand, the model can be used for all trenchers, which was one of the goals prior to the study.

All the processes that make a frontal impact or work in the direction of travel logically affect mobility. Any force acting in this direction must be additionally overcome by traction to form a horizontal balance. The possible currents and pitch angles should therefore be known during the risk assessment.

One thing that stands out in cohesive soils is that the CBT2400 has poorer mobility in soils with higher undrained shear strengths. This has two causes that are important to know. The first is that a decrease in the adhesion factor causes the track-soil shear forces to become smaller from a certain point with increasing undrained shear strength. When the undrained shear strength is above 110 kPa, there will be no more track-soil shear interaction. This constitutes an upper limit to the model. The second cause is that, from a certain point, the penetration depth decreases very rapidly and the traction becomes completely dependent on track-soil shear forces. With the CBT2400, the grousers' percentage is already zero at twenty kPa, in the most standard situation without slopes. So it is interesting to look at the grouser's length to increase penetration depth and mobility. This will be elaborated on in a later section.

Another result that stands out is that the roll and currents from the side have little influence on the trencher's mobility in cohesive soils. These two processes influence the force redistribution on the tracks. This causes one track to have to deal with a greater vertical force than the other. Because vertical stability is almost non-existent in cohesive soils, the increase in vertical pressure has little influence. The large pressure does result in more penetration of the grousers, but this results in a larger traction force. So, where vertical pressure is less, penetration depth will be less, but in most of the operational area, traction is already dependent on track-soil interaction. In granular soils, the vertical model is normative for large parts of the lower boundary. As a result, the roll and flow impact on the sides is of greater influence than in cohesive soils. In addition, it is logical that these processes have more influence on the mobility process because, where the redistribution of vertical forces only influences penetration depth in cohesive soils, in granular soils it also influences the available shear strength in the soil, which is used in the traction calculations for the horizontal stability.

The influence of sensitivity also stands out: very sensitive cohesive soils lose a large part of their strength at a certain shear displacement. The sensitivity of the clay is easy to estimate by making a shear displacement graph. It is also possible to determine from this graph the shear displacement required for the residual shear strength to become effective. The last influence on this process is the slip ratio. The slip ratio can be easily measured when the trencher is operational. The slip ratio can be seen as the failure limit in the horizontal stability. How much absolute slip distance is accepted before it is called failure. In Boskalis' prior soil research the sensitivity is not measured. This causes that risk assessment is less precise.

What is also noticeable in both soils is that the influence of the driving resistances (the bulldozing resistance, the static compaction resistance and the dynamic compaction resistance) are small on the operation area. This makes parameters such as the elastic modulus and undrained elasticity modulus correlation factor less critical. Therefore these parameters are less vital to measure prior to the risk assessment.

In the case study with the smaller grousers, the previously described process of penetration and track-soil interaction can be clearly observed. In cohesive soils, the trencher's mobility increases in soils with an undrained shear strength below 40 kPa. This is a logical consequence of the grousers becoming smaller and thus penetrating deeper. In soils with a higher undrained shear strength, however, there is still no penetration, and traction is therefore dependent on the track-soil interaction. However, since the grousers are smaller, the areas where this interaction takes place will also be smaller. As a result, the trencher's mobility will deteriorate here. In sandy soils, the penetration is better than in clay soils; therefore the decrease in grouser length will result in an increase in mobility at all soil strengths. In cohesive soils that are more dependent on track-soil interaction, the flat track belt is therefore a more logical improvement. This can also be seen in the mobility envelopes. For granular soils, a decrease in mobility can be seen at all soil strengths. There can only be one explanation for this: the track now being used also penetrates well into denser soils. The traction is more significant when the grousers penetrate, so it cannot be said that it does not help to increase workability in some circumstances. This will mainly be in soils where a greater force is applied to the trenching tools. This, in turn, is expected in stronger soils where the penetration of the grousers is worse than in weak soils. Therefore it is essential to look at the option of even smaller grousers. It is crucial that the grousers penetrate in these conditions anyway.

When increasing the width and length of the track, it was a logical consequence that mobility would improve in both cases. Both the vertical forces are distributed over a larger area and the shearing surface becomes larger in the traction calculations. It is good to keep in mind that increasing the width will be mechanically easier than increasing the length.

Shifting the centre of gravity mainly affects vertical stability. With the jet sword in operation, the centre of gravity is now in the best place. However, this should be investigated more precisely. For this, it is important that the vertical and horizontal forces on the cutting tools are better mapped. With the help of case studies, it can be determined where the centre of gravity should be placed to achieve the best mobility, both in the situations with and without operation.

When validating the horizontal model, little soil research was available at the failure location. Using assumptions based on soil investigations further away from the failure location, a full case study was eventually carried out. This does allow for validation of the model as to whether it gives a good estimate of risks. Note that this is the most important application of the model as it is intended for use at an earlier stage to identify potential risks in the trajectory. What is true, however, is that many essential parameters are currently missing from the ground surveys that do influence mobility to some extent. It would be valuable to examine these parameters. Especially in situations where mobility seems to be critical. In cohesive soils, this mainly concerns the sensitivity of the soil, while in granular soils, it concerns the influence of contractancy. Both can be determined through a shear-displacement graph. Besides, it is not possible, to see how accurate the model is. The actual accuracy of the horizontal model might be tested by assessing trencher mobility in locations where the soil details are known. Further explanatory notes will be provided in the recommendations section.

In the case study done in this research, a maximum horizontal cutting force is taken into account everywhere on the trench tool. This means that the same force is applied in very loose granular soil as in firm cohesive soil. In reality, this will not be the case. It can be valuable to link a model in which the cutting forces on the trenching tools are calculated. In this way, the horizontal stability can be precisely calculated, and the mobility envelope will be more precise.

As discussed earlier, the track-soil interaction planes are an important part of the traction calculations. Here, however, two major assumptions (adhesive factor and external friction angle) were made in determining the shear strength. Should these values deviate, this will have consequences for the mobility envelopes. Also, it can be expected that when the adhesion diminishes there will be an increasing friction angle in cohesive soils. This relationship is not yet clear and is therefore not included. Another shortcoming is that this model approaches the process statically, while driving the trencher is a dynamic process. In the dynamic process, successive events may cause soil parameters to change. It is also difficult to accurately determine the strength of the soil from a CPT. However, this is of great importance for the accuracy of the model. This is also a knowledge gap, and should be further researched.

8.2. Conclusion

This research sought to answer the following question: ”Which different operational environments and soil conditions have a critical influence on the deployabilty of a subsea tracked trencher regarding the vertical stability and horizontal mobility of the soil-track interaction system?” To answer this question, a computational model was formed, and with that model a case study was carried out with the vehicle CBT2400. The conclusions are listed below:

- The mobility of the CBT2400 is better in granular soils than in cohesive soils.
- In looser granular soils (rd < 30%) the vertical stability (sinking) determines the mobility to a greater extent than the horizontal stability (slipping). This confirms the expectations from the practical knowledge. In denser granular soils (rd > 30 %) the mobility is limited by the horizontal stability (slipping). However, there must be extreme circumstances (slopes > 10°; currents > 0.5m/s) to slip in denser granular soils.
- In weaker cohesive soils (< 15 kPa) the vertical stability (sinking) determines the mobility. This confirms the expectations from the practical knowledge. In stronger cohesive soils (> 15 kPa) the horizontal stability (slipping) determines the mobility, with a trenching depth of 3.3 m. From the practical expertise slipping was expected in soils stronger than 50 kPa. From the research it can be concluded that this boundary is lower. But it can be seen that from 50 kPa the mobility decreases in high rate.
- In all granular and cohesive soils, pitch angles are of importance in the mobility process. The presence of pitch angles increase the chance of horizontal failure (slipping). In cohesive soils a pitch of 10° is the maximum slope, which is smaller than the expectation(15°). In granular soils the maximum pitch is 25°, which is larger, but with angles steeper than 15° the mobility decreases rapidly. In general, a downward slope will be less critical than an upward slope. In addition, the influence is more significant in stronger (> 40 kPa) than in weaker cohesive soils. In contrast to cohesive soils, the influence is greater in granular soils with a relative density between the 70% and 30%.
- Roll angles influence the mobility in granular soils significantly, while the change in cohesive soils the influence is almost negligible. The influence in granular soils is in particular in the horizontal stability and causes even larger influence in combination with pitch angles.
- The current conditions can be divided into frontal impact and side impact. In cohesive soils, frontal impact has a lot of influence, while side impact has little effect. Especially areas where there is a positive pitch angle and a frontal flow are areas at additional risk. In granular soils, flow from both directions has a significant influence on mobility. Therefore, it is crucial to make a good analysis of the currents in granular soils. Currents mainly influence the horizontal stability (slipping).

- The sensitivity is of significant influence on the mobility of the trencher in cohesive soils. When the sensitivity of the soil increases, the horizontal stability (slipping) will be more normative, another critical factor to the influence of sensitivity is from which track element the shear strength is expected to be in its residual state. The accepted slip ratio and the slip displacement before the residual state begins determines this element. Increasing sensitivity influence the mobility in weaker soils deteriorate at a higher rate than stronger soils.

- The influence of the dilatancy and contractancy depends on the grain size particle grading and the progress velocity. From the research it can be concluded that when all three parameters are right, there is an influence on the mobility. In looser soils (rd<50%) the mobility will decrease while in denser soils (rd>50%) the mobility will increase. With smaller median grain sizes (d_{50} < 0.001 m) and larger particle grading (d_{50}/d_{10} > 7) the influence should be considered. When the influence is to high it can be considered to lower the progress velocity in order to enlarge the mobility.

- With a lower elasticity modulus, mobility will decrease in cohesive soils. The impact of the elasticity modulus in granular soils is almost negligible. The effect of the dynamic compaction resistance caused by the slip ratio is small but cannot be neglected.

- The grouser size influences the horizontal stability. It can be concluded that increasing or decreasing the grouser's length, which increases or decreases the grouser's bottom contact area, can positively influence mobility. Reducing the grousers length causes the traction force to improve, but only if the grousers do penetrate the soil. If the grousers do not penetrate, it will decrease the traction force. If the length of the grouser increases, the traction force increases when the smaller grousers are not penetrated. In other situations, it will decrease.

- Increasing the length or width of the tracks would improve the trencher's mobility, both the vertical stability (sinking) as horizontal stability (slipping). The largest changes will be in looser granular soils and weaker cohesive soils.

- Changing the centre of gravity does change the vertical stability and thereby affect mobility. A more thorough analysis should be made whether this can improve mobility in a way.

- It can be concluded that the model can be used in a prior risk assessment. With a less extensive soil survey, the model identifies risks in specific locations. However, after the first risk assessment, a more comprehensive examination will be necessary to determine whether the trencher can operate in that environment. The more insightful ground parameters and external factors are, the more reliable the risk analysis will be.

8.3. Recommendations

The recommendation section will be divided into two parts: operational and follow-up research recommendations. The operational recommendations can be split up into operational use and possible trencher recommendations. The recommendations are discussed below:

- Operational use: From the two case studies done during the validation, it appears that the model can identify risky locations, with the soil research now being done within Boskalis. However, additional assumptions need to be made. These assumptions directly influence whether or not the trencher will fail and are thus essential. Therefore it is wise to do the risk assessment in 4 steps. The first step is the initial soil investigation. The trajectory's bathymetry should be known, and there should be a profile of the material of the top layer and the underlying layer. Finally, several CPTs must be carried out along the trajectory, and the soil in the areas between the CPT's should be approximated. The CPT locations should be chosen with the conclusions from this study in mind to ensure that the assumptions around the risk areas are adequate. Once the soil is evaluated along the trajectory, the model can do a first risk assessment. The first risk analysis marks specific locations, which can be further investigated. Preferably, this second investigation includes the drawing up of stress-displacement graphs. With the help of these graphs, the sensitivity and the influence of contractancy or dilatancy are known. Besides, a more exact estimation of the forces on the tools should be determined. If both are known, a more precise failure analysis

can be made. If the trencher's mobility is still at risk of failing, preventive measures can be taken. If it turns out that there is no risk, after all, the trencher can operate as usual.

- Track dimensions change: It can be interesting to adjust the dimensions of the trencher's tracks and especially the grousers to the circumstances. For example, narrower grousers than in the case of heavy loads, but also a set with flat tracks can be interesting. Here, however, other factors such as wear, assembly speed and costs play an essential role. In any case, increasing the size of the tracks (width/length) is something that improves mobility.

From the implications of this study, there are a number of logical further research steps. A number of follow-up studies will be suggested below:

- Track-soil interaction: Logical follow-up research might study more precisely the track-soil interaction. This can be done by testing the external friction angle of the granular soil with the track material. In addition, it would be interesting to test the adhesion factor for cohesive soils with the track material. If these relationships are further clarified, the model becomes more accurate.
- CPT interpretation: A future study on the interpretation of the CPT for the top layer of soil is of interest. For the mobility of the trencher, the top 20 cm of soil is the most important. At the moment, this is determined with CPT's. But, is this the best way to determine this part of the soil, and how can the results best be translated into a soil strength?
- Cutting forces: A potential follow-up step in modelling is to integrate the tool already available within Boskalis that calculates the forces operating on the cutting tool. This would ensure a better early estimate of where potential risks lie, especially where they are absent. If the soil is less strong, the forces on the tool will also be less, and there will be less need for traction.
- Validation studies: Additional validation tests will need to be carried out to clarify how accurate the boundary regions in the model are. There are two options for this: testing in a controlled environment, perhaps using a scale model, or additional testing after a trencher has failed, to determine the specific soil parameters at precisely that location. While the latter option would, of course, require a failed operation - which, in itself, is not desirable - it will probably be less costly and time-consuming.

Bibliography

Abuhajar, O., Hesham El Naggar, M., Newson, T., & Abuhajar Hesham El Naggar Tim Newson, O. M. (2010). Review of Available Methods for Evaluation of Soil Sensitivity for Seismic Design. *International Conferences on Recent Advances in Geotechnical Earthquake Engineering and Soil Dynamics*, *5*, 27.

Al-Karni, A. A. (2011). Evaluation of shear strength of cohesionless soil due to excess pore water pressure. *Arabian Journal of Geosciences*, *4*(7-8), 1095–1101.

Alwalan, M. (2018). Interaction of closely spaced shallow foundations on sands and clays: A review. *5*, 101–110. https://doi.org/10.22161/ijaers.5.9.11

Baek, S. H., Shin, G. B., & Chung, C. K. (2018). Assessment of the side thrust for off-road tracked vehicles based on the punching shear theory. *Journal of Terramechanics*, *79*, 59–68.

Baek, S. H., Shin, G. B., & Chung, C. K. (2019). Experimental study on the soil thrust of underwater tracked vehicles moving on the clay seafloor. *Applied Ocean Research*, *86*(March), 117–127.

Baek, S. H., Shin, G. B., Lee, S. H., Yoo, M., & Chung, C. K. (2020). Evaluation of the slip sinkage and its effect on the compaction resistance of an off-road tracked vehicle. *Applied Sciences (Switzerland)*, *10*(9).

Budhu, M. (2011). *Soil Mechanics and Foundations* (Third Edition). JOHN WILEY & SONS, INC.

Carman, P. (1956). *Flow of gases through porous media*. Academic Press.

Chen, X., Hong, G., & Miedema, S. A. (2019). A study on the clay adhesion factor. *Dredging Summit & Expo '19 Proceedings*, (June).

Cherubini, C., & Vessia, G. (2008). Reliability approach for the side resistance of piles by means of the total stress analysis (α method). *Canadian Geotechnical Journal*, *44*, 1378–1390. https://doi.org/10.1139/T07-061

Das, B. M. (2011). *Geotechnical engineering handbook.* J. Ross Publishing.

Feng, X., Gourvenec, S., Randolph, M. F., & Teng, R. (2019). Effectiveness of Effective Area Method for Assessing Undrained Capacity of Shallow Rectangular Foundations. *Journal of Geotechnical and Geoenvironmental Engineering*, *145*(2), 06018013.

Journée, J. M. J., Massie, W. W., & Huijsmans, R. H. M. (2015). OFFSHORE HYDROMECHANICS Third Edition (2015).

Kézdi, Á., & Rétháti, L. (1974). *Handbook of soil mechanics* (Vol. 1). Elsevier Amsterdam.

Lambe, T. W., & Whitman, R. V. (1969). Soil Mechanics.

M. Takechi, C. Uno, Y. T. (1994). Maximum and minimum void ratio characteristics of sands. *Chemical Pharmaceutical Bulletin*, *17*(11), 1460–1462.

Meyerhof, G. (1953). The Bearing Capacity of Foundations under Eccentric and Inclined Loads.

Miedema, S. A. (2019). *The Delft Sand, Clay & Rock Cutting Model* (Third edition). TU Delft open.

Mitchell, J. k., & Soga, K. (2005). *Fundamentals of Soil Behavior* (Third Edition, Vol. 158). JOHN WILEY & SONS, INC.

Mocera, F., Somà, A., & Nicolini, A. (2020). Grousers effect in tracked vehicle multibody dynamics with deformable terrain contact model. *Applied Sciences (Switzerland)*, *10*(18).

Morgan, N., Cathie, D., Pyrah, J., & Steward, J. (2007). Tracked subsea trencher mobility and operation in soft clays. *Proceedings of the International Offshore and Polar Engineering Conference*, 1366–1373

(9/10) Geeft goed het probleem aan dat ik moet gaan oplossen.

Obrzud, R. (2010). *The hardening soil model: A practical guidebook*. Zace Services.

Papadopoulou, A., & Tika, T. (2008). The effect of fines on critical state and liquefaction resistance characteristics of non-plastic silty sands. *Soils and foundations*, *48*(5), 713–725.

Prat, M., Bisch, E., Millard, A., Mestat, P., & Cabot, G. (1995). The modeling of the structures (la modelisation des ouvrages).

Rosenqvist, I. (1952). CONSIDERATIONS ON THE SENSITIVITY OF NORWEGIAN QUICK-CLAYS. *Ge´otechnique*, *3*, 195–200.

Schmertmann, J. H. (1978). Guidelines for cone penetration test : performance and design.

Shill, S., & Hoque, M. M. (2015). Comparison of Bearing Capacity Calculation Methods in Designing Shallow Foundations. *International Journal of Engineering Technology*, *3*(9), 29–39.
Terzaghi, K., Peck, R. B., & Mesri, G. (1996). Soil Mechanics in Engineering Practice.
Verruijt, A. (2010). *Soil Mechanics Book*.
Wang, M., Wu, C., Ge, T., Gu, Z. M., & Sun, Y. H. (2016). Modeling, calibration and validation of tractive performance for seafloor tracked trencher. *Journal of Terramechanics*, *66*, 13–25.
Wong, J. (2001). *Theory of ground vehicles* (Third edition). JOHN WILEY & SONS, INC.
Wong, J. (2010). *Terramechanics and off-road vehicle engineering* (Second edition). Elsevier.